Physics Library
QC
1
.U56

Volume 65A
Number 5
Sept.–Oct. 1961

THE UNIV. OF MICH.
OCT 27 1961
PHYSICS LIBRARY

Physics and Chemistry

U.S. DEPARTMENT OF COMMERCE

SECTION A

JOURNAL OF RESEARCH

NATIONAL BUREAU OF STANDARDS

Journal of Research

of the

National Bureau of Standards

A. Physics and Chemistry

SEPT.–OCT. • 1961

VOLUME • 65A

NUMBER • 5

Editor: U. Fano

Associate Editors: L. M. Kushner
I. M. Richardson

Publication dates:
Feb. 1, Apr. 1, June 1, Aug. 1, Oct. 1, Dec. 1, 1961.

JOURNAL OF RESEARCH

The National Bureau of Standards Journal of Research reports research and development in the fields of activity shown at right. Also included from time to time are survey articles on topics closely related to the Bureau's scientific and technical program.

The Journal is published in four separate sections as follows:

A. Physics and Chemistry

Contains papers of interest primarily to scientists working in these fields. Issued six times a year. Annual subscription: domestic, $4.00; foreign, $4.75.

B. Mathematics and Mathematical Physics

Presents studies and compilations designed mainly for the mathematician and the theoretical physicist. Issued quarterly. Annual subscription: domestic, $2.25; foreign, $2.75.

C. Engineering and Instrumentation

Reports research and development results of interest chiefly to the engineer and the applied scientist. Issued quarterly. Annual subscription: domestic, $2.25; foreign, $2.75.

D. Radio Propagation

Reports work in radio propagation, upper atmospheric physics and communications. Issued six times a year. Annual subscription: domestic, $4.00; foreign, $4.75.

Functions and Activities

The functions of the National Bureau of Standards are set forth in the Act of Congress, March 3, 1901, as amended. These include the development and maintenance of the national standards of measurement and the provision of means and methods for making measurements consistent with these standards; the determination of physical constants and properties of materials; the development of methods and instruments for testing materials, devices, and structures; advisory services to government agencies on scientific and technical problems; invention and development of devices to serve special needs of the Government; and the development of standard practices, codes, and specifications. The work includes basic and applied research, development, engineering, instrumentation, testing, evaluation, calibration services, and various consultation and information services. The Bureau also serves as the Federal technical research center in a number of specialized fields. The scope of activities of the National Bureau of Standards is suggested in the following listing of the divisions and sections engaged in technical work.

Washington, D.C.

Electricity. Resistance and Reactance. Electrochemistry. Electrical Instruments. Magnetic Measurements. Dielectrics.

Metrology. Photometry and Colorimetry. Refractometry. Photographic Research. Length. Engineering Metrology. Mass and Scale. Volumetry and Densimetry.

Heat. Temperature Physics. Heat Measurement. Cryogenic Physics. Equation of State. Statistical Physics.

Radiation Physics. X-ray. Radioactivity. Radiation Theory. High Energy Radiation. Radiological Equipment. Nucleonic Instrumentation. Neutron Physics.

Analytical and Inorganic Chemistry. Pure Substances. Spectrochemistry. Solution Chemistry. Standard Reference Material. Applied Analytical Research.

Mechanics. Sound. Pressure and Vacuum. Fluid Mechanics. Engineering Mechanics. Rheology. Combustion Controls.

Organic and Fibrous Materials. Rubber. Textiles. Paper. Leather. Testing and Specifications. Polymer Structure. Plastics. Dental Research.

Metallurgy. Thermal Metallurgy. Chemical Metallurgy. Mechanical Metallurgy. Corrosion. Metal Physics. Electrodeposition.

Mineral Products. Engineering Ceramics. Glass. Refractories. Enameled Metals. Crystal Growth. Physical Properties. Constitution and Microstructure.

Building Research. Structural Engineering. Fire Research. Mechanical Systems. Organic Building Materials. Codes and Safety Standards. Heat Transfer. Inorganic Building Materials.

Applied Mathematics. Numerical Analysis Computation. Statistical Engineering. Mathematical Physics.

Data Processing Systems. SEAC Engineering Group. Components and Techniques. Digital Circuitry. Digital Systems. Analog Systems. Applications Engineering.

Atomic Physics. Spectroscopy. Radiometry. Solid State Physics. Electron Physics. Atomic Physics.

Instrumentation. Engineering Electronics. Electron Devices. Electronic Instrumentation. Mechanical Instruments. Basic Instrumentation.

Physical Chemistry. Thermochemistry. Surface Chemistry. Organic Chemistry. Molecular Spectroscopy. Molecular Kinetics. Mass Spectrometry. Molecular Structure and Radiation Chemistry.

• Office of Weights and Measures.

Boulder, Colo.

Cryogenic Engineering. Cryogenic Equipment. Cryogenic Processes. Properties of Materials. Gas Liquefaction.

Ionosphere Research and Propagation. Low Frequency and Very Low Frequency Research. Ionosphere Research. Prediction Services. Sun-Earth Relationships. Field Engineering. Radio Warning Services.

Radio Propagation Engineering. Data Reduction Instrumentation. Radio Noise. Tropospheric Measurements. Tropospheric Analysis. Propagation-Terrain Effects. Radio-Meteorology. Lower Atmosphere Physics.

Radio Standards. High Frequency Electrical Standards. Radio Broadcast Service. Radio and Microwave Materials. Atomic Frequency and Time Interval Standards. Electronic Calibration Center. Millimeter-Wave Research. Microwave Circuit Standards.

Radio Systems. High Frequency and Very High Frequency Research. Modulation Research. Antenna Research. Navigation Systems. Space Telecommunications.

Upper Atmosphere and Space Physics. Upper Atmosphere and Plasma Physics. Ionosphere and Exosphere Scatter. Airglow and Aurora. Ionospheric Radio Astronomy.

U.S. DEPARTMENT OF COMMERCE
Luther H. Hodges, Secretary

NATIONAL BUREAU OF STANDARDS
A. V. Astin, Director

Order all publications from the Superintendent of Documents
U.S. Government Printing Office, Washington 25, D.C.

Use of funds for printing this publication approved by the Director of the Bureau of the Budget (June 19, 1961).

JOURNAL OF RESEARCH of the National Bureau of Standards—A. Physics and Chemistry
Vol. 65A, No. 5, September–October 1961

Calibration of a Monitor for Use in Bremsstrahlung Beams

E. G. Fuller and Evans Hayward

(June 6, 1961)

The calibration of a thick-walled ionization chamber by means of a sodium iodide scintillation spectrometer is described. The calibration was made for six bremsstrahlung energies in the range 6 to 19 Mev.

1. Introduction

A thick-walled, parallel-plate, aluminum ionization chamber has been designed and constructed [1] [1] as a standard to measure the X-ray intensity of the bremsstrahlung beams of betatrons and synchrotrons. This chamber is of simple, rugged construction and presumably can be reproduced in any laboratory. It has already been calibrated for peak bremsstrahlung energies in the range 20 to 180 Mev by caliormetry [1] and by means of a scintillation spectrometer [2]. The present paper describes its calibration by the latter method [3] for bremsstrahlung energies in the range 6 to 19 Mev. This calibration then permits for the first time the measurement in different laboratories of photonuclear cross sections in the giant resonance regions with reference to the same monitor.

2. Method

The object of this calibration was to relate the number of coulombs collected from the thick-walled ionization chamber to the amount of energy in the bremsstrahlung beam incident on it. This calibration was performed in two steps. First, the reading on a transmission monitor (see fig. 1) was related to the charge collected from the standard chamber by taking the ratios of their readings. For this comparison the standard chamber was carefully located in the betatron bremsstrahlung beam in the position later occupied by a sodium iodide scintillation spectrometer. The second step was to use the spectrometer to relate the amount of energy in this beam to the reading of the transmission monitor. These two measurements then yield the number of coulombs collected from the standard chamber per Mev of bremsstrahlung energy incident on it for the beam filtration equivalent to 7.25 g/cm^2 of aluminum normally used with this betatron. In a subsidiary experiment the effects of filtration were studied by varying the aluminum thickness between a thin transmission chamber and the standard chamber.

The relationship between the amount of energy incident on the scintillation spectrometer and the charge collected from the transmission ionization chamber was determined by measuring the total number of interactions in the crystal produced by the beam. For this measurement a thick absorber was placed between the transmission ionization chamber and the crystal. (See fig. 1.) This absorber was introduced to reduce the intensity of the X-ray beam at the crystal so that it could be counted without pulse pile-up and at the same time accurately monitored by the ionization chamber. The absorber also removed the lowest energy photons from the beam, making the pulse height distributions obtained more amenable to interpretation. In the previous calibration [2] that employed this method carbon absorbers were used. This approach was not possible in the work reported here, because the physical dimensions of the experimental area in front of the betatron are not great enough to provide the good geometry required. It has already been shown [4], however, that it is possible to calibrate this beam using lead absorbers for which the Compton scattering cross section is much less important and geo-

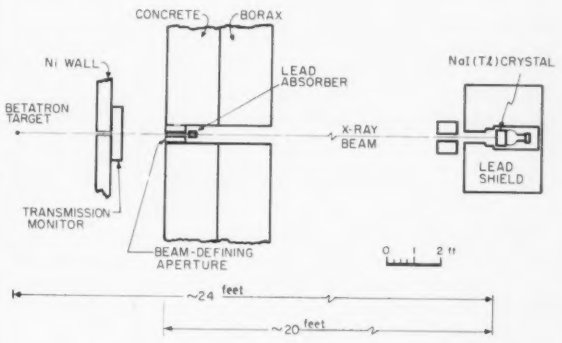

FIGURE 1. *Geometry of the experiment.*

[1] Figures in brackets indicate the literature references at the end of this paper.

metrical considerations are therefore minimized. Lead absorbers were therefore used in the final calibration.

The physical arrangement is shown in figure 1. The bremsstrahlung beam traversed the betatron donut wall and the parallel-plate transmission chamber before being defined by a small hole (1/16 in. in diameter) in an 8-in. long lead block. This aperture produced a beam approximately 2 in. in diameter at the back of the experimental area about 24 ft from the betatron target. Before reaching the sodium iodide crystal this beam passed through but did not strike a secondary aperture that removed stray radiation. The absorbers were placed in the beam just after the beam-defining aperture.

The use of a scintillation spectrometer to calibrate a bremsstrahlung beam depends on the ability to relate the total number of photons materialized in the sodium iodide crystal to the amount of energy in the beam. This calibration is based on a knowledge of the X-ray attenuation coefficients for all the absorbing materials in the beam, as well as for the sodium iodide itself. The assumed shape of the bremsstrahlung spectrum, $I(E_0,E)$, is of less importance. If $A(E_0)=\int dE\, I(E_0,E)$ represents a unit of bremsstrahlung energy leaving the betatron target lying in the cone transmitted by the beam-defining aperture when electrons of energy E_0 strike the internal betatron target, then the number of photons materialized in the sodium iodide crystal is

$$P(L,E_0)=\int dE\, \frac{I(E_0,E)}{E}\, e^{-L(E)}[1-e^{-T(E)}]. \quad (1)$$

The symbol $L(E)$ represents the number of mean free paths of material between the bremsstrahlung-producing target and the detector and $T(E)$ the number in the sodium iodide crystal itself. At the same time, the amount of energy passing through the beam-defining aperture is

$$A'(E_0)=\int dE\, I(E_0,E)e^{-L'(E)}, \quad (2)$$

where $L'(E)$ is the number of mean free paths of absorber in the donut wall and the transmission monitor. If $C(L,E_0)$ stands for the total number of spectrometer counts registered per volt measured on the transmission monitor, and $R(E_0)$ is the number of coulombs collected from the standard chamber per volt measured on the same monitor, then the calibration of the standard chamber in coulombs/Mev is

$$\alpha(E_0)=\frac{R(E_0)}{C(L,E_0)}\,\frac{P(L,E_0)}{A'(E_0)}. \quad (3)$$

This method is based on the assumption that each photon interacting in the absorbing material results in its removal from the beam. The applicability of this assumption can be checked experimentally by performing the calibration for several values of absorber thickness, L. This test was used as the criterion of acceptability of the results. A valid calibration must be independent of L.

3. Details of the Measurement

The scintillation spectrometer consisted of a NaI(Tl) crystal and associated electronics. The sodium iodide crystal was 5 in. in diameter and 4 in. long and was viewed by a 5-in. photo-multiplier tube. This assembly was encased in the lead box shown in figure 1. The pulses were amplified and analyzed by a 20-channel pulse height analyzer. The analyzer was gated so as to accept pulses only during a 25-μsec interval around the betatron yield pulse. To avoid pulse pile-up the counting rates were at all times maintained at less than five counts per second for all pulses above a bias corresponding to the absorption of $\sim$300 kev by the crystal. The repetition rate of the betatron was 180 pulses/sec.

The charge collected from the transmission monitor (and from the standard chamber as well) was determined by measuring the voltage developed across a polystyrene film capacitor. This voltage was cancelled by that supplied and measured by a potentiometer. The null condition was established with a vibrating reed electrometer. The capacitors were calibrated against a standard, using a bridge operated at 1,000 cycles. The resulting errors in the absolute charge measurements are small compared to those inherent in the determination of the absolute number of counts in the sodium iodide crystal.

The data to be reported here were taken in a two-week period during which the following measurements were made as a daily routine: (1) The sensitivity of the transmission chamber, which was closed to the atmosphere, was checked by measuring the time required to charge a capacitor to a standard voltage when a radioactive source was placed in a standard position. This reading was reproducible to within 0.5 percent. (2) The leak-rate of this monitor was measured. It was large enough to produce corrections to the monitor reading varying from 0.1 to 2 percent. (3) The stability of the counting equipment was checked by measuring the pulse height distribution produced by a Na^{22} source and by using a pulser to determine the bias of the top and bottom of the pulse height analyzer. The overall gain of the system changed by less than 2 percent. This variation has a negligible effect on the calibration.

The absorbers used in this calibration were lead disks 2 in. in diameter and 1 in. long. They were carefully machined so that their thickness in g/cm^2 could be determined by weighing and accurately measuring their diameters. They were placed in the beam just after the beam-defining aperture. The choice of absorber thickness was determined empirically. It was found that at least 5 in. of lead were required between the transmission monitor and the spectrometer to reduce the X-ray intensity at the crystal enough so that the counting could be done without pulse pile-up, and to maintain a high enough intensity at the ionization chamber to make a reliable measurement possible. The upper limit on the thickness was set at 7 in. by the magnitude

of the multiple scattering in the absorber. The use of eq (1) to calculate the number of photons materialized in the sodium iodide crystal assumes that every interaction of a photon in the absorber results in its removal from the beam. As will be seen in the following, for sufficiently thick absorbers the buildup of secondaries is great enough to make this assumption invalid.

At each of the six bremsstrahlung energies used in this calibration, the pulse height distributions produced by the photons transmitted by 5, 6, 7, and 8 in. of lead were recorded. Two runs were made under each condition to yield a total of 10^4 counts. The statistical uncertainty of the calibration is therefore of the order of 1 percent.

The principal source of background was that resulting from cosmic rays and general background radioactivity. This was determined by measuring the counting rate with the X-rays off and the pulse height analyzer ungated. The background for each run was then determined by multiplying this counting rate by the time for each run and reducing by the duty cycle of 4.6×10^{-3}. An attempt was made to evaluate the betatron-produced backgrounds. For this purpose the number of counts registered per monitor reading was recorded when an additional 8-in. lead barrier was placed in front of the sodium iodide crystal. These measurements were made at selected bremsstrahlung energies and for various absorber thicknesses, $L(E)$, in the incident beam. These yields were found to be negligible compared with those measured with the 8 in. removed, indicating that there was no serious contribution to the background from this source.

4. Treatment of the Data

A typical pulse height distribution is shown in figure 2. It was obtained using a 13 Mev bremsstrahlung spectrum and 6 in. of lead absorber in the beam. As a result of the steep energy dependence of the lead X-ray attenuation coefficient, the spectrum of transmitted photons consists of a broad maximum peaking near 3 Mev, i.e., channel 10. An appreciable fraction (1,815 counts in this case) of the distribution lies above the top of the analyzer. The flat part of the distribution below channel 6 results from the incomplete absorption of higher energy photons in the sodium iodide crystal. The dotted histogram in the first five channels has been corrected for background. The dotted area that extends 1.38 channels below the threshold of the pulse height analyzer is an extrapolation of the distribution to include the pulses too small to be recorded. The total number of counts in the distribution then was obtained by taking the number above the threshold of the analyzer, subtracting the gated room background and adding a correction for the pulses below the threshold. The two corrections are small and tend to cancel so that the total correction was usually less than 1 percent.

The results are presented in table 1. The quantities, $C(L,E_0)$ and $R(E_0)$, are the experimental data. The ratios, $P(L,E_0)/A'(E_0)$, were obtained

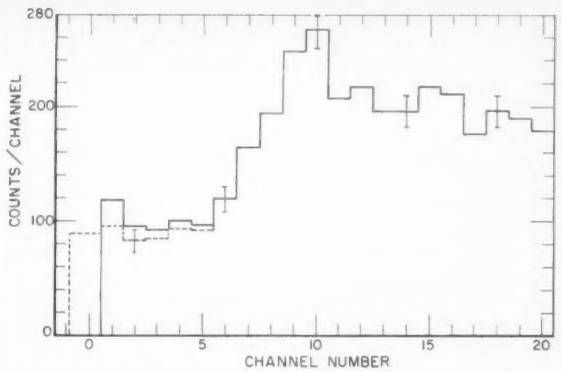

FIGURE 2. *Pulse height distribution produced when the 13-Mev bremsstrahlung spectrum traversed 6 in. of lead.*

In this spectrum there were an additional 1815 counts registered above the top of the analyzer. The errors indicated are based on the number of counts. The dotted histogram in the first five channels has been corrected for the cosmic ray background. The dotted area below the first channel is an extrapolation and was taken to represent the number of pulses too small to be recorded in the analyzer.

TABLE 1

E_0	Lead thickness	$C(L, E_0)$	$R(E_0)$	$P(L, E_0)/A'(E_0)$	$a(E_0)$	RMS deviation
Mev	*in.*	*counts/volt* $\times10^3$	*coulombs/volt* $\times10^{-11}$	*counts/Mev* $\times10^{-4}$	*coulombs/Mev* $\times10^{-19}$	%
6	5	129.3	9.121	5.597	3.948	1.6
	6	40.26		1.756	3.983 3.92	
	7	12.54		0.5277	3.838	
	8	3.946		0.1615	3.733	
8	5	134.9	10.07	5.205	3.891	2.0
	6	42.04		1.637	3.921 3.85	
	7	13.25		0.4923	3.741	
	8	4.150		0.1507	3.657	
10	5	128.6	10.83	4.775(4.771)	4.021	.86
	6	41.11		1.504(1.503)	3.962 4.01	
	7	12.13		0.4529(.4529)	4.044	
	8	3.887		0.1386(.1388)	3.862	
13	5	119.7	11.78	3.961(3.946)	3.898	.45
	6	37.24		1.241 (1.236)	3.926 3.92	
	7	11.11		0.3716 (0.3704)	3.940	
	8	3.452		0.1132 (0.1130)	3.863	
16	5	107.6	12.66	3.340 (3.318)	3.930	1.1
	6	34.30		1.041 (1.035)	3.842 3.90	
	7	10.00		0.3106 (0.3089)	3.932	
	8	3.115		0.09430(0.09392)	3.833	
19	5	99.16	13.43	2.868 (2.845)	3.884	1.0
	6	31.52		0.8914 (0.8847)	3.798 3.83	
	7	9.361		0.2651 (0.2633)	3.803	
	8	2.903		0.08031(0.07990)	3.715	

by evaluating the integrals of eqs (1) and (2). The bremmstrahlung spectra were obtained from the tabulation of Penfold and Leiss [5] and the X-ray attenuation coefficients from the tabulation of White [6]. The absorption by the donut wall, equivalent to 1.59 g/cm^2 of aluminum, the transmission monitor 5.66 g/cm^2 of aluminum, and the thick lead absorbers were all taken into account. The values in parentheses are the result of carrying out the same integrations with the pair production cross section for lead increased by 2.5 percent. Wyckoff and Koch [7] have pointed out that this modification would be more consistent with the results of their attenuation measurements. This

adjustment decreases the magnitudes of the integrals by only 0.5 percent. Reasonable changes in the shape of the assumed bremsstrahlung spectrum have an even smaller effect.

The calibrations of the standard chamber, $\alpha(E_0)$, obtained using the four different lead absorber thicknesses are also given in the table. At each energy the value of $\alpha(E_0)$ obtained using the 8-in. lead absorber is the smallest, and it differs from the average by the largest amount. This systematic trend was taken as an indication that a small fraction of the photons detected by the spectrometer had already been scattered and that the assumptions underlying the calibration procedure were failing. Only the calibrations obtained using 5, 6, and 7 in. of lead as absorbers have therefore been included in the final average. The errors quoted in the table are based on the internal consistency of these three numbers.

The effect of secondary processes on the calibration was even more dramatic when carbon absorbers were used. The calibrations were inconsistent for any pair of thicknesses differing by a mean free path and great enough to make the ion chamber measurements compatible with the scintillation counting.

The final numbers in the table represent the calibration of the standard chamber for a beam diameter of 2.25 in. and a filtration of the incident bremsstrahlung beam equivalent to 7.25 g/cm^2 of aluminum. The calibration does not depend critically on either of these quantities. It has been shown [1] that this calibration varies with beam diameter by less than 1 percent for beam diameters up to 6 in.

In the transmission ionization chamber used for this calibration the bremsstrahlung beam passed through 5.66 g/cm^2 of aluminum. To check the effect of filtration on the calibration this chamber was replaced by one that contained only 1.37 g/cm^2 of aluminum, At each bremsstrahlung energy the reading of the standard chamber was compared to that of the thin transmission monitor as a function of aluminum thickness placed between them. The thicknesses used bracketed the filtration used in in the present calibration. It was found that the charge collected from the standard chamber was essentially proportional to the amount of bremsstrahlung energy incident on it, i.e., proportional to $A'(L',E_0)$ calculated from eq (2), for L' ranging from 2.96 (donut plus thin-walled ionization chamber) to 10 g/cm^2 of aluminum. Deviations from proportionality as large as 2 percent may exist for the extreme thickness at the two lowest energies, 6 and 8 Mev. For reasonable thickness, then, the calibration presented here is independent of the distortions produced in the spectrum by absorbers and gives a measure of the energy incident on the monitor chamber.

The results of this calibration are plotted in figure 3 as a function of bremsstrahlung energy, E_0. The uncertainty in this calibration results from the statistical uncertainties ($\pm 1\%$), the possible errors in the methods used to subtract background and extrapolate the pulse height distribution to zero ($\pm 0.3\%$), the uncertainty in the determination of $R(E_0)$ ($\pm 1\%$), and the uncertainties in the evaluation of $P(L,E_0)$ and $A'(E_0)$ ($\pm 0.7\%$). The uncertainty of ± 2 percent given in figure 3 has been made larger than the value obtained by combining these uncertainties to take into account possible unknown systematic errors. Also shown in figure 3 are the results of the other two calibrations of the standard chamber [1,2] in the energy range up to 30 Mev. It is satisfying to note that in the small energy range in which these calibrations overlap that there is good agreement in the absolute magnitude. The results of the present calibration are essentially independent of bremsstrahlung energy, E_0. Only the point at $E_0=10$ Mev fails to include the average value for the six energies of 3.905 10^{-19} coulombs/Mev within its error bar. In using this calibration it is therefore sufficient to use this single number at all energies.

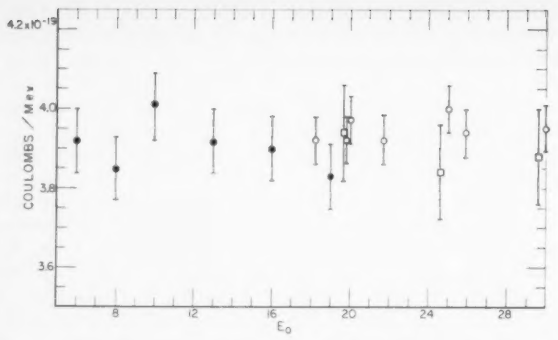

FIGURE 3. *Calibration of the standard chamber in coulombs/Mev as a function of the incident bremsstrahlung energy E_0.*

The closed circles are the data obtained in the calibration reported here. The open circles represent the data obtained by calorimetry and reported in [2]. The squares represent the results of Leiss, Pruitt, and Schrack [3], who made a calibration very similar to the one described here. Their data have been decreased slightly to take into account a modification of the standard chamber made since their calibration.

The authors thank R. A. Schrack for his help in evaluating the integrals of eq (1).

5. References

[1] J. S. Pruitt and S. R. Domen (to be published).
[2] J. E. Leiss, J. S. Pruitt, and R. A. Schrack (unpublished report).
[3] H. W. Koch, J. E. Leiss, and J. S. Pruitt, Bull. APS II, **1,** 199 (1956).
[4] J. H. Hubbell, E. Hayward, and W. F. Titus, Phys. Rev. **108,** 1361 (1957).
[5] A. S. Penfold and J. E. Leiss, Physics Research Laboratory Report (University of Illinois, Champaign, Ill., 1958).
[6] G. R. White (unpublished report). Beta and gamma ray spectroscopy K. Siegbahn (1955). (North Holland Publ. Co. Amsterdam p. 587).
[7] J. M. Wyckoff and H. W. Koch, Phys. Rev. **117,** 1261 (1960).

(Paper 65A5–119)

JOURNAL OF RESEARCH of the National Bureau of Standards—A. Physics and Chemistry
Vol. 65A, No. 5, September–October 1961

Mass Spectrometric Study of NF_2, NF_3, N_2F_2, and N_2F_4

John T. Herron and Vernon H. Dibeler

(May 22, 1961)

Appearance potentials have been measured for selected ions from NF_2, NF_3, N_2F_2, and N_2F_4. Ionization-dissociation processes are identified and bond dissociation energies are calculated. In addition, the bond dissociation energy, $D(F_2N–NF_2)$, has been directly measured to be 5.14 ± 0.38 kj/mole (21.5 ± 1.6 kcal/mole). A summary is made of available thermochemical and mass spectrometric data for N—F compounds and some evidence is presented to support the designation of *cis* and *trans* structures for the N_2F_2 isomers.

1. Introduction

The synthesis of a new series of compounds containing nitrogen and fluorine atoms has aroused considerable interest in their chemical and physical properties; in particular, heats of formation, bond dissociation energies, and ionization processes. Some of these data have been obtained from mass spectrometric studies [1, 2, 3].[1] In general, however, the data are fragmentary and in some cases are based on doubtful assumptions by analogy to N—H compounds. In a previous paper [3], we reported an electron impact study of tetrafluorohydrazine in which a value of 53 kcal/mole for the $F_2N–NF_2$ bond dissociation energy was calculated from estimated values of the N–F bonds in NF_3 [1]. It was also suggested that the failure of other workers to find ions of m/e greater than that corresponding to NF_2^+ in the mass spectrum of N_2F_4 was due to decomposition of N_2F_4 into NF_2 radicals in the mass spectrometer ion source. In light of the recently reported [4] value of 19.2 kcal/mole for the dissociation energy of the N–N bond in N_2F_4 this seems quite reasonable. We have made measurements of the effect of temperature on the $N_2F_4^+/NF_2^+$ ratio in the mass spectrum of N_2F_4. In addition, we have made a mass spectrometric study of the thermal dissociation of N_2F_4, and re-examined the ionization-dissociation processes for this molecule. We report appearance potentials of various ions in the related N—F compounds: NF_2, NF_3, and the two available isomers of N_2F_2.

A recent study [5] of the absorption spectra of the N_2F_2 isomers has given rise to a controversy concerning their structure. Although not unequivocal, the data reported here give evidence for the similarity in bond energies and heats of formation of these isomers and hence support the designation of the N_2F_2 isomers as *cis* and *trans*.

2. Experimental Procedure

The mass spectrometer used in this research is a first order, direction focusing instrument with a nominal 60° sector field and a 12-in. radius of curvature. The analyser tube and the source and collector housings are fabricated from nonmagnetic stainless steels and made vacuum tight with gold wire gaskets. Separate pumping systems are provided for the source housing and analyser tube. The source housing contains a flanged re-entrant port to admit thermal reactors or electrodeless discharge tubes for the introduction of free radicals or other active species to the ion source with a minimum of wall collisions. In addition, the electron impact source is provided with a conventional gas introduction system.

Carefully regulated power supplies are utilized for the magnet current, the ion accelerating voltage and focusing controls and the electron emission circuit. The latter circuit is designed to permit the precise measurement of appearance potentials of either positive or negative ions and to examine ionization probability curves over the range from zero to 100 ev.

The resolved ion currents are detected by means of a 14-stage electron multiplier. The integrated ion current is measured with a vibrating-reed electrometer and pen recorder. The nominal detection limit for this system was about 10^{-17} amps.

A simple thermal reactor was attached to the mass spectrometer to study the dissociation of N_2F_4. The reactor, shown schematically in figure 1, was connected to a 2-liter reservoir volume which remained at room temperature. The N_2F_4 at a pressure of about 0.2 mm effused from the reactor through a 1-mil glass leak located at the line-of-sight inlet to the ion source. The temperature of the N_2F_4 vapor was measured by a glass-encased thermocouple located about 1 mm from the leak.

The temperature variation of the mass spectrum of N_2F_4 was studied using the technique described by Reese, Dibeler, and Mohler [6]. Briefly, the mass spectrometer filament is turned off and the ion source allowed to cool to room temperature. The N_2F_4 at normal operating pressures is admitted to the ion source through the conventional gas inlet and the filament turned on. Ion currents for the NF_2^+ and $N_2F_4^+$ ions were measured immediately and remeasured at frequent intervals using nominal 70 ev electron energies. The temperature was monitored by means of a thermocouple attached directly to the ion source.

Appearance potentials of NF_2, NF_3, the *cis* and *trans* isomers of N_2F_2, and N_2F_4 were measured as

[1] Figures in brackets indicate the literature references at the end of this paper.

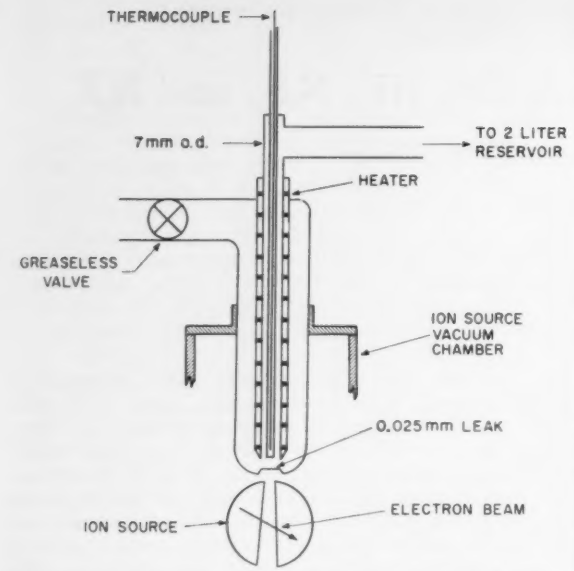

FIGURE 1. *Thermal reactor for kinetic studies of the dissociation of* N_2F_4

described in previous work [7]. For NF_2, measurements were made on the vapors effusing from the reactor containing N_2F_4, at 170 °C.

The NF_3 and N_2F_4 were obtained through D. E. Mann. Their purity has been noted elsewhere [1, 3]. The *cis* and *trans* isomers of N_2F_2 were kindly prepared and purified for us by Charles S. Cleaver of the E. I. Du Pont de Nemours Experimental Station, Wilmington, Del. Immediately after separation by gas chromatography, the isomers were placed in Monel cylinders and cooled with solid CO_2. They were transported and maintained at this temperature until introduced to the mass spectrometer. Gas chromatographic analysis reported by Cleaver indicated the following compositions:

trans–N_2F_2: 0.2% air, <0.1% NF_3, <0.1% N_2O, > 99.6% *trans*–N_2F_2;

cis–N_2F_2: 0.6% air, 0.2% N_2O, 5.2% *trans*–N_2F_2, 94.0% *cis*–N_2F_2.

These analyses were supported by our mass spectrometric observations.

For conversion from electron volts to joules, 1 ev is taken to be 9.6496×10^{4} joules. For conversion to the thermochemical calories, 1 cal is taken to be 4.1840 joules.

3. Results and Discussion

3.1. Thermal Dissociation of N_2F_4

A typical set of data for the thermal dissociation of N_2F_4 is summarized in table 1. Column 1 gives the absolute temperature of the reactor, and columns 2 and 3 the observed ion currents of the $N_2F_4^+$ and NF_2^+ ions in arbitrary units.

For a first approximation, it is assumed that no NF_2 is formed at the lowest reactor temperature, i.e., 333.0 °K. The ratio of $NF_2^+/N_2F_4^+$ at this temperature was taken as characteristic of the mass spectrum of N_2F_4 and was applied to the data in column 2, table 1 to calculate the contribution to the observed NF_2^+ peak of NF_2^+ ions resulting from dissociative ionization of N_2F_4 (column 4). The contribution resulting from the ionization of NF_2 is obtained by difference (column 5). On the further assumption that the observed $N_2F_4^+$ ion abundance and the calculated NF_2^+ ion abundance are measures of the partial pressures of N_2F_4 and NF_2, respectively, an equilibrium constant can be obtained from the relation

$$K_p = k(NF_2)^2/N_2F_4 \qquad (1)$$

where k is a factor relating measured ion abundances to partial pressures. Values of K_p/k are given in column 6.

From the usual integrated van't Hoff equation, we plot log K_p versus $1/T$ to obtain the enthalpy, ΔH, of the reaction. In this case, however, the slope of the plot must be obtained by successive approximation. The data of table 1 are plotted as the open circles of figure 2. The best straight line through these points is extrapolated to the lowest temperature (333.0 °K) and a first estimate made of the ratio NF_2/N_2F_4 from eq (1). This is then used to calculate a more nearly correct set of data. The process is repeated until the indicated constant slope is obtained, shown as solid circles in figure 2. The mean of four such determinations, resulted in a value of $\Delta H = 5.14$

TABLE 1. *Summary—calculation of the equilibrium constants for the thermal dissociation of* N_2F_4

T(°K)	Observed ion currents		$(NF_2^+)_{N_2F_4}$	$(NF_2^+)_{NF_2}$	$\frac{K_p}{k}=\frac{(NF_2)^2}{N_2F_4}$	$(NF_2^+)_{N_2F_4}$	$(NF_2^+)_{NF_2}$	$\frac{K_p}{k}=\frac{(NF_2)^2}{N_2F_4}$	$(NF_2^+)_{N_2F_4}$	$(NF_2^+)_{NF_2}$	$\frac{K_p}{k}=\frac{(NF_2)^2}{N_2F_4}$
	$N_2F_4^+$	NF_2^+									
450.7	28.0	16320	660	15660	8.76×10^{6}	640	15680	8.78×10^{6}	630	15690	8.79×10^{6}
434.3	68.5	16140	1620	14520	3.09	1260	14580	3.11	1550	14590	3.11
423.9	111.0	16110	2620	13490	1.64	2540	13570	1.66	2510	13600	1.67
412.0	184	16110	4350	11760	7.50×10^{5}	4200	11910	7.72×10^{5}	4160	11950	7.76×10^{5}
401.6	259	16200	6110	10090	3.92	5920	10280	4.08	5900	10300	4.10
382.4	440	17070	10400	6670	1.01	10040	7030	1.12	9950	7120	1.15
362.0	650	18150	15330	2820	1.22×10^{4}	14840	3310	1.69×10^{4}	14700	3450	1.83×10^{4}
343.6	740	18300	17470	830	9.32×10^{2}	16900	1400	2.65×10^{3}	16720	1580	3.37×10^{3}
333.0	750	17700	17700	0	0	17120	580	4.49×10^{2}	16920	775	8.01×10^{2}

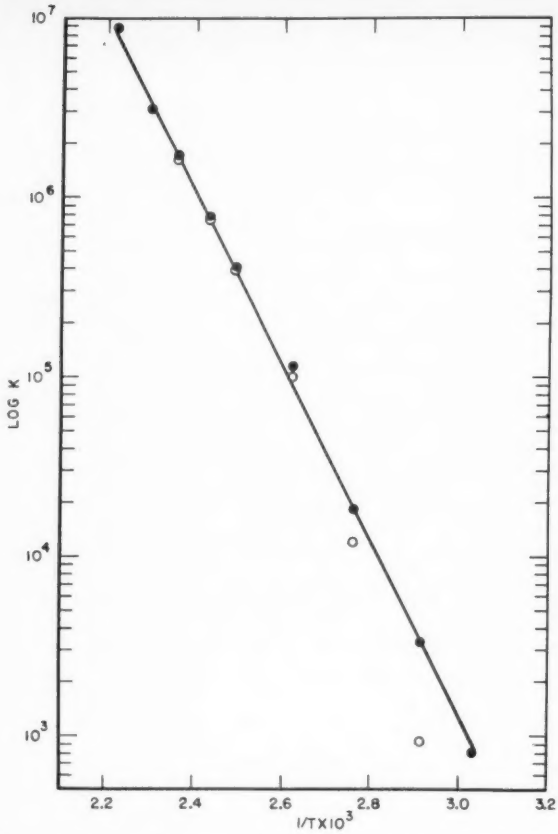

FIGURE 2. *Log* K_p *versus* 1/T *for the equilibrium* $N_2F_4 \rightleftarrows 2NF_2$.

± 0.38 kj/mole(21.5 ± 1.6 kcal/mole). The uncertainty given is the estimated standard deviation. The value of the gas constant used in the calculations was $R=8.314$ joule/degree mole. This is in good agreement with the previously reported value of 19.2 kcal/mole [4].

From the value, $\Delta H = 21.5 \pm 1.6$ kcal/mole for the reaction $N_2F_4 \rightarrow 2NF_2$, and the $\Delta H_f(N_2F_4) = -2.0 \pm 2.5$ kcal/mole [8] we calculate $\Delta H_f(NF_2) = 9.8 \pm 2.1$ kcal/mole. Further, from $\Delta H_f(NF_3) = -29.7 \pm 1.8$ kcal/mole [9] and $\Delta H_f(F) = 18.9 \pm 0.5$ kcal/mole [10], we calculate $D(NF_2\text{-}F) = 58.4 \pm 4.4$ kcal/mole. Similarly, from $NF_2 \rightarrow N + 2F$, we calculate D(N–F) average, in $NF_2 = 70.5 \pm 1.6$ kcal/mole. Finally, from $NF_2 \rightarrow NF + F$, we calculate $\Delta H_f(NF) = 61.4 \pm 4.2$ kcal/mole.

As the average bond energy in NF_3 is 66.3 kcal/mole [9], it would appear that the first N—F bond is the weakest bond in NF_3. This is contrary to the observed bond order in NH_3, in which the first and subsequent N—H bond dissociation energies are reported to be 104, 88, and 88 kcal/mole, respectively [11]. This would negate the assumptions made by Reese and Dibeler [1] in their calculations of the ionization potentials of NF_2 and NF radicals.

3.2. Appearance Potential Data

Two studies of N_2F_4 have been reported [2,3] but the original interpretation of the NF^+ and NF_2^+ appearance potentials did not account for the dissociation of N_2F_4 into NF_2 radicals within the ion source.

The effect of ion source temperature on the $N_2F_4^+/NF_2^+$ ratio in the mass spectrum of N_2F_4 is shown in figure 3. Although an extrapolation of the data to lower temperatures is difficult, it seems apparent that the limiting value of the ratio is about 0.08. The change in mass spectrum of N_2F_4 with temperature, due to decomposition of N_2F_4 in the ion source, thus accounts for the differences in the mass spectrum of N_2F_4 reported by different workers [2, 3, 4, 12]. The data of Loughran and Mader [2] have already been reinterpreted assuming the presence of NF_2 [4] in the ion source.

A summary of the available appearance potential data for the N—F compounds is shown in table 2. Column 1 identifies the molecule, columns 2 and 3 give the ion and the probable process of formation, column 4 gives the observed appearance potential and column 5 reports the source.

NF_2. The ionization potential of NF_2 measured in this work was 12.0 ± 0.1 ev in good agreement with that of Loughran and Mader. The average of the two values is 11.9 ± 0.2 ev.

Differences in the reported NF^+ appearance potentials from NF_2 are much greater. We observe two processes leading to the formation of NF^+. The difference in the appearance potentials of these processes is almost equal to the electron affinity of the fluorine atom (3.6 ev) [13]. This gives considerable support to the present identification.

From

$$NF_2 \rightarrow NF^+ + F$$
$$A(NF^+) \geq D(NF\text{—}F) + I(NF)$$

where the inequality accounts for any excess energy involved in the reaction, we calculate an upper limit for $I(NF) = 12.4 \pm 0.3$ ev, assuming D(NF—F)=D(N—F) average in NF_2. This differs from the previous estimate of $I(NF) = 12.0$ ev [1]. However, the present value is considered the more reliable for reasons stated in the previous section.

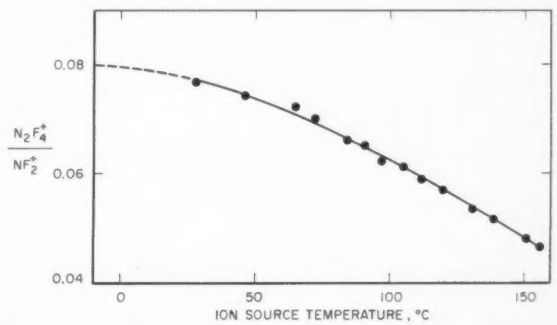

FIGURE 3. *Effect of ion source temperature on the* $N_2F_4^+/NF_2^+$ *ratio in the mass spectrum of* N_2F_4.

TABLE 2. *Summary of appearance potential data for N–F compounds*

Parent molecule	Ion	Probable process	Appearance potential	Reference
			ev	
NF_2	NF_2^+	$NF_2 \rightarrow NF_2^+$	12.0±0.1	This work.
			11.8±0.2	[2]
	NF^+	$NF_2 \rightarrow NF^+ + F^-$	11.8±0.2	This work.
		$\rightarrow NF^+ + F$	15.5±0.2	Do.
NF_3	NF_3^+	$NF_3 \rightarrow NF_3^+$	15.0±0.2	[2]
			13.2±0.2	[1]
			13.2[a]	This work.
	NF_2^+	$NF_3 \rightarrow NF_2^+ + F$	14.2±0.3	[1]
			14.6	[2]
			14.2→14.6[a]	This work.
	NF^+	$NF_3 \rightarrow NF^+ + 2F$	17.9±0.3	[1]
trans-N_2F_2	$N_2F_2^+$	$N_2F_2 \rightarrow N_2F_2^+$	13.1±0.1	This work.
	N_2F^+	$N_2F_2 \rightarrow N_2F^+ + F$	13.9±0.2	Do.
		$N_2F_2^+ \rightarrow N_2F^+ + F$ (metastable)	13.4±0.2	Do.
	NF^+	$N_2F_2 \rightarrow NF^+ + NF$	17.0±0.2	Do.
cis-N_2F_2	N_2F^+	$N_2F_2 \rightarrow N_2F^+ + F$	14.0±0.2	Do.
	NF^+	$N_2F_2 \rightarrow NF^+ + NF$	16.9±0.2	Do.
N_2F_4	$N_2F_4^+$	$N_2F_4 \rightarrow N_2F_4^+$	12.0±0.1	[3]
	$N_2F_3^+$	$\rightarrow N_2F_3^+ + F^-$	12.0[a]	This work.
		$\rightarrow N_2F_3^+ + F$	15.6[a]	Do.
	NF_2^+	See text.		
	NF^+	See text.		

[a] Single observation.

NF_3. The two reported values for the appearance potential of the NF_2^+ ion from NF_3 differ by 0.4 ev. Different methods of evaluating the appearance potential were used by each investigator. We also find it possible, by using different graphical methods, to interpret our data so as to obtain either limiting value from the same set of measurements. However, the appearance potential is readily calculated from the equation

$$NF_3 \rightarrow NF_2^+ + F$$

from which

$$A(NF_2^+) \geq D(NF_2-F) + I(NF_2)$$
$$\geq 14.4 \pm 0.4 \text{ ev.}$$

The calculated value lies just between the two limiting experimental values.

The NF^+ appearance potential has been reported as 17.9±0.3 ev [1], and ascribed to the reaction

$$NF_3 \rightarrow NF^+ + 2F.$$

From the relation

$$A(NF^+) \geq D(NF_2-F) + D(NF-F) + I(NF)$$

and the values of $D(NF_2-F)$, $D(NF-F)$, and $I(NF)$ given above, we calculate $A(NF^+) \geq 18.0 \pm 0.6$ ev, in good agreement with the measured value. Thus there appears to be no evidence for a lower energy process for this reaction which would result in the formation of molecular fluorine.

N_2F_2. The mass spectra of the *cis* and *trans* N_2F_2 were similar in most respects to those reported previously [5,13]. However, additional very diffuse peaks in the mass spectra at nonintegral m/e ratios were observed and attributed to metastable transitions [15]. These metastable ions were observed only in the mass spectrum of the *trans* species. This is consistent with the fact that the *cis* isomer apparently produces no parent ion. The relative abundance of the metastable ion appearing at the nominal m/e=33.5 was 0.22 percent of the largest normal ion peak and was attributed to the transition, $N_2F_2^+ \rightarrow N_2F^+ + F$. The ion appearing at m/e=16.5 was 0.02 percent of the maximum peak and was attributed to the transition, $N_2F_2^+ \rightarrow NF^+ + NF$. Appearance potential measurements of the ions at m/e=33.5 and 16.5 ruled out the possibility of doubly charged ions.

The relatively large abundance of the m/e=33.5 metastable peak in *trans* N_2F_2 made it possible to measure the appearance potential of this ion with good precision. As might be expected on the basis of the statistical theory of mass spectra [12], the appearance potential is somewhat lower than that of the same ions collected at m/e=47. However, the magnitude of the difference is unexpectedly large.

The appearance potentials of the normal fragment ions NF^+ and N_2F^+ are identical within experimental uncertainty for both *cis* and *trans* N_2F_2. The heats of formation of the two isomers are also very similar; thus Armstrong and Marantz [16] report $\Delta H_f(N_2F_2)$ *cis*=16.4 kcal/mole and $\Delta H_f(N_2F_2)$ *trans*=19.4 kcal/mole with an uncertainty of about 1.5 kcal/mole. Thus if there is no excess kinetic or excitational energy involved in the dissociative ionization of either of the isomers, it would appear that they are similar in molecular structure.

This argues in favor of the *cis* and *trans* designations for the N_2F_2 isomers contrary to the recent suggestion by Sanborn [5] that the isomer presently designated "*cis*" actually has the 1,1-difluorodiazine structure as first considered by Bauer [17].

Similarly, these data do not support the recently reported [18] heat of isomerization of 27.5±5.0 kcal/mole for the N_2F_2 isomers. However, we have been unable to calculate this value from the data as given in the reference.

On the basis of nearly equal heats of formation for the *cis* and *trans* isomers, we can calculate the N=N bond dissociation energy for either isomer of N_2F_2 from the reaction:

$$N_2F_2 \rightarrow NF^+ + NF$$

and the relation $D(FN=NF) \leq A(NF^+) - I(NF)$. Using the values $A(NF^+)=17.0\pm0.2$ ev and $I(NF)=12.4\pm0.3$ ev, we obtain $D(FN=NF) \leq 4.6\pm0.5$ ev, or $\leq 106\pm12$ kcal/mole.

A check on this calculation can be made using the measured values for ΔH_f (N_2F_2) and the reaction

$$N_2F_2 \rightarrow 2NF$$

from which $D(FN=NF)=2\Delta H_f NF - \Delta H_f N_2F_2$. Using the previously calculated value for $\Delta H_f NF = 64.4 \pm 4.2$, we calculate $D(FN=FN)$ *cis*=106±10 kcal/mole and $D(FN=NF)$ *trans*=103±10 kcal/mole.

These values may be compared with the value of $D(HN=NH)=104\pm6$ kcal/mole in diimide as reported by Foner and Hudson [19]. However, it should be emphasized that both methods used to

calculate D(FN=NF) involve a common approximation, i.e., that the bond dissociation energy D(FN−F)=D(N−F) average in NF_2. The uncertainty in these and previous calculations are conservatively estimated from the algebraic sum of uncertainties in the contributing measurements.

A summary of measured and derived thermochemical data for the N—F compounds is given in table 3.

TABLE 3. *Summary of thermochemical data for N–F compounds*

Molecule	$\triangle H_f$	Ionization potential	Bond dissociation energy
	kcal/mole	*ev*	*kcal/mole*
NF	61.4±4.2	≤12.4±0.3	D(N−F)av=70.5±1.6
NF_2	9.8±2.1	12.0±0.1	$D(F_2N-F)=58.4\pm4.4$
NF_3	−29.7±1.8[9]	13.2±0.2[1]	D(FN=NF)=106±10
cis N_2F_2	16.4±1.5[16]		D(FN=NF)=103±10
trans N_2F_2	19.4±1.5[16]	13.1±0.1	$D(F_2N-NF_2)=21.5\pm1.6$
N_2F_4	−2.0±2.5[8]	12.0±0.1[3]	

4. References

[1] R. M. Reese and V. H. Dibeler, J. Chem. Phys. **24,** 1175 (1956).

[2] E.D. Loughran and C. Mader, J. Chem. Phys. **32,** 1578 (1960).

[3] J. T. Herron and V. H. Dibeler, J. Chem. Phys. **33,** 1595 (1960).

[4] C. B. Colburn and F. A. Johnson, J. Chem. Phys. **33,** 1869 (1960).

[5] R. H. Sanborn, J. Chem. Phys. **33,** 1855 (1960).

[6] R. M. Reese, V. H. Dibeler, and F. L. Mohler, J. Research NBS **46,** 79 (1951).

[7] J. T. Herron and V. H. Dibeler, J. Am. Chem. Soc. **82,** 1555 (1960).

[8] G. T. Armstrong, S. Marantz, and C. F. Coyle, private communication (1960).

[9] G. T. Armstrong, S. Marantz, and C. F. Coyle, J. Am. Chem. Soc. **81,** 3798 (1959).

[10] W. H. Evans, T. R. Munson, and D. D. Wagman, J. Research NBS **55,** 147 (1955).

[11] A. P. Altshuller, J. Chem. Phys. **22,** 1947 (1954).

[12] C. B. Colburn and A. Kennedy, J. Amer. Chem. Soc. **80,** 5004 (1958).

[13] H. O. Pritchard, Chem. Revs. **52,** 537 (1953).

[14] H. M. Rosenstock, M. B. Wallenstein, A. L. Wahrahaftig, and H. Eyring, Proc, National Academy of Sciences **38,** 667 (1952).

[15] J. A. Hipple and E. U. Condon, Phys. Rev. **68,** 54 (1945).

[16] G. T. Armstrong and S. Marantz, private communication (1961).

[17] S. H. Bauer, J. Amer. Chem. Soc. **69,** 3104 (1947).

[18] C. B. Colburn, F. A. Johnson, A. Kennedy, K. McCallum, L. C. Metzger, and C. O. Parker, J. Am. Chem. Soc. **81,** 6397 (1959).

[19] S. N. Foner, and R. L. Hudson, J. Chem. Phys. **28,** 719 (1958).

(Paper 65A5–120)

599651—61——2

JOURNAL OF RESEARCH of the National Bureau of Standards—A. Physics and Chemistry
Vol. 65A, No. 5, September–October 1961

Rate of the Reaction NO+N, and Some Heterogeneous Reactions Observed in the Ion Source of a Mass Spectrometer*

John T. Herron

(May 19, 1961)

The rate of the reaction $NO+N \rightarrow N_2+O$ has been measured to be $1.0\pm0.5\times10^{13}$ cm^3 $moles^{-1}$ sec^{-1} at room temperature. The heterogeneous reactions $N+O \rightarrow NO$ and $O+O \rightarrow O_2$ were observed to occur in the ion source of the mass spectrometer.

1. Introduction

The reaction of active nitrogen with nitric oxide has been studied mass spectrometrically by Kistiakowsky and Volpi [1,2].[1] They concluded that the reaction taking place was

$$NO+N \rightarrow N_2+O \qquad (1)$$

and that the rate constant for the reaction had a lower limit of about $5\times10^{13}cm^3$ $mole^{-1}$ sec^{-1} at room temperature.

In view of the importance of this reaction in certain atmospheric phenomena as well as its practical value as a method of measuring nitrogen atom concentrations, it has been re-examined using a mass spectrometer of high sensitivity.

In addition, a mass spectrometric study of active nitrogen has been made.

In one of the previous mass spectrometric studies, there was some evidence to suggest the presence of a highly energetic species other than nitrogen atoms [3]. This was not observed by a second group of investigators [4]. The present study was undertaken in the hope of resolving this difference.

2. Experimental Procedure

The mass spectrometer was a 60° sector type instrument of 12-in. radius of curvature. Magnetic scanning was used at a constant ion accelerating potential of 5,000 v.

The gas inlet system and ion source were so designed that gas could pass directly from the reactor or discharge zone into the electron beam of the mass spectrometer. Thus a certain fraction of the gas entering the ion source could be ionized without suffering wall collisions in the ion source.

Ion currents were measured by means of a 14 stage ion multiplier, vibrating reed electrometer, and pen recorder. The minimum detectable signal was about 10^{-18} amp.

Active nitrogen was produced by passing dry nitrogen through a 2450 Mc/s electrodeless discharge. Two types of flow system were used, one for studying active nitrogen, and another for studying its reactions. In the former, gas at about 0.1 mm total pressure was taken directly from the discharge zone, through a 1 mm diameter "leak" leading to the mass spectrometer ion source which was about 10 cm from the leak. The appearance potentials of the ions produced in the ion source by electron impact were measured by varying the electron energy in 0.2 ev steps.

The reaction of active nitrogen with nitric oxide was studied in the reactor shown in figure 1. Nitric

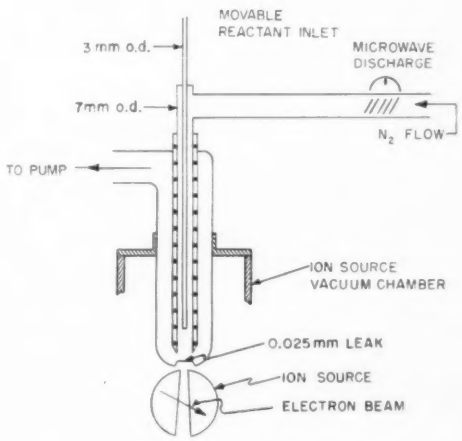

FIGURE 1. *Reactor.*

*This research was supported in part by the Advanced Research Projects Agency.

[1] Figures in brackets indicate the literature references at the end of this paper.

oxide entered the reactor through the movable central tube, and active nitrogen through the outer tube. Gas leaving the reactor passed over a 0.025 mm diameter leak for continuous sampling by the mass spectrometer.

Although the reactor was equipped with a heater, all the experiments reported here were made at room temperature.

In any given experiment, all experimental conditions were fixed except the initial nitric oxide concentration. The range of experimental conditions used in the various experiments was, pressure, 0.33 to 0.87 mm, nitrogen flow, 16 to 65 cm^3/min, length of reaction zone, 1.1 to 2.7 cm, and reaction time, 0.5×10^{-3} to 1.7×10^{-3} sec.

Partial pressures of stable reactants and products were measured by conventional mass spectrometric techniques using an ionizing energy of 50 ev. Relative nitrogen atom partial pressures were measured using a nominal ionizing energy of 24 ev, i.e., at sufficiently low energy to minimize formation of N^+ ions from dissociative ionization of nitrogen. Small corrections were made for contributions of N^+ ions from nitric oxide. The relative values were related to absolute units of pressure by equating the N^+ signal due to nitrogen atoms (with no reactant present) to the limiting amount of nitric oxide consumed via reaction (1), assuming this to be the correct stoichiometry.

In some experiments 96 percent $N^{15}O$ was used as a reactant instead of normal $N^{14}O$.

3. Results and Discussion

The ionization efficiency curve for the N^+ ion produced by electron impact from active nitrogen is shown in figure 2. The ionization potential of argon, 15.76 ev [5], was used to calibrate the energy scale.

The lowest N^+ appearance potential was 14.53 $\pm$0.12 ev. This is equal to the ionization potential of the ground state nitrogen atom, 14.54 ev [5]. The sharp break upwards in the curve at 23.5 ev corresponds to the formation of N^+ ions from N_2. The break in the ionization efficiency curve at 16.1 ev, reported by Jackson and Schiff [3] was not observed. However, the N_2^+ ionization efficiency curve did show a small shift (less than 1 ev) to lower energy when the discharge was turned on. This may have been due to vibrationally excited nitrogen molecules which have been reported to be present in active nitrogen [6, 7].

It seems safe to conclude that the only reactive species involved in the nitric oxide reaction under the conditions of the present work are ground state nitrogen atoms.

Since the nitric oxide is in its ground state at room temperature, the reaction under study can be more properly written as

$$NO(^2\Pi)+N(^4S)\rightarrow N_2+O.$$

The energetic states of the products are not known, although there is some evidence to suggest that the N_2 is in a vibrationally excited state [6]. This is not surprising, since the reaction is 80 kcal exothermic.

Although experiments were made with both $N^{14}O$ and $N^{15}O$, it is more illustrative to discuss the results in terms of the $N^{15}O$ experiments. A typical set of results is shown in figure 3.

The products of the reaction are $N^{14}N^{15}$, $N^{14}O$, and O_2. Other than confirming its presence, no attempt has been made to analyze for atomic oxygen. Over the range of initial $N^{15}O$ partial pressures used, the partial pressure of $N^{14}N^{15}$ produced was equal to the amount of $N^{15}O$ consumed, as would be expected from eq (1). This was not exactly true for the change in partial pressure of nitrogen atoms, although the uncertainty in nitrogen atom measurements was considerably greater.

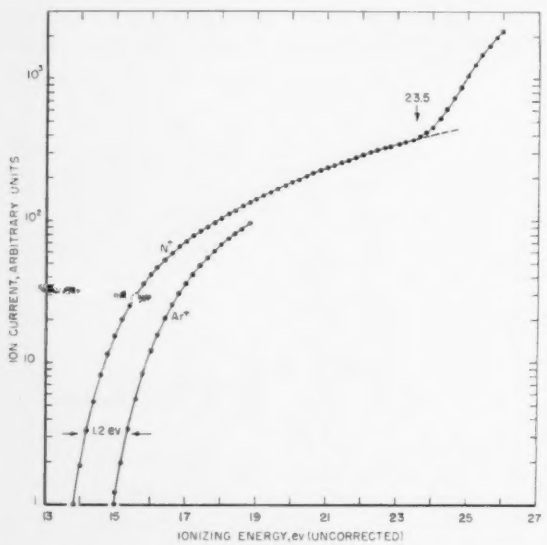

FIGURE 2. *Ionization efficiency curve for the N^+ ion from active nitrogen.*

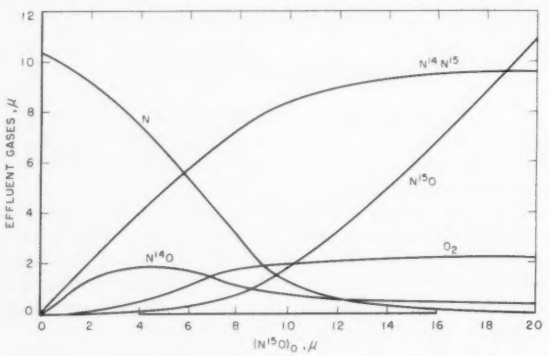

FIGURE 3. *Steady state partial pressures of effluent gases as a function of initial $N^{15}O$ partial pressure.*

The second order rate equation for the reaction can be written as

$$\log \left\{ \frac{N_0(NO_0-x)}{NO_0(N_0-x)} \right\} = \frac{k}{2.303} (NO_0-N_0)t$$

where N_0 and NO_0 are the initial nitrogen atom and nitric oxide concentrations respectively, x is the extent of reaction, and t the reaction time.

A plot of log $[N_0(NO_0-x)]/[NO_0(N_0-x)]$ versus $(NO_0-N_0)t$ gives a straight line, the slope of which, as determined by a least squares fit of the data, yields k. The best value of k, taken as the unweighted average of 6 experiments was $k=(1.0\pm0.5)\times10^{13}$cm^3 mole^{-1} sec^{-1}. The deviation given is 3 times the standard deviation of the average. All the data for the 6 separate experiments are plotted together in figure 4. Points shown in open circles were not used in determining k.

The major source of uncertainty in this value is due to incomplete mixing of the reactants, since the time for a molecule to diffuse across the reactor is comparable with the reaction time.

Under conditions of constant flow of nitrogen and nitric oxide, it was found that the distance between nitric oxide inlet and leak had no effect on the nitric oxide partial pressure until the distance was 1 cm or less. The average distance used in the experiments was 2.1 cm.

The value of k given above agrees, within the limits of experimental error, with that calculated from the data of Clyne and Thrush for the reaction at 300 °K, i.e., $k=(2.2\pm0.6)\times10^{13.0\pm0.5}$ cm^3 mole^{-1} sec^{-1}.

The $N^{14}O$ and O_2 observed as products of the reaction are probably due to secondary reactions. The rate controlling steps for homogeneous reactions giving rise to these products would involve termolecular reactions, which, under the conditions of this work, would be too slow to account for the amount of products observed.

It seems almost certain that these reactions are occurring on the walls of the mass spectrometer ion source. If this is the case, then the partial pressures of $N^{14}O$ and O_2 shown in figure 3, have no absolute significance, but are relative partial pressures within the ion source. With a total pressure in the reactor of 0.5 mm the pressure at a point just below the ion source housing was about 10^{-6} mm. The pressure in the ion source probably would be no greater than 5×10^{-6} mm, so that the pressure differential between reactor and ion source is about 10^{-5}. Therefore, the absolute partial pressures of $N^{14}O$ and O_2 in the ion source were of the order of 10^{-8} mm. As might be expected at such low pressures, these heterogeneous reactions appear to follow second order kinetics.

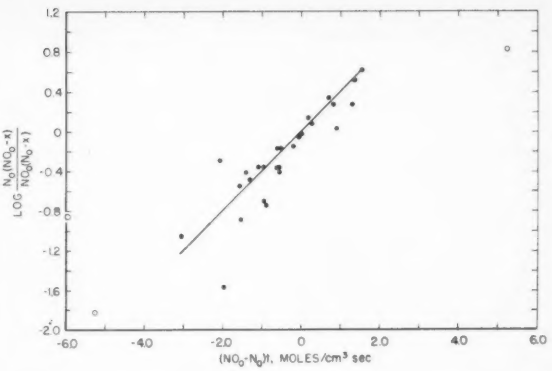

FIGURE 4. *Summation of rate data for the reaction* NO+N

It should be noted that atomic recombination in the ion source has been postulated previously to explain the low sensitivity of highly reactive atomic species such as N or O [1,2,9]. Under the usual experimental conditions, however, the recombination product is inseparable from the original molecules used as a source of atoms. Similarly, in the present work, N_2 formed in the ion source was not separable from that passing unchanged through the discharge.

4. References

[1] G. B. Kistiakowsky and G. G. Volpi, J. Chem. Phys. **27,** 1141 (1957).
[2] G. B. Kistiakowsky and G. G. Volpi, J. Chem. Phys. **28,** 665 (1958).
[3] D. S. Jackson and H. I. Schiff, J. Chem. Phys. **21,** 2233 (1953), **23,** 2333 (1955).
[4] J. Berkowitz, W. A. Chupka, and G. B. Kistiakowsky, J. Chem. Phys. **25,** 457 (1956).
[5] C. E. Moore, NBS Circ. 467 (1958).
[6] F. Kaufman, and J. R. Kelso, J. Chem. Phys. **28,** 510 (1958).
[7] K. Dressler, J. Chem. Phys. **30,** 1621 (1959).
[8] M. A. A. Clyne and B. A. Thrush, Nature **189,** 56 (1961).
[9] J. T. Herron and H. I. Schiff, Can. J. Chem. **36,** 1159 (1958).

(65A5–121)

JOURNAL OF RESEARCH of the National Bureau of Standards—A. Physics and Chemistry
Vol. 65A, No. 5, September–October 1961

Synthesis of the Humites $n Mg_2SiO_4 \cdot Mg(F, OH)_2$

A. Van Valkenburg

(June 7, 1961)

The humite group comprises four minerals having the general formula $n Mg_2SiO_4 \cdot Mg(F, OH)_2$ where $n=1$, 2, 3, and 4. These have been synthesized in the laboratory from melts, by solid state reactions, and by hydrothermal techniques. Complete substitution of GeO_2 for SiO_2 has been accomplished in three of the humites and partial substitution of OH ions for F, Fe for Mg, and Ti for Mg or possibly Si, has been accomplished in one or more of the series. Indices of refraction of the synthetic humites are given and powder X-ray diffraction data have been obtained for the fluorine end members. Also, infrared data from 4,000 to 300 cm^{-1} are given for the fluorine end members and these are compared to the corresponding spectra of the natural analogs.

1. Introduction

The term "humites" as used by mineralogists refers to four minerals that have the general formula $n Mg_2SiO_4 \cdot Mg(F, OH)_2$, where n-1, 2, 3, or 4. The individual mineral names are norbergite, $n=1$, named from the Norberg locality, Vasmanland, Sweden; chondrodite, $n=2$, named from the Greek word meaning "a grain," alluding to the granular texture of the material as it occurs in aggregate form; humite, $n=3$, named after Sir Abraham Hume; and clinohumite, $n=4$.

The synthesis of the humites was undertaken as part of a general study to determine the factors governing the isomorphous substitution of fluorine for hydroxyl groups in hydrous silicate structures. The natural humites contain both fluorine and hydroxyl anions, but fluorine is always present as the major constituent. This fact suggests that a complete isomorphous substitution of hydroxyl for fluorine may not be possible in the humites. The hydrothermal studies of Bowen and Tuttle [1][1], Roy and Roy [2], and Carlson et al., [3] in the system SiO_2–MgO–H_2O failed to produce a hydrous analog of the humites and their results support the idea that a complete isomorphous substitution of fluorine by hydroxyl cannot take place.

The primary objectives of the humite synthesis were to (1) determine the minimum ratio of F^{-1} to $(OH)^{-1}$ that can exist in a given structure; (2) determine some of the properties of end members; and (3) determine the possible existence of humite members having $n=5$, 6, etc., or ½, ¼, etc.

Daubree in 1851 [4] and Dolter [5] in 1889 may have synthesized one or more of the humites by reacting fluorides with silicates in the absence of water, although their identifications were not conclusive. W. Jander and V. R. Fett [6] in 1939 made a series of hydrothermal syntheses in which they claimed to have synthesized chondrodite and humite, using formula proportions of oxides and HF. Their data on pressure and temperature relationships are lacking and they apparently placed no significance on the presence of extra lines or absence of lines in the X-ray powder diffraction data of their synthetic materials. During World War II, German scientists [7] reported the synthesis of the humites as impurities in the flakes of synthetic fluorophlogopite. The presence of the humites in the mica was attributed to an incorrect composition of the mica melt. In 1947 [8] Rankama synthesized norbergite and chondrodite by fusing forsterite with magnesium fluoride in a graphite crucible. His attempts to produce hypothetical members of the group where $n=5$, 6, etc., were not successful.

[1] Figures in brackets indicate the literature references at the end of this paper.

2. Synthesis Techniques

The humites were synthesized at the National Bureau of Standards using the techniques of crystallization from melts, hydrothermal reactions, and solid state reactions. The fluorohumites, containing all fluorine and no hydroxyl groups, were synthesized using solid state reactions and crystallization from melts. The hydroxyl-bearing humites were synthesized under hydrothermal conditions. The starting materials consisted of reagent grade magnesium carbonate, magnesium fluoride and silicic acid or quartz. In special cases natural forsterite (Mg_2SiO_4) and olivine $(Mg,Fe)_2SiO_4$ were used with MgF_2 to give the desired formula proportions. The raw batches were prepared by first sintering together magnesium carbonate and silica to drive off CO_2 and water vapor before adding MgF_2. This practice was undertaken to prevent the MgF_2 from prematurely decomposing, releasing F_2 at temperatures below fusion. After sintering, MgF_2 was added in formula proportions to the batch and the ingredients were reground in a mechanical mortar to insure thorough mixing. To obtain maximum reactivity of a batch using solid state reaction techniques, the powder was compressed into ½-in. diam wafers at a pressure of 20,000 psi. The wafers were then placed in platinum envelopes which were sealed by crimping adjacent edges. Another technique employed was to tamp powder into a platinum cylinder of ½ mm ID by ½ cm long and hermetically seal both ends. Platinum resistance furnaces with controllers were used to heat and

melt the specimens. Temperatures were measured in degrees C to a precision of ±3° using Pt-Pt 10 percent Rh thermocouples. The thermocouples were placed on the outside wall of the platinum envelopes and cylinders.

3. Thermal Dissociation Characteristics of the Synthetic Fluorohumites

The dissociation temperature of norbergite was the only dissociation temperature determined in the humites as the experimental conditions were not satisfactory for the other humites. Two techniques were used to determine the norbergite dissociation temperature. The first employed the well-known soak-quench technique developed by the Geophysical Laboratory, and the second employed a differential thermal apparatus. Initially experiments were designed to quench materials in a platinum envelope that was not sealed. It was found that volatiles escaped from the envelope changing the composition, thus giving erroneous results. Sealed platinum envelopes were then used and these gave reproducible results. Unfortunately, the dissociation temperatures of the remaining humites were too high for the sealed envelopes and they burst at temperatures above 1,300 °C. The dissociation temperature of the fluoronorbergite, using the quench technique, was 1,180±5 °C. A differential thermal analysis curve, figure 1, obtained from a sealed platinum envelope indicates dissociation at approximately 1,195 °C, as observed in the endothermic peak at this temperature. The small exothermic peak at 1,050 °C is unexplained and the broad endothermic peak at 200 °C is due to the elimination of hygroscopic water. On cooling an exothermic peak occurred at 1,180 °C, indicating recrystallization. This point is not recorded on the heating curve in figure 1. The differential curve was made on a conventional apparatus employing a heating rate of 12 °C/min.

Evidence from sealed tube experiments indicated that norbergite melts incongruently. At temperatures above 1,180 °C, a norbergite composition yielded chondrodite as the major phase.

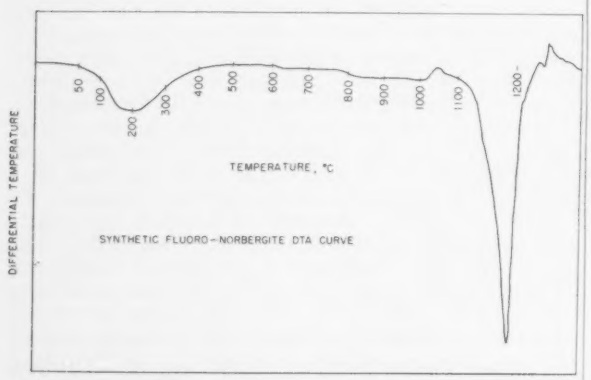

FIGURE 1. *Synthetic fluoronorbergite DTA heating curve.*

4. Synthesis of the Fluorohumites by Solid State Reactions

The fluorohumites were readily synthesized using solid state reaction techniques. The advantages of using these techniques are that the series can be crystallized at temperatures lower than their fusion temperatures and losses of volatile constituents can be kept at a minimum. The reactions yielding the best results were those in which the powdered ingredients were compressed into pellets and then enclosed in platinum tubes. Norbergite was readily synthesized by reacting at temperatures of 1,150 °C for periods of several hours. The remaining humites were synthesized at higher temperatures in the range of 1,250 to 1,300 °C. Hot pressing methods were also employed in which wafers 1 in. in diameter and ¼ in. thick were pressed and heated in a carbon resistance furnace at 1,400 psi and 1,100 to 1,300 °C.

Considerable difficulty was experienced in identifying the individual synthetic humites from microscopic examinations until it was realized that the synthetic analogs of chondrodite and clinohumite may exhibit apparent orthorhombic symmetry. Natural chondrodite and clinohumite are monoclinic and in chondrodite the extinction angle of $X \wedge a = 26$ to 30°, while in clinohumite $X \wedge a = 9° \pm$. As in the reaction products of the chondrodite and clinohumite compositions straight extinction was observed, it was assumed that these compounds were not synthesized. However, the disturbing feature was the presence of phases that had indices of refraction equivalent to a fluorochondrodite and fluoroclinohumite. This problem was discussed with H. F. W. Taylor, who has synthesized a hydroxyl calcium analog of chondrodite [10]. He has concluded from calculations that a chondrodite structure can exhibit orthorhombic symmetry providing certain conditions are met. These conditions are based on the stacking arrangements of the alternating layers of Mg_2SiO_4 and MgF_2 found in the humites [11], and the layering is governed by repeated twinning on a unit cell scale.

Table 1 lists the refractive indices of the synthetic fluorohumites as measured by oil immersion techniques and white light. These indices and all others given in this paper are accurate to ±.002. The value of $2V$ is estimated.

Since the compositions of the humites depend on the alternate layering of Mg_2SiO_4 and $Mg(F,OH)_2$ it was thought that compositions corresponding to $5Mg_2SiO_4 \cdot MgF_2$ or $\frac{1}{2}$ $Mg_2SiO_4 \cdot MgF_2$ might be synthesized. Stoichiometric compositions of these were prepared and heated at various temperatures. An examination of the rection products did not indicate the formation of other humite compounds.

TABLE 1

	α	β	γ	$2V$
Norbergite	1.548	1.552	1.570	33°
Chondrodite	1.582	1.594	1.612	50°
Humite	1.598	1.606	1.630	60°
Clinohumite	1.608	1.618	1.636	75°

5. Infrared Spectra

The infrared spectra of the synthetic fluorohumites are presented to show differences in the spectra of individual compounds that can be used in diagnostic identifications. The spectra were made on a double-beam spectrophotometer using a NaCl prism in the region of 4,000 to 900 cm^{-1} and a CsBr prism in the region 800 to 300 cm^{-1}. The samples were prepared by grinding in a boron carbide mortar, then mixing the powder with dry ground KBr and firmly pressing the ingredients into pellets at 100,000 psi using standard techniques. The sample concentration ranged from 2 to 3 mg per gram of KBr.

In figures 2a to 5b are plotted infrared spectrograms of the synthetic fluoro and natural humites between 4,000 and 300 cm^{-1}. The major absorption bands of these compounds are located in the region between 1,050 and 850 cm^{-1} and they are believed to be caused by the stretching modes of the Si–O bond. The specific assignments of individual bands were not attempted in these studies. The natural norbergite samples came from Franklin, N.J., and contained adhered impurities of calcite in estimated amounts of 5 percent or less by volume. The natural chondrodite sample was also from Franklin, N.J., and it contained some calcite impurities that were estimated to be less than 5 percent by volume. The natural humite and clinohumite samples were from Monte Somma, Italy, and these were quite pure, with impurities estimated to be less than 0.5 percent by volume.

5.1. Norbergite Spectra

The infrared spectra of the natural and synthetic norbergites show differences. The band at 3,500 cm^{-1} in the synthetic material is due to O–H stretching of water in the KBr pellet, while in the same band of the natural material the O–H stretching is due to hydroxyl groups in the norbergite. These hydroxyl groups can be distinguished from the water found in KBr by their greater intensity when compared to a test KBr pellet. In the natural norbergite, the bands located at 1,460 cm^{-1} and 880 cm^{-1} are caused by calcium carbonate impurities. The band at 760 cm^{-1} in the natural sample is absent in the synthetic sample. The band occurring at 625 cm^{-1} in the natural sample has shifted to 630 cm^{-1} in the synthetic sample: also, the band at 565 cm^{-1} in the natural sample has shifted to 570 cm^{-1} in the synthetic material.

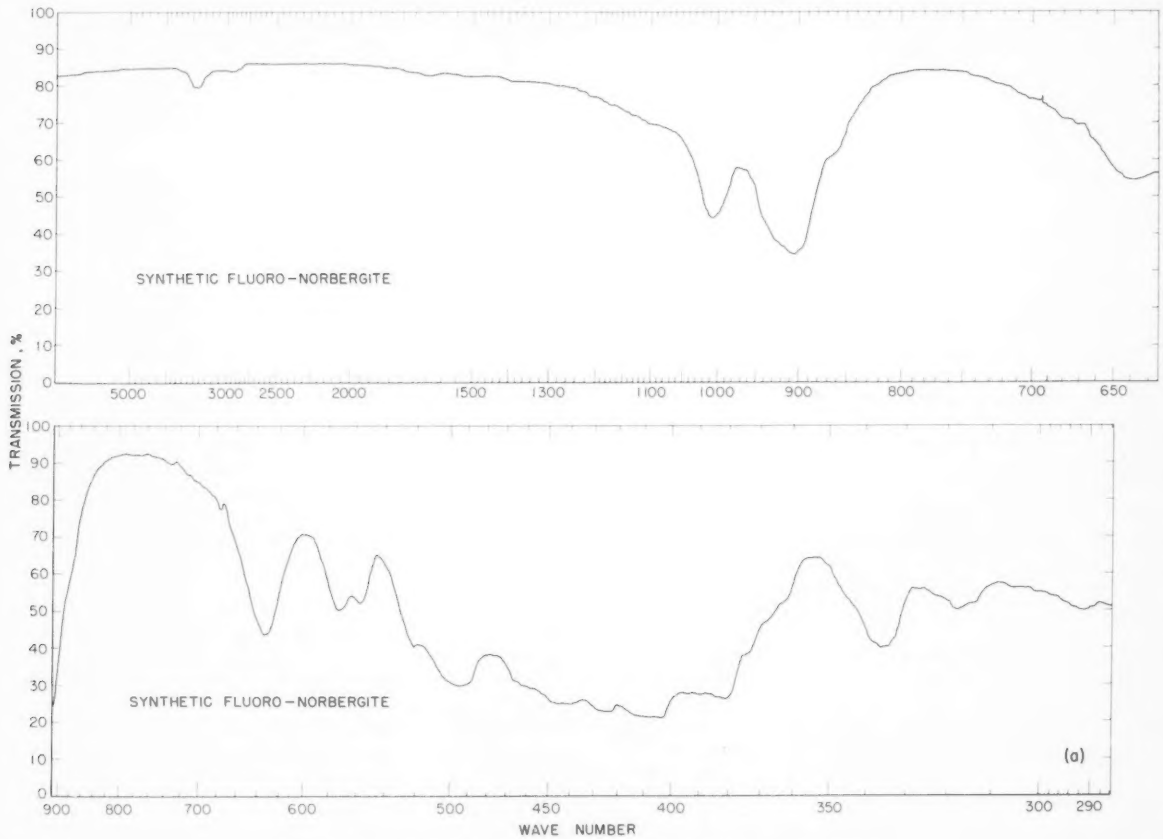

FIGURE 2a. *Infrared absorption spectra of synthetic fluoro norbergite.*

5.2. Chondrodite Spectra

The synthetic chondrodite spectra show two major differences as compared to the natural chondrodite. The band at 760 cm^{-1} in the natural sample is entirely absent in the synthetic. A similar absence is noted in the synthetic material for the band at 960 cm^{-1}. The sharp peak at 3,500 cm^{-1} indicates the presence of OH in the structure of the natural chondrodite. The bands at 618 cm^{-1} and 555 cm^{-1} in the natural material have shifted to 625 cm^{-1} and 560 cm^{-1} in the synthetic material. The band at 768 cm^{-1} in the natural material is absent in the synthetic sample.

5.3. Humite Spectra

The humite patterns are essentially the same except for the differences in the OH bands at 3,500 cm^{-1}. The sharper band in the natural humite indicates hydroxyl groups. The band at 755 cm^{-1} in the natural sample is absent from the synthetic sample and the band at 560 cm^{-1} in the synthetic is missing or obscured in the natural pattern. In the pattern of the synthetic sample there are bands at 493, 420, and 365 cm^{-1} which may be obscured or missing in the patterns of the natural material. Again a shift is noted from band 615 cm^{-1} of the natural material to 620 cm^{-1} in the synthetic sample.

5.4. Clinohumite Spectra

The clinohumite spectra show differences in the intensities of the 1,000 cm^{-1} and 890 cm^{-1} bands. In the synthetic sample, the band at 890 cm^{-1} is more intense than the 1,000 cm^{-1} band. The reverse is true for the natural clinohumite. The pattern of the natural mineral has a band at 725 cm^{-1} that is absent for the synthetic sample. The band at 610 cm^{-1} for the mineral is displaced to 620 cm^{-1} in the pattern of the synthetic humite. The band at 540 cm^{-1} in the synthetic-sample pattern is obscured by the shoulder of the mineral pattern. Bands found at 425, 390, and 370 cm^{-1} for the synthetic humite are not identified in the pattern of the mineral.

The differences between the patterns of the synthetic and natural humites are not explained as no assignments of the absorption bands were attempted. The synthetic fluorohumites differ chemically from

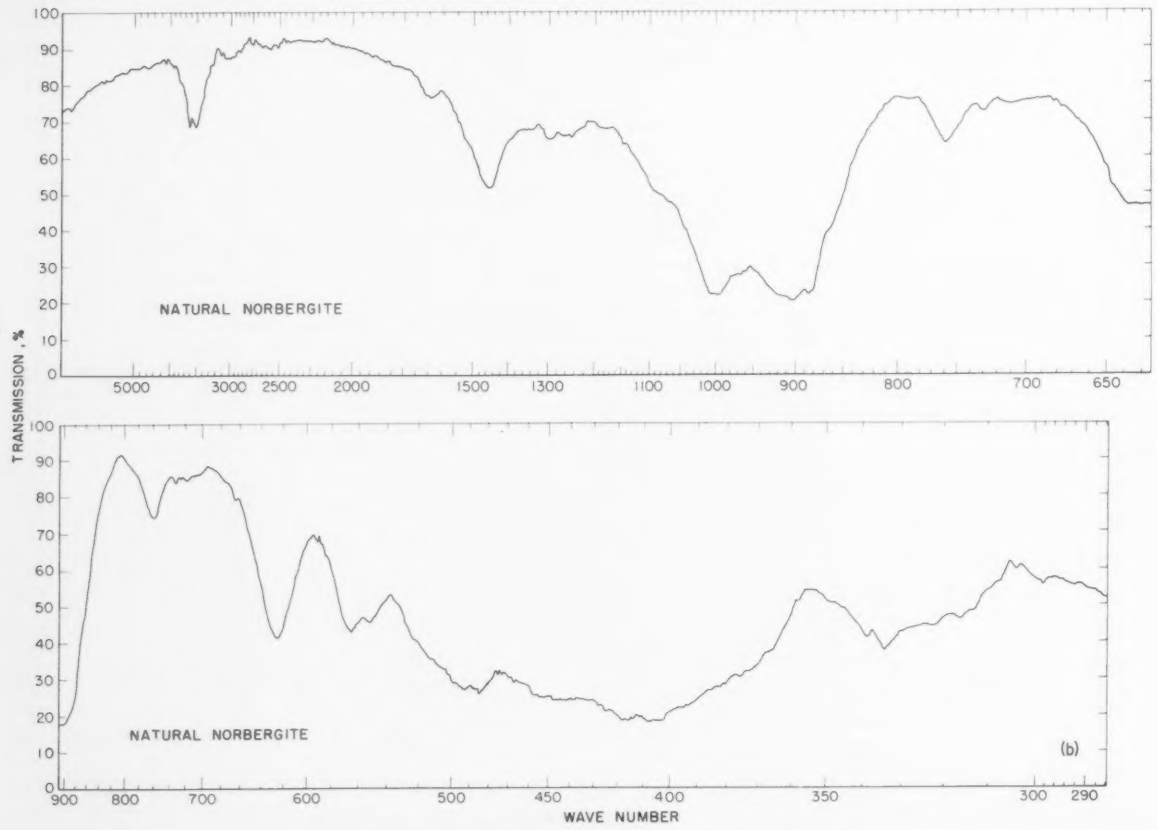

FIGURE 2b. *Infrared absorption spectra of natural norbergite.*

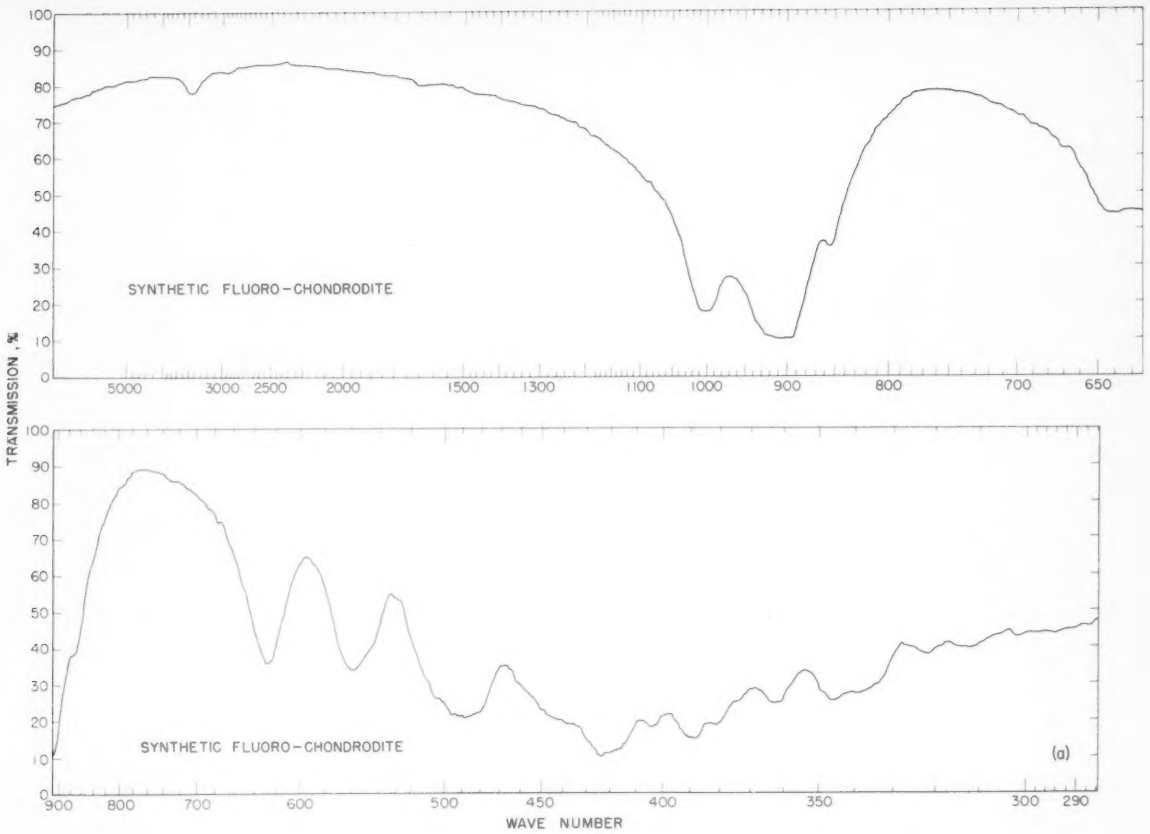

FIGURE 3a. *Infrared absorption spectra of synthetic fluoro chondrodite.*

the natural analogs in that no hydroxyls are present in their structures. The natural samples all contain hydroxyls in addition to fluorine. Also, the analyzed natural samples show the presence of FeO, Fe_2O_3, Al_2O_3, and TiO_2 and these oxides may perturb the bonds between atoms sufficiently to account for some shifting of the bands. It is also known that the synthetic chondrodite and clinohumite show apparent orthorhombic symmetry as compared to the monoclinic symmetry of the natural analogs. These differences should also affect the absorption patterns.

X-ray powder diffraction patterns were made of the synthetic fluorohumites using an X-ray diffractometer with Cu K_α radiation, (1.5405 A) at 25° C. The samples used for X-ray analysis were estimated under the microscope to contain 1 percent or less impurities by volume. A spectrographic analysis showed the following impurities; less than 1.0 percent iron; 0.1 percent each of aluminum and calcium; and less than 0.01 percent each of boron, chromium, manganese, nickel, strontium, and titanium. The norbergite and humite samples have been indexed and the results are given in tables 2 and 4. In tables 3 and 5 the *d*-spacings for chondrodite and clinohumite are given. For purposes of comparison a norbergite examined by the British Museum, ASTM card number 2–1345, and a norbergite reported by Sahama [12] have been included in table 2. Also, natural chondrodite, humite, and clinohumite, as reported by Sahama [12], have been included in tables 3, 4, and 5. It should be noted that the natural humites contain hydroxyl units as well as fluorine.

Taylor and West [11] in 1929 determined that norbergite has the space group Pnma (No. 62) and $4(Mg_2SiO_4 \cdot MgF_2)$ per unit cell. Table 2a gives a comparison of the lattice constants of Taylor and West's norbergite with the NBS synthetic fluoronorbergite.

The humite structure as determined by Taylor [11] and West has a space group Pnma (No. 62) and $4(3Mg_2SiO_4 \cdot MgF_2)$ per unit cell. Table 4a gives a comparison of the lattice constants of Taylor and West's humite with NBS synthetic fluorohumite.

6. Hydrothermal Synthesis of the Humites

The two major objectives in the hydrothermal synthesis of the humites were to determine (1) the

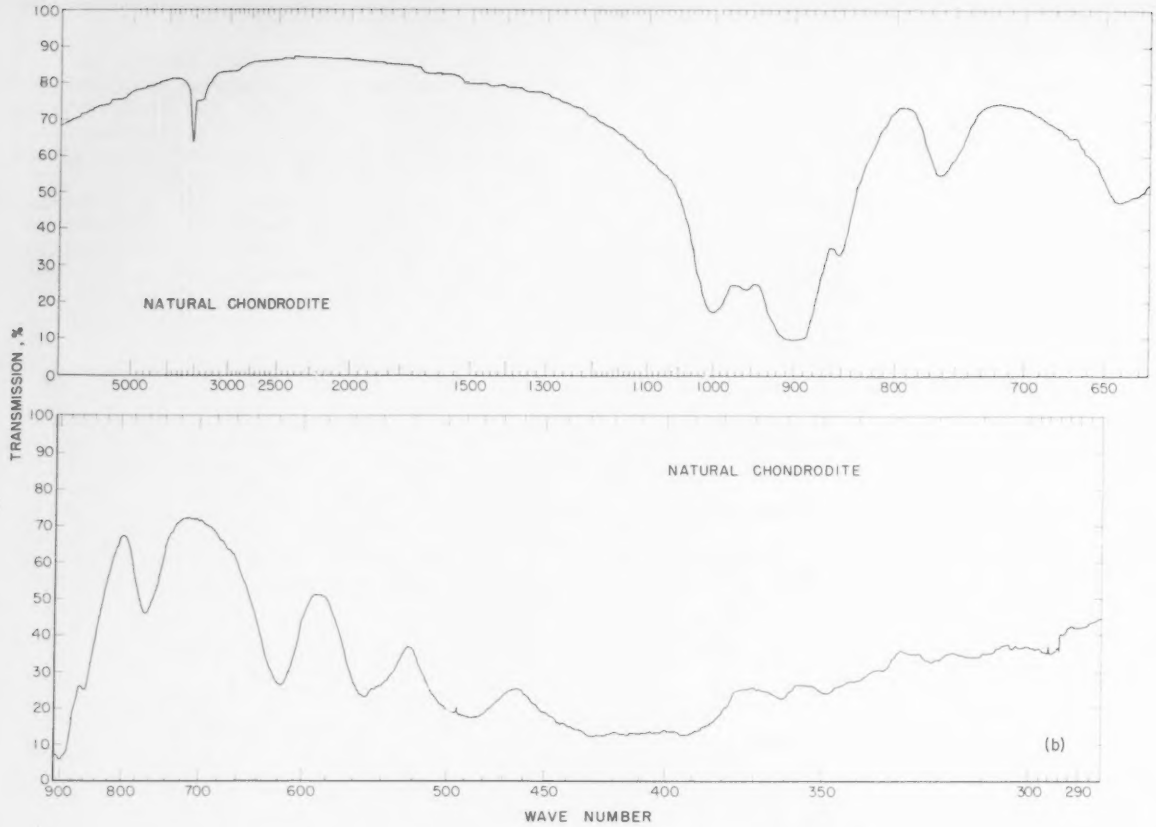

FIGURE 3b. *Infrared absorption spectra of natural chondrodite.*

maximum amount of hydroxyl ions $(OH)^{-1}$ that can replace fluorine ions F^{-1} in the structure of a given humite and (2) the hydrothermal stability range of the series.

The apparatus used in the hydrothermal experiments is the same as that developed at the Geophysical Laboratory [9]. The ingredients used in all experiments consisted of MgO, SiO_2 as precipitated silica and MgF_2 as the fluorinating agent. The ingredients were ground in a mechanical mortar to ensure thorough mixing and to increase the grain surface area for better reactivity. Charges weighing about 0.2 g and distilled water were hermetically sealed in platinum tubing ½ in. long by ⅛ in. O.D. The platinum tubing was then placed in the hydrothermal apparatus. The distilled water was always added to the charge in excess of that required for stoichiometric proportions.

The reaction products obtained from the hydrothermal experiments were usually fine grained and it was difficult to identify the phases microscopically although an occasional grain was observed that was large enough to obtain optical properties. Consequently, identification of fine-grained phases was made using X-ray powder diffraction data. However, it was thought unreliable to determine by this means whether hydroxyl ions were substituting for fluorine ions in any given experiment. Past experiences have indicated there is very little structural change in the unit cell, and certainly there is very little change in X-ray scattering power, when substitution occurs. Thus there is little or no change in the X-ray patterns.

However, owing to the relatively large differences in optical refractivities of hydroxyl compounds relative to isomorphous fluorine analogs, refractive index measurements are likely to yield values of the extent of replacement, if use is made of Gladstone and Dale's principle [13] stating

$$K=\frac{n-1}{d}.$$

d is the density which can be assumed constant for OH/F replacements in isomorphous silicates owing to the similarity of radius and mass of the ions; the average refractive index is $n=\sqrt[3]{\alpha\beta\gamma}$; and K is the specific refraction, a simple additive function:

$$K=\Sigma m_i K_i.$$

TABLE 2. *Norbergite*

hkl	NBS synthetic fluoro Cu, 1.5405 A at 25 °C		British Museum Natural Cu, 1.5418 A		Sahama Natural Cu, 1.5405 A	
	d	*I*	*d*	*I*	*d*	*I*
	A		*A*		*A*	
200	5.145	18	5.2	40	5.13	m
			4.8	40		
210	4.428	10	4.41	50		
020	4.371	28			4.38	w
101	4.283	12			4.27	vw
011	4.149	20			4.14	vw
220	3.327	22	3.37	60	3.32	m
211	3.227	27			3.22	m
121	3.058	100	3.08	80	3.06	vs
			2.94	40		
301	2.771	14	2.77	40	2.76	vw
221	2.716	12			2.72	vw
311	2.639	73	2.66	70	2.63	s
410	2.466	15	2.52	60	2.46	w
131	2.408	36	2.43	40	2.41	m
321	2.337	34	2.35	40	2.34	m
102	2.296	16			2.29	w
401	2.255	68	2.26	80	2.25	m
231	2.230	80			2.23	s
112	2.214	8				
411	2.184	8				
122	2.0320	10	2.03	20	2.03	vw
240, 331	2.0068	5				
141	1.9442	14	1.94	60	1.948	vw
430	1.9243	6				
222	1.9201	5				
241	1.8472	8	1.86	20		
511	1.8408	9	1.81	20	1.838	vw
322	1.7733	4				
402	1.7357	32	1.74	100	1.733	m
232	1.7241	48	1.74	20	1.723	s
341	1.7125	5			1.721	m
412	1.7022	14			1.699	vw
270	1.6529	10	1.65	50		
151	1.6160	7	1.60			
332, 422	1.6125	10				
042	1.6004	9				
620	1.5938	10			1.592	vw
611, 142	1.5808	6				
441	1.5678	4				
103	1.5518	2				
502, 013	1.5470	2	1.54	20		
242, 113	1.5280	6				
432	1.4890	16			1.480	w
213, 351	1.4763	45	1.49	80	1.475	m
123	1.4621	6	1.47	40	1.471	w
522	1.4582	6			1.460	w
060	1.4547	20				
450	1.4435	6				
301	1.4265	4				
313, 631	1.4080	7	1.41	40		
701, 260	1.3990	6	(a)		1.398	vw

[a] Eight additional lines were omitted.

TABLE 2a. *Lattice constants*

		a	*b*	*c*
		A	*A*	*A*
1929	Taylor and West [12] natural	10.2	8.74	4.71
1959	NBS synthetic fluoro	10.271	8.727	4.709 at 25 °C

The density of norbergite calculated from the NBS lattice constants is 3.194 g/cm³ at 25 °C.

TABLE 3. *Chondrodite*

NBS synthetic fluoro Cu, 1.5405 A at 25 °C		Sahama from Hangelby Natural Cu, 1.5405 A	
d	*I*	*d*	*I*
A		*A*	
7.418	10		
4.854	40	4.83	s
3.992	20		
3.948	18		
3.897	11	3.92	w
3.685	23	3.69	w
3.554	42	3.55	m
3.477	30	3.47	m
3.390	27	3.37	m
3.007	45	3.00	s
2.910	15	2.91	vw
2.842	15	2.83	w
2.764	35	2.75	m
2.672	43	2.66	s
2.605	57	2.61	m
2.512	41	2.50	s
2.461	11		
2.428	18	2.42	w
2.318	27	2.31	m
2.301	21	2.29	w
2.272	100	2.27	m
2.252	100	2.25	vs
2.149	16	2.14	vw
2.025	9	2.10	vw
2.009	10		
1.945	9		
1.882	8		
1.851	9		
1.795	16	1.790	vw
1.789	16		
1.737	98	1.735	s
1.693	16	1.688	vw
1.633	5		
1.617	18	1.611	w
1.603	11		
1.574	12	1.570	vw
1.561	5		
1.542	6		
		1.498	vw
		1.478	m
		1.395	vw
		1.340	m

The m_i's are the mass fractions of constituents of specific refraction K_i. Experience shows [13] that the values of K are most reliable when they are computed from a closely similar compound of known composition and specific refraction $K=K_0$. For the humite group one can compute K_0 for the fluorinated compounds and then write

$$K=K_0+Zm_A[K_{Mg(OH)_2}-K_{MgF_2}].$$

Z is the desired fraction of F^- groups replaced by $(OH)^-$; m_A is the average of the mass fractions of $Mg(OH)_2$ and MgF_2 in the hydroxylated and fluorinated formulas, respectively. Using known values for refractive indices and densities of sellaite and brucite $K_{Mg(OH)_2}-K_{MgF_2}=0.114$. Thus,

$$Z=\frac{K-K_0}{0.114m_A}=\frac{\partial n}{d\cdot 0.114m_A}.$$

$+\partial n$ is the difference in average refractive index observed between the compound of unknown composition and the fluorinated analog. The calculation can be readily followed from table 5a.

TABLE 4. *Humite*

hkl	NBS synthetic fluoro Cu, 1.5405 A at 25° C.		Sahama Natural Cu, 1.5405 A	
	d	*I*	*d*	*I*
	A		*A*	
020	10.42	5	----	---
042	5.17	9	----	---
200	5.11	9	----	---
210	4.97	18	4.96	w
220	4.59	19	4.57	w
111	4.20	1	----	---
121	3.97	5	----	---
031	3.90	12	3.90	vw
131	3.66	5	3.65	m
240	3.34	49	----	---
201	3.47	5	3.46	vw
060	3.453	32	----	---
211	3.430	25	3.42	w
141	3.312	32	3.31	m
051	3.119	7	3.12	vw
023	3.102	7	----	---
151	2.980	6	2.98	vw
241	2.885	6	2.89	vw
301	2.770	23	2.76	w
311	2.744	32	2.74	m
161	2.691	50	2.69	m
321	2.674	5	----	---
080	2.589	7	----	---
331	2.572	38	2.57	m
420	2.490	4	----	---
261	2.453	4	----	---
341	2.443	30	----	---
171	2.438	70	2.44	s
430	2.399	21	2.40	w
022	2.308	8	----	---
351	2.304	12	2.30	vw
440	2.297	7	----	---
271	2.256	100	2.26	vs
401, 122	2.251	35	----	---
181	2.218	17	----	---
132	2.189	7	----	---
361	2.158	6	----	---
142	2.107	38	----	---
222	2.103	30	----	---
460	2.057	6	----	---
2·10·0,291	1.920	5	----	---
501	1.881	7	----	---
1·10·1	1.867	8	----	---
521	1.850	1	----	---
531	1.814	6	----	---
471	1.794	2	----	---
2·10·1	1.779	6	----	---
391	1.772	5	----	---
082	1.7477	6	----	---
272	1.7387	65	1.740	s
182	1.7229	5	----	---
490, 551	1.7117	4	----	---
481	1.6995	3	----	---
432	1.6859	12	1.685	vw
3·10·1,630	1.6581	10	----	---
442	1.6486	1	----	---
372	1.6256	2	----	---
640	1.6213	15	1.621	w
452	1.6032	4	----	---
621	1.5863	5	----	---
3·11·1	1.5575	4	----	---
462	1.5525	13	----	---
1·10·2,123	1.5419	3	----	---
2·13·0	1.5223	10	----	---
---	*1.5192	15	1.520	vw
4·11·0	1.5176	5	----	---
1·13·1	1.4948	1	----	---
---	*1.4895	8	1.485	m
670	1.4786	69	1.478	w
3·12·1	1.4644	1	----	---
1·11·2	1.4588	1	----	---
303	1.4226	1	----	---
163,2·14·0	1.4223	4	----	---
---	------	--	1.396	vw
---	------	--	1.392	vw
---	------	--	1.380	vw
---	------	--	1.344	w

*These "d" spacings cannot be indexed, but since they occur in Sahama's natural material, they have been included for comparison.

TABLE 4a. *Lattice constants*

		a	*b*	*c*
1929	Taylor and West, natural material.	10.23	20.86	4.738
1960	NBS, synthetic material	10.243	20,72	4.735 at 25 °C

The density of humite calculated from NBS lattice constants is 3.201 g/cm³ at 25 °C.

TABLE 5. *Clinohumite*

NBS synthetic fluoro Cu, 1.5405 A at 25 °C		Sahama from Hameenkyla Natural Cu, 1.5405 A	
d	*I*	*d*	*I*
A		*A*	
5.029	25	5.02	s
4.453	22	4.44	w
3.870	29	3.86	w
3.696	47	3.70	s
3.487	30	3.48	w
3.450	30	3.44	w
3.338	16	3.35	vw
3.224	21	3.22	m
2.919	9	2.91	vw
2.768	58	2.76	s
2.675	7	2.68	vw
2.604	27	2.60	w
2.538	54	2.54	s
2.512	59	2.51	s
2.459	19	-----	---
2.405	22	2.40	w
2.391	16	2.39	vw
2.354	32	2.36	m
2.312	14	2.30	vw
2.257	100	2.26	s
2.218	7	-----	---
2.188	9	2.15	vw
2.156	15	-----	---
1.879	10	-----	---
1.826	5	-----	---
1.796	8	-----	---
1.790	6	-----	---
1.768	8	-----	---
1.741	80	1.742	s
-----	---	1.738	vs
1.683	14	1.681	vw
1.656	4	-----	---
1.636	7	-----	---
1.624	17	1.624	vw
1.609	16	1.612	vw
1.541	8	1.537	vw
-----	---	1.479	m
-----	---	1.396	vw
-----	---	1.345	w

TABLE 5a

Name	n Fluorinated	n Unknown composition containing hydroxyls	δn	$\frac{0.002}{\delta n}$	*d*	m_A	*Z* for unknown composition
					g/cm³		%
Norbergite	1.557	1.568	0.011	0.2	3.19	0.314	10±2
Chondrodite	1.569	1.613	.017	.1	3.12	.179	26±3
Humite	1.612	1.633	.021	.1	3.12	.130	45±5
Clinohumite	-----	-----	-----	-----	-----	-----	-----

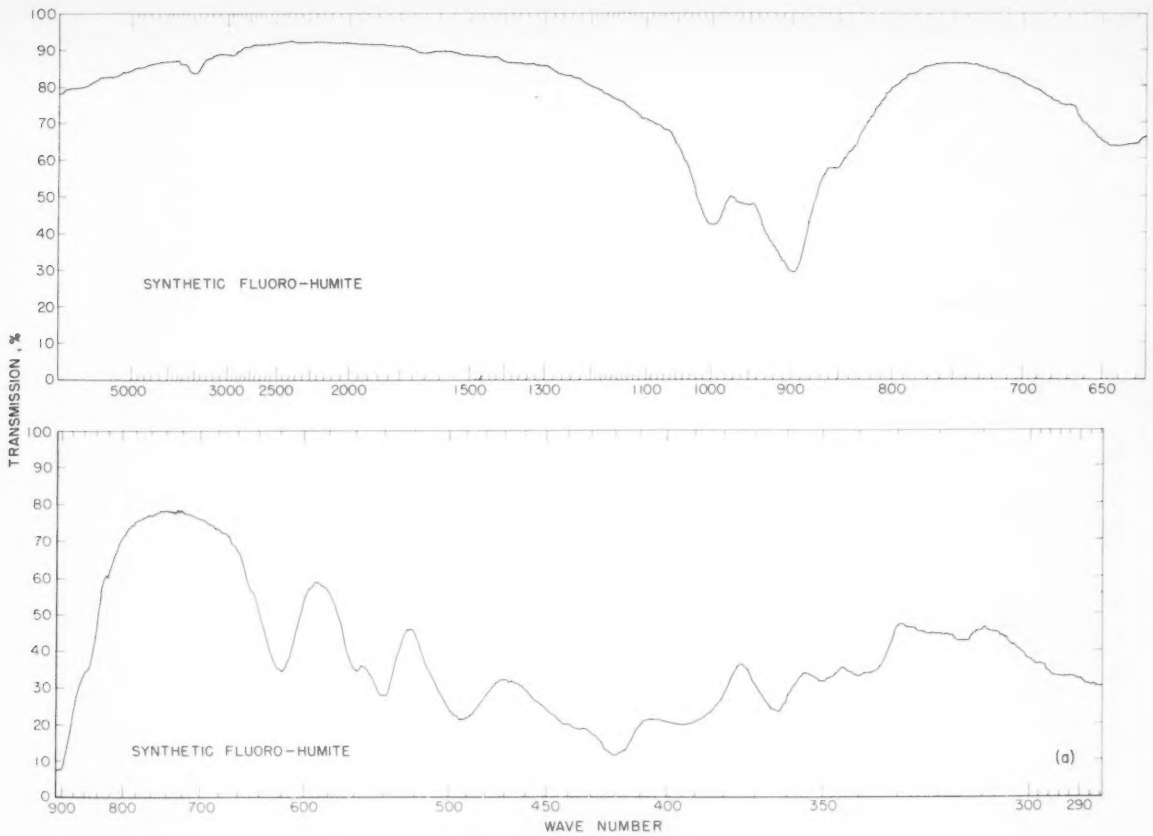

FIGURE 4a. *Infrared absorption spectra of synthetic fluoro humite.*

A brief consideration of the sources of error in the calculation of the values of Z will show readily that the mathematical simplifications in the above analysis introduce an error of less than 1 percent. Similarly the density values are better than would correspond to a ½ percent accuracy, and the assumption of density constancy with composition over the limited range is unlikely to affect Z by more than 1 percent. Uncontrolled compositional variations in the synthetic humites are not only small, but are known to affect the refractive index but narrowly.

A further possible source of error could arise from Gladstone and Dale's principle not applying within the accuracies here considered. From experience [15] one can be confident that for the limited replacements here discussed the application of the principle is sound.

It remains only to discuss the experimental uncertainties introduced from the refractive index measurements. The commonly claimed third decimal figure is rightly suspected owing to some systematic errors which, however, are largely eliminated when only a difference in refractive indices is involved as in this experiment. The $0.002/\partial n$ values given in table 52 are the author's estimate of the fractional errors which account for the largest uncertainties in the determinations of Z. An approximate estimate of the probable error in Z is obtained by multiplying $0.002\ \partial n$ by Z (see table 5a).

7. Norbergite Compositions

Fourteen hydrothermal experiments were completed on the norbergite composition as shown in table 6. The first seven experiments were made using a calculated F^{-1} to $(OH)^{-1}$ ratio of 1:1. These ratios and the subsequent ratios were obtained in the raw batch composition by varying the proportions of MgF_2 to $Mg(OH)_2$. The next six experiments were run on compositions that were calculated to yield a completely fluorinated norbergite. In experiment 14 fluorine was eliminated from the composition with the objective of synthesizing norbergite having only hydroxyl groups.

The norbergite compositions containing a calculated ratio of 1:1, F^{-1} to $(OH)^{-1}$ indicate that chondrodite forms as the stable phase at 700 to 800 °C and 20,000 psi. At 700 °C crystallization is inhibited and the presence of some chondrodite and

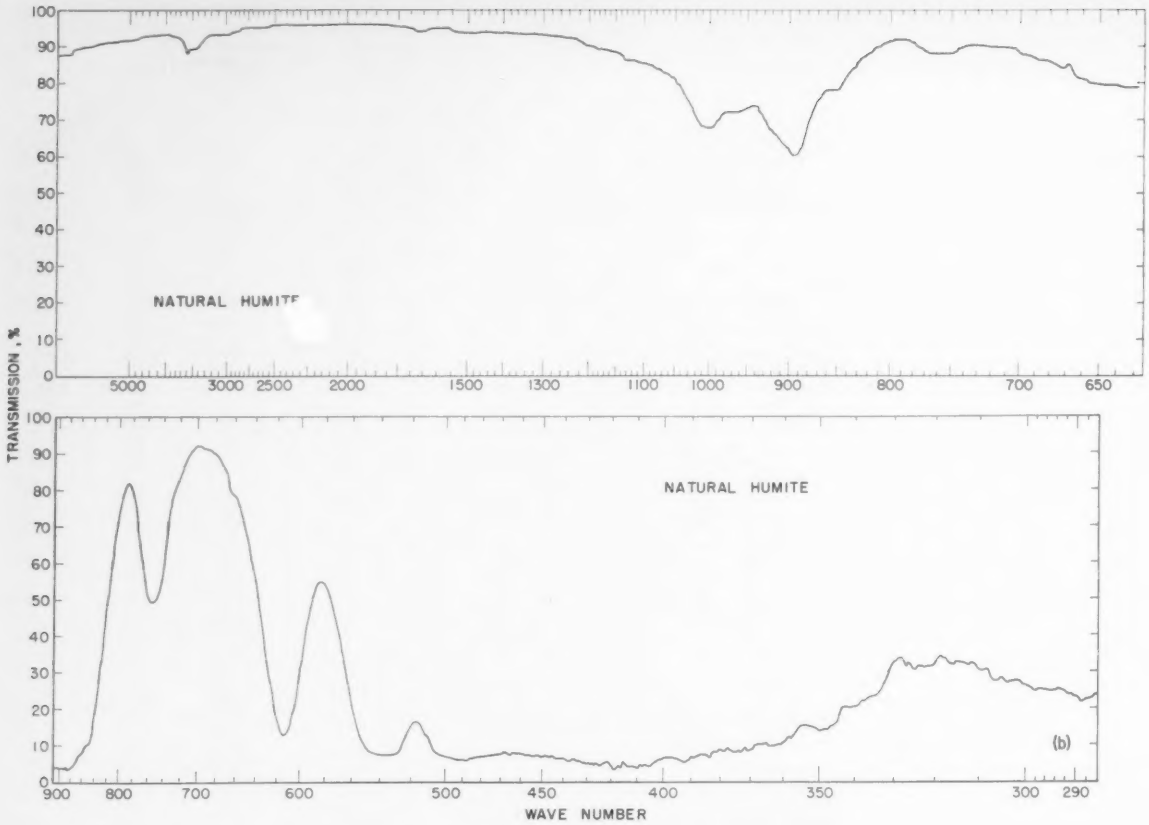

FIGURE 4b. *Infrared absorption spectra of natural humite.*

TABLE 6. *Norbergite compositions hydrothermal experiments*

Experiment	%F in (F,OH)	Temp. °C	Psi	Time	Results
1	50	810	20,000	1 week	Major phase as determined by X-ray Chondrodite α=1.600, β=1.611, γ=1.628.
2	50	800	20,000	21 hr	Same as above.
3	50	800	8,000	16 hr	Chondrodite major phase.
4	50	700	20,000	16 hr	Some brucite. Chondrodite is beginning to crystallize.
5	50	700	8,000	5 days	Chondrodite. Material not well crystallized.
6	50	600	20,000	1 week	Material not well crystallized. Major phase norbergite as determined by X-ray.
7	50	400	16,000	1 week	Under microscope, reaction appeared very poor. X-rays indicated the presence of some talc.
8	100	810	16,000	1 week	Norbergite plus small amount of talc.
9	100	700	20,000	3 days	Norbergite major phase. α=1.560, β=1.564, γ=1.580.
10	100	700	20,000	16 hr	Norbergite.
11	100	600	20,000	1 week	Norbergite major phase.
12	100	500	16,000	1 week	Norbergite major phase.
13	100	400	20,000	3 days	Talc major phase.
14	0	700	18,000	5 days	Forsterite, periclase with some brucite.

talc indicates that this temperature may be near the lower stability limit of chondrodite formation. At 600 °C the presence of norbergite was determined by X-ray analysis. Below 600 °C talc appears to be the stable phase and this talc may contain fluorine in its structure. These hydroxyl bearing chondrodites also showed orthorhombic symmetry under the microscope, as zero extinction angles were observed parallel to the major crystallographic axes. The chondrodite obtained from the norbergite composition of experiment 1 contained a few grains that were large enough to measure indices of refraction: α=1.600, β=1.611, and γ=1.628. These indices are higher than the indices measured on a completely fluorinated chondrodite grown from solid state reactions where α=1.582, β=1.594, and γ=1.612. The higher indices indicate the presence of hydroxyl groups in the structure. Calculations further show that 26 percent of the F^{-1} ions have been replaced by $(OH)^{-1}$ ions (see table 5a).

Experiments 8 to 13 were made using a norbergite composition calculated to give an anhydrous fluoronorbergite. Since the ingredients were exposed to water vapor there was always the possibility of

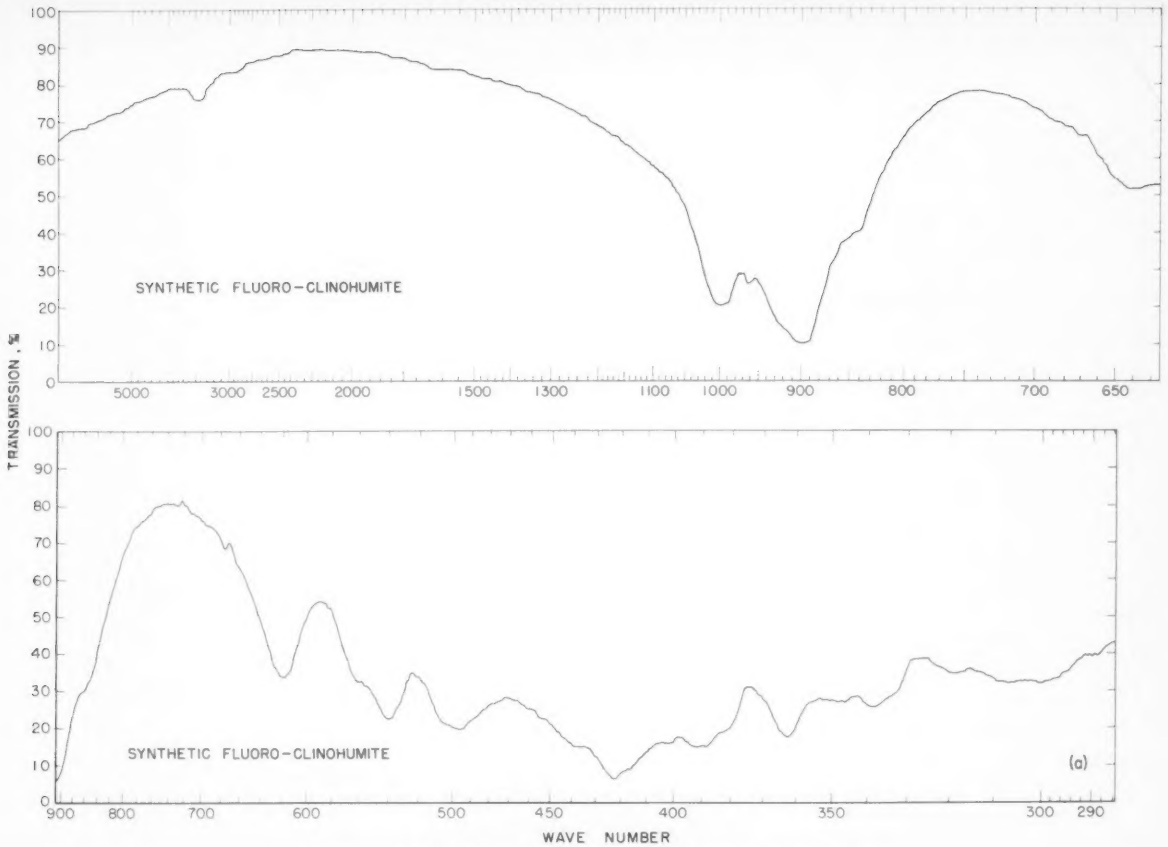

FIGURE 5a. *Infrared absorption spectra of synthetic fluoro clinohumite.*

$(OH)^{-1}$ entering the structure in preference to F^{-1}. In these experiments norbergite formed in the temperature range of 500 to 800 °C and a pressure range of 16,000 to 20,000 psi. In experiment 9 a few grains of norbergite were large enough to measure indices of refraction: $\alpha=1.560$, $\beta=1,564$, and $\gamma=1.580$. In comparison the indices of an anhydrous synthetic norbergite made from solid state reactions are $\alpha=1.548$, $\beta=1.552$, and $\gamma=1.570$. Again the higher indices of refraction indicate that hydroxyl units are present in the norbergite structure and that 10 percent of the F^{-1} have been replaced by hydroxyls (see table 5a). It is significant to note here that the composition was calculated to give an anhydrous norbergite. In the reaction, however, $(OH)^{-1}$ ions were incorporated in the structure and there was no optical evidence of any variation in the indices of refraction indicating that the OH content was the same for all the grains examined. This suggests that the maximum amount of $(OH)^{-1}$ has entered the structure as none of the experiments showed norbergite grains with higher indices of refraction.

In these norbergite experiments it is to be noted that the amount of fluorine present may alter the course of reaction. For example, in experiment 1, where the ratio of F^{-1} to $(OH)^{-1}$ is 1:1, the major phase as determined by X-ray powder data was chondrodite. In comparison, experiment 9 was calculated to have 100 percent F and the pressure, temperature and time are essentially the same. The major phase, however, was norbergite.

Experiment 14 was one of several attempts to synthesize a hydroxyl norbergite but none of these was successful. The reaction products were the same as those found by Bowen and Tuttle, namely, talc, brucite, forsterite, etc. [1]. Fluorine appears to be a necessary constituent in norbergite.

8. Chondrodite Compositions

Chondrodite compositions were prepared in the same manner as the norbergite compositions and a list of experimental results are given in table 7. Experiments 1, 2, and 3 contained a calculated 1:1 ratio of F^{-1} to $(OH)^{-1}$. Chondrodite formed in all three experiments and, in addition, brucite was present in the reaction products formed at 500 °C and 20,000 psi (experiment 3), while humite formed at 800 °C and 20,000 psi (experiment 1). The humite of this experiment had indices of $\alpha=1.620$, $\beta=1.629$, and $\gamma=1.650$. In comparison the anhydrous

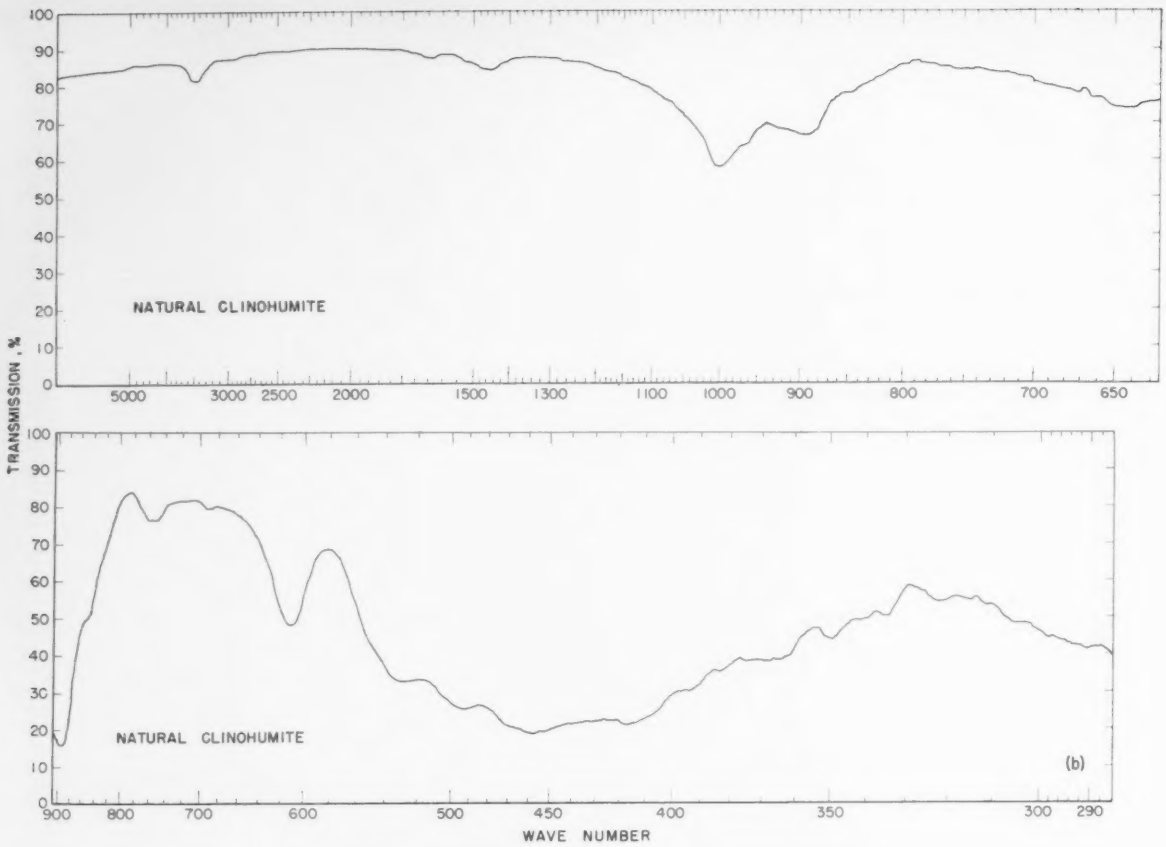

FIGURE 5b. *Infrared absorption spectra of natural clinohumite.*

TABLE 7. *Chondrodite compositions hydrothermal experiments*

Experiment	%F in (F,OH)	Temp.	Psi	Time	Results
		°C			
1	50	800	20,000	16 hr	Crystals of humite present. α=1.620, γ=1.650 Major phase chondrodite.
2	50	700	8,000	2 weeks	Chondrodite.
3	50	500	20,000	3 days	Major phases brucite and chondrodite.
4	100 (F)	800	20,000	16 hr	Chondrodite and talc. No humite.
5	100 (F)	700	8,000	2 weeks	Chondrodite and talc.
6	100 (F)	500	20,000	3 days	Talc, brucite, and chondrodite.
7	0	700	10,000	2 weeks	X-ray pattern close to that of forsterite.

humite containing fluorine gave α=1.598, β=1.606, and γ=1.630. It would appear that hydroxyl groups had also entered the humite structure. The hydroxyl content in humite was calculated to be 45 percent (see table 5a). Experiments 4, 5, and 6 contained a calculated 100 percent F in (F, OH) and their reaction products contained chondrodite. Experiment 7 did not contain any fluorine and it was made under the same conditions as experiment 6 with the idea of synthesizing a hydroxyl chondrodite. Forsterite was the major constituent in this experiment and there was no evidence of any chondrodite.

9. Humite Compositions

Table 8 lists the results of experiments on humite compositions. The major phases obtained in these experiments are either forsterite or talc, and humite did not appear as a reaction product. It should be noted again that water was added to the humite composition in excess of that required for the hydroxyl content, and this excess water may well be responsible for decreasing the fluorine ion concentration thus shifting the course of reaction away from humite.

TABLE 8. *Humite compositions hydrothermal experiments*

Experiment	%F in (F,OH)	Temp.	Psi	Time	Results
		°C			
1	50	900	20,000	3 days.	Major phase forsterite.
2	50	800	20,000	3 days.	Small leak developed. Forsterite, talc and possible humite.
3	50	600	20,000	3 days.	Major phase is talc.
4	50	700	8,000	5 days.	Forsterite and some talc.
5	100	900	20,000	3 days.	Forsterite and second phase not identified.
6	100	800	20,000	3 days.	Forsterite major phase.
7	100	700	8,000	5 days.	Forsterite major phase.
8	100	600	20,000	3 days.	Talc major phase.
9	0	700	10,000	5 days.	Forsterite and talc major phase.

10. Clinohumite Compositions

Compositions corresponding to clinohumite were prepared and run under the same conditions as the humite experiments. The results of these experiments were the same as the humite experiments, and there was no optical evidence that a clinohumite containing hydroxyl units was synthesized. A table of the clinohumite compositions was not prepared.

11. Substitutions

It is well known that germanium will proxy for silicon atoms in many of the silicate structures. Robbins and Levin [13] have succeeded in synthesizing a germanium forsterite, Mg_2GeO_4. Since the forsterite structure is one of the fundamental building blocks in the humites, it was thought that germanium humites could be synthesized. Using solid state reaction techniques, germanium analogs of silicon fluorohumites were synthesized with the exception of clinohumite. This analog was not identified in any of the reaction products. However, the search was not exhaustive and it is thought likely that the compound can be synthesized provided the correct condition of temperature, composition, etc., is found. As with the other synthetic fluorochondrodites, the germanium fluorochondrodite shows orthorhombic symmetry under the polarizing microscope. The germanium analogs are positive in optical character with the following indices as determined by oil immersion techniques and white light.

	α	β	γ
Germanium norbergite	1.590	1.598	1.638
Germanium chondrodite	1.658	1.670	1.735
Germanium humite	1.716	1.732	1.758

Buckle and Taylor [10] were successful in obtaining a calcium analog of chondrodite, $Ca_5(SiO_4)_2(OH)_2$, using hydrothermal techniques. The other three members of the humite group were not reported but it seems reasonable that, given the proper conditions, they also can be synthesized. One of the important features of this synthesis is that a hydroxyl humite without fluorine can be obtained. The author repeated the synthesis of Buckle and Taylor and confirmed their results. Attempts by the author, however, to substitute fluorine for hydroxyl in the calcium analog were not successful.

As titanium has been reported in several analyses of the natural humites [12], a few preliminary experiments were made to introduce TiO_2 synthetically into the norbergite structure. Two fluoronorbergite compositions were formulated to replace approximately 10 and 20 percent of MgO by TiO_2. The two compositions were fired at 1,150 °C in one experiment and at 1,250 °C in another. For comparison a TiO_2 free norbergite was run at the same time for each experiment. In all the TiO_2 experiments the reaction products yielded a norbergite that had higher indices of refraction than that of the control norbergite. The α index of refraction for the TiO_2 norbergite, and this includes both the 10 and 20 percent compositions, was 1.557 as compared to 1.546 for the control norbergite and the γ index was 1.578 as compared to 1.570. No attempt was made to substitute TiO_2 in the other humite structures, but it is probable that TiO_2 will go into these structures.

Ferrous iron is found in most natural humites substituting for magnesium and two experiments were designed to incorporate ferrous iron in the synthetic fluorochondrodite structure. This structure was chosen to observe the possible effect of iron on the crystal symmetry of chondrodite. Since previous attempts to synthesize a monoclinic form were unsuccessful it was thought the presence of the slightly larger ferrous ion might change the layering or stacking characteristics of the structure, producing monoclinic symmetry similar to that of the natural analog. A fluorochondrodite composition was prepared using a natural olivine $(MgFe)_2SiO_4$ that contained approximately 15 percent of ferrous iron. To this MgF_2 was added in formula proportions and the batch heated to 1,380 °C with one sample exposed to atmospheric conditions and a second sample exposed to the inert gas helium to prevent oxidation of the iron. In both experiments a reaction product was obtained that appeared optically to be orthorhombic. There was no evidence of monoclinic symmetry. The reaction products of both experiments had the same indices of refraction with $\alpha=1.612$ and $\gamma=1.642$ and their X-ray diffraction patterns were the same and typical of synthetic chondrodites.

12. Summary

The humites have been synthesized using the techniques of solid state reactions, hydrothermal

reactions, and crystallization from melts. The synthetic fluoro analogs of chondrodite and clinohumite did not have the monoclinic symmetry characteristic of the natural minerals; in comparison they showed orthorhombic symmetry under the microscope. This anomaly is interpreted as a difference in structural stacking in which layered segments are arranged to give either monoclinic or orthorhombic symmetry. X-ray, optical, and infrared data are given for the synthetic fluorohumites and they are compared to those of their natural analogs. The substitutions of germanium for silicon, calcium for magnesium, titanium for magnesium or possibly silicon, ferrous iron for magnesium, and hydroxyls for fluorine were successfully achieved in one or more of the humite series. Experimental evidence indicates that the humite series does not extend beyond compositions corresponding to norbergite or clinohumite.

The author gratefully acknowledges the help of colleagues who assisted in preparations and who contributed valuable suggestions to the study. These include R. G. Pike, G. F. Rynders, E. N. Bunting, E. Lippincott, and M. Cook.

13. References

[1] N. L. Bowen and O. F. Tuttle, Bull. Geol. Soc. Amer. **60,** 439 (1949).
[2] D. M. Roy and R. Roy, Am. Mineralogist **40,** 147 (1955).
[3] E. T. Carlson, R. Peppler, and L. S. Wells, J. Research NBS **51,** 179 (1953) RP2448.
[4] A. Daubree, Compt. rend. **32,** 625 (1851).
[5] C. Dolter, Mineralog. u. petrog. Mit. **X,** 67 (1889).
[6] W. Jander and U. R. Fett, Z. anorg. Chem. **242** (1939).
[7] N. Koeppen and N. N. Padurew, Gesetzmaessige Verwachsungen von synthetischem Phlogopit mit Mineralien der Humitgruppe, Fiat Final Report No. 749, Office of Military Government for Germany, U.S. Field Information Agency Technical, March 1946.
[8] K. Randama, Am. Mineralogist **32,** 146 (1947).
[9] J. Van den Heurk, Bull. Geol. Soc. Amer. **64,** 993 (1953).
[10] E. R. Buckle and H. F. W. Taylor, Am. Mineralogist **43,** 818 (1958).
[11] W. H. Taylor and J. West, Proc. Roy. Soc. (London) A., CXVII, 517 (1928).
[12] Th. G. Sahama, Ann. Acad. Sci. Fennicae, Ser. A. (1953).
[13] E. S. Larsen and H. Berman, Geol. Survey Bull. **848,** 31 (1943).
[14] C. R. Robbins and E. M. Levin, Am. J. Sci. **257,** 63 (1959).
[15] H. W. Jaffe, Am. Mineralogist **41,** 757 (1956).

(Paper 65A5–122)

JOURNAL OF RESEARCH of the National Bureau of Standards—A. Physics and Chemistry
Vol. 65A, No. 5, September–October 1961

Phase Equilibria in Systems Involving the Rare Earth Oxides. Part III. The Eu_2O_3–In_2O_3 System

S. J. Schneider

(April 14, 1961)

The equilibrium phase diagram was determined for the Eu_2O_3–In_2O_3 system. An induction furnace, having an iridium crucible as the heating element (susceptor), was used to establish the solidus and liquidus curves. The 1:1 composition melts congruently at 1745 ±10 °C. Melting point relations suggest that the 1:1 composition is a compound with solid solution extending both to 31 mole percent In_2O_3 and 71 mole percent In_2O_3. The compound is pseudohexagonal with a_H=3.69 A and c_H=12.38 A. Isostructural phases also occur in the 1:1 mixtures of both Gd_2O_3 and Dy_2O_3 with In_2O_3. The melting points of Eu_2O_3 and In_2O_3 were determined to be 2,240±10 °C and 1910±10 °C respectively. A eutectic occurs in the Eu_2O_3–In_2O_3 system at 1,730 °C and about 73 mole percent In_2O_3. The indicated uncertainties in the melting points are conservative estimates of the overall inaccuracies of temperature measurement.

1. Introduction

This paper is the third in a series concerning phase equilibria in systems involving the trivalent rare earth oxides. The first paper [1][1] described the polymorphic forms of these oxides. The second [2] dealt with solid state reactions between these materials. This investigation reports results obtained in a complete study of one specific system, Eu_2O_3–In_2O_3.

Two polymorphic forms of Eu_2O_3 have been reported [1]. The stable modification is monoclinic having a B-type[2] rare earth oxide structure. The other form is metastable having the cubic C-type (Tl_2O_3–type) rare earth oxide structure. The transformation from the C- to the B-type occurs above about 1,075 °C and is apparently irreversible. The melting point of Eu_2O_3 has been reported as 2,050 °C [3].

Although In_2O_3 is not a member of the lanthanide series of rare earth oxides, it does have the cubic C-type structure. Indium sesquioxide becomes somewhat volatile at elevated temperatures. It has been reported to volatilize predominantly by decomposition to the gaseous elements at temperatures of 677 °C [4] and 850 °C [5]. However, as shown by the present investigation, volatilization of In_2O_3 does not become significant until temperatures in excess of 1,350 °C are reached and maintained for several hours. Goldschmidt et al., [6] reported the melting point of In_2O_3 to be over 2,000 °C.

Because of the relatively high melting points encountered in this system, induction heating was employed exclusively for the determination of the solidus and liquidus curves.

[1] Figures in brackets indicate the literature references at the end of this paper.
[2] This structure type has not yet been fully described in the crystallographic literature.

2. Materials

The starting materials used in this study were found by general qualitative spectrochemical analysis to have the following impurities:

Eu_2O_3—Ba, Ca, Er, and Si; each present in amounts less than about one hundredth percent.
Cr, Cu, Fe, Mg, and Ni; each present in amounts less than about one thousandth percent.
As and Yb; perhaps present.

In_2O_3—Al, Ca, Cu, Fe, Mg, Ni, Pb, and Si; each present in amounts less than about one hundredth percent.
Er; present in amounts less than about one thousandth percent.
Ag and Mn; each present in amounts less than about one ten thousandth percent.
Tl; perhaps present.

3. Experimental Procedure

Specimens were prepared from 1 g batches of various combinations of Eu_2O_3 and In_2O_3. Calculated amounts of each oxide, corrected for ignition loss at 800 °C, were weighed to the nearest milligram. Each batch was mechanically mixed, pressed at 10,000 lb/in.$_2$ into a ¾ in. diam pellet and fired on platinum foil in a muffle furnace at 800 °C for about 20 hr. The specimens were then ground in an agate mortar, remixed, again pressed into pellets, and then fired at 1,350 °C for 6 hr.

Following the preliminary heat treatments, the specimens were ground, sealed in Pt tubes and fired at various temperatures for different periods of time in a platinum alloy quench furnace. The Pt tubes containing the specimens were quenched into ice water and then examined for evidence of leaks.

If leakage occurred, as indicated by small pin holes in the tube or by the presence of water in the specimen, the results were discarded and the experiment repeated.

Temperatures in the quench furnace, controlled to ± 5 °C, were measured with a platinum-platinum-10-percent-rhodium thermocouple. Inasmuch as Pt thermocouples deteriorate rapidly above 1,400 °C, the temperatures recorded for all quenching experiments are only accurate to about ± 10 °C.

All quenched specimens were examined by X-ray diffraction techniques at room temperature using a high-angle recording Geiger-counter diffractometer and Ni-filtered Cu radiation. Equilibrium was assumed to have been attained when the X-ray pattern showed no change after successive heat treatments of a specimen or when the data were consistent with the results from a previous set of experiments.

It was necessary, in mixtures containing greater than 50 mole percent In_2O_3, to heat treat the specimen for a relatively long time before equilibrium was even approached. The Pt tubes invariably failed due to the high internal pressure. Therefore the equilibrium phases had to be extrapolated from the results obtained from a series of short-time heat treatments.

An induction furnace, having as the heating element (susceptor) a small iridium crucible, was used exclusively to determine all solidus and liquidus temperatures. Temperatures in excess of 2,300 °C were easily attained with this furnace. The crucible with cover was formed by powder metallurgical techniques and had the following overall nominal dimensions; height, ¾ in.; outer diameter, ½ in.; and wall thickness, 1/16 in. A small fragment of a 1,350 °C calcined specimen was placed on a small iridium button which in turn was set inside the crucible. Temperatures were controlled manually and were measured with an optical pyrometer sighted through a calibrated 45° glass prism and a 1/16 in. diam hole in the crucible cover.

Nearly perfect blackbody conditions were obtained with this arrangement. The specimen generally could not be seen. All heatings were performed in a normal atmosphere. Vaporization of IrO_2 and/or Ir apparently did not affect the specimen in any way. Solid state reaction between the specimen and these materials was never indicated by the X-ray patterns of the various specimens.

The crucible was heated very quickly at first and then more slowly as the desired temperature was approached. When the appropriate temperature was reached and maintained for about 15 sec, the furnace was turned off. The temperature of the crucible dropped below red heat in less than 1 min. The entire heating and cooling cycle consumed about 10 min. or less. The cooled specimen was examined visually with the binocular microscope for evidence of melting. The solidus temperature was indicated by slight rounding of the corners of the specimen. The liquidus temperature, usually more difficult to determine, was indicated by the formation of an essentially flat button with no sharp or irregular corners.

The apparent temperatures indicated by the pyrometer were dependent upon the physical setup of the equipment and geometry of the crucible. The temperature measuring system was calibrated against Au, Pt, and Rh (set on alumina) and as expected, each metal appeared to melt at a temperature lower than its reported value. The deviations between apparent and actual melting points were accounted for in part by errors caused by the pyrometer and prism. After correcting for the pyrometer and prism errors, the deviations amounted to 3 °C at 1,063 °C (Au), 11 °C at 1,769 °C (Pt), and 13 °C at 1,960 °C (Rh). A plot of temperature deviation against apparent temperature results in a linear curve which was used throughout this investigation to correct all observed temperature to a precision of at least ± 5 °C. The average emissivity for the three calibration points was 0.953 with a range of ± 0.012, which is smaller than the inaccuracy of the pyrometer. For these reasons the calibration curve was extended above the last calibration point (1,960 °C) with reasonable expectancy that the emissivity will not change.

The reasons for the small deviation from blackbody conditions are unknown at this time. At first it was thought possible that part of the deviation was due to IrO_2 and/or Ir vapor. This assumption was disproved, however, by an experiment in which the filament of a standard pyrometer lamp showed no temperature deviation when sighted on through vapor of IrO_2 and/or Ir. The experiment consisted of sighting through a hollow iridium cylinder on the lamp filament which was maintained at a constant temperature. The temperature of the filament was determined with an optical pyrometer both before and during the heating of the cylinder. The cylinder was maintained at various temperatures, ranging between about 1,000 °C and the melting point of iridium. Within the limits of the precision of the pyrometer, any absorption of radiation by the vapor of IrO_2 and/or Ir produced by the heated cylinder would have been easily detected. An imperfect crucible (variation in density) is the most probable explanation for the deviation from blackbody conditions. These imperfections could cause nonuniform heating and thus result in deviation from blackbody conditions. However, nonuniform heating was not detected by the optical pyrometer when sighted on various parts of the crucible.

Because of the tendency for In_2O_3 to volatilize, it is probable that the measured melting point might actually represent the melting point of some mixture lower in In_2O_3 content than the starting composition. This error was greatly minimized by the rapid heating technique employed. Extensive volatilization of In_2O_3 was easily detected by a scoriaceous appearance of the specimen. It should be emphasized that the problem of volatilization of In_2O_3 was not as serious as had been anticipated. Weight loss data on In_2O_3 after heat treatment at 1,350 °C for 6 hr in air showed that a maximum compositional error of only about 0.25 mole percent would result for the 25

mole percent Eu_2O_3:75 mole percent In_2O_3 mixture. The error for the 50:50 composition would be even less. Furthermore, weight loss data on In_2O_3 heated to high temperatures in a manner similar to the melting point experiments indicated that additional compositional errors would not be excessive. For specimens heated to 1,730 °C and 1,900 °C the compositional error (calculated) for the 75:25 mixture would be about 0.34 mole percent and 1.02 mole percent respectively. For this system these possible errors were probably reduced even further by solid state reaction which would tend to inhibit the loss of In_2O_3. Nevertheless, considering the various errors, it is estimated that the solidus and liquidus temperatures up to about 2,000 °C, as recorded, are accurate to ±10 °C and ±20 °C, respectively. Exact estimates of the accuracy for temperatures between 2,000 and 2,300 °C are not available because of lack of calibration data. However, it is believed that the accuracy of temperatures in this range is no worse than the values previously stated for lower temperatures provided that the calibration curve can be extended above 2,000 °C. The reproducibility of results was found to be better than ±5 °C.

4. Results and Discussion

The equilibrium phase diagram for the Eu_2O_3–In_2O_3 system is given in figure 1. It was constructed from the data listed in tables 1 and 2. Only the more significant data are shown on the diagram. The difficulty in obtaining equilibrium in many mixtures as well as the inability to quench solid solutions without causing exsolution made it necessary to rely on the shape of the solidus and liquidus curves to determine the different subsolidus boundary limits.

The melting point of Eu_2O_3 was found to be 2,240 ±10 °C. The X-ray pattern of melted Eu_2O_3 was very diffuse and therefore difficult to interpret. It showed essentially only those diffraction peaks attributable to the B-type structure. Wisnyi and Pijamowski [3], using a tungsten strip furnace in a hydrogen atmosphere, determined the melting point of Eu_2O_3 as 2,050 ±30 °C. One possible explanation for the large difference in the two melting points is that Eu_2O_3 probably partially reduces to EuO in hydrogen.

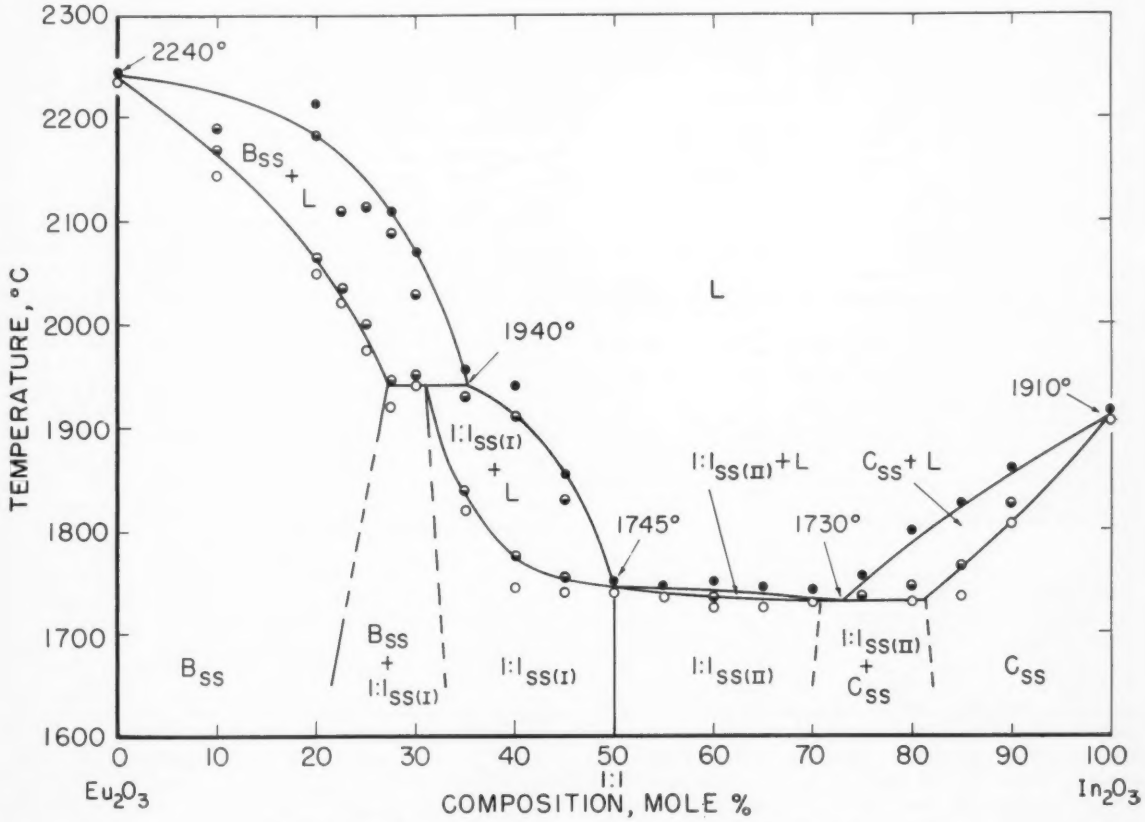

FIGURE 1. *Phase equilibrium diagram for the system* Eu_2O_3-In_2O_3.

B—Eu_2O_3, having the B-type rare earth oxide structure.
C—In_2O_3, having the C-type rare earth oxide structure.
I:I—$Eu_2O_3 \cdot In_2O_3$ compound.
L—liquid
ss—solid solution.
○—no melting.
◒—partial melting.
●—completely melted.

TABLE 1. *Experimental data for compositions in the Eu_2O_3–In_2O_3 system*

Composition		Heat treatment [2]		X-ray diffraction analyses [3]	Remarks
Eu_2O_3	In_2O_3 [1]	Temp.	Time		
Mole %	*Mole %*	°C	*hr*		
100	0	1,500	1.5	B [5]	
		2,245	—[4]	B	Specimen melted.
90	10	1,600	6	B_{ss} [5]	
		1,650	1.5	B_{ss}	
85	15	1,650	1.5	B_{ss}	
80	20	1,600	1	B_{ss}	
		1,600	6	B_{ss} [5]	
		1,650	1.5	B_{ss}	Extraneous X-ray peak at d=2.9079 A.
77.5	22.5	1,650	1.5	B_{ss}	Extraneous X-ray peaks at d=2.9079 A and 2.7684 A.
75	25	1,600	6	B_{ss}+1:1 [5]	
		1,600	1.5	B_{ss}+1:1	Extraneous X-ray peak at d=2.9079 A.
70	30	1,600	6	B_{ss}+1:1 [5]	
		1,600	1.5	B_{ss}+1:1	
65	35	1,600	2	1:1+B_{ss}	
60	40	1,600	6	1:1+B_{ss} [5]	
55	45	1,600	2	1:1+B_{ss}	
54	46	1,650	2	1:1+B_{ss}	
53	47	1,650	2	1:1+B_{ss}	
52	48	1,650	2	1:1+B_{ss}	
51	49	1,650	2	1:1+B_{ss}	
50	50	1,350	6	1:1 [5]	
		1,600	6	1:1 [5]	
		1,650	6	1:1 [5]	
		1,650	2	1:1	
		1,730	.5	1:1+B_{ss}	Specimen lost In_2O_3. Heated in Ir crucible, non-equilibrium for equimolar mixture.
49	51	1,650	2	$1:1_{ss}$	
48	52	1,650	2	$1:1_{ss}$	
47	53	1,650	2	$1:1_{ss}$	
46	54	1,650	2	$1:1_{ss}$	
45	55	1,650	1	$1:1_{ss}$+P	Nonequilibrium.
			2 [6]	$1:1_{ss}$	
40	60	1,600	1	P+$1:1_{ss}$+C_{ss}	Nonequilibrium.
		1,650	3 [6]	$1:1_{ss}$+P	Nonequilibrium.
		1,650	2	$1:1_{ss}$	
35	65	1,650	3	P+$1:1_{ss}$+C_{ss}	Nonequilibrium.
		1,650	2 [6]	$1:1_{ss}$+P	Nonequilibrium.
30	70	1,650	2	P+C_{ss}+$1:1_{ss}$	Nonequilibrium.
		1,650	3 [6]	$1:1_{ss}$+P	Nonequilibrium.
	100	1,650	6	C	
		1,905	—[4]	C	
		1,915	—[4]	C	Specimen melted.

[1] Results of experiments on compositions intermediate between 70 and 100 mole percent In_2O_3 are not included. Pt tube always failed during heat treatments, giving erroneous results.

[2] All specimens calcined at 800 °C for 20 hr and 1,350 °C for 6 hr prior to listed heat treatment. Unless otherwise noted, all specimens were quenched from indicated temperature.

[3] The phases identified are given in order of relative amount present at room temperature.
B—Eu_2O_3 having B-type rare earth oxide structure.
1:1—Eu_2O_3·In_2O_3 compound.
C—In_2O_3 having C-type rare earth oxide structure.
P—1:1 compound having perovskite-type structure.
ss—solid solution.

[4] Melting point experiment; specimen held at temperature for 15 sec; specimen not quenched.

[5] Specimen not quenched.

[6] Additional heat treatment of previous specimen.

Solid solution of In_2O_3 in Eu_2O_3 (B_{ss}) occurs from 0 to about 27 mole percent In_2O_3 at the solidus. X-ray patterns of various quenched specimens in this region contained two diffraction peaks (d= 2.9079 A and 2.7684 A) which normally are not associated with those of the B-type structure. The occurrence of the two extraneous peaks was not a consistent phenomena, thus suggesting that the peaks represent a metastable second phase. The X-ray patterns of heat treated rare earth oxides commonly show diffraction peaks attributable to rare earth oxide structures other than those of the stable phase [1]. The two extra peaks occur at d-spacings that correspond closely to the spacings of the two strongest reflections, 002 and 101, predicted for Eu_2O_3 having the hexagonal A-type (La_2O_3-type) structure. If this is the correct interpretation Eu_2O_3 apparently has a metastable A-type polymorph, not previously reported.

The phase diagram (fig. 1) was drawn to indicate a congruently melting (1,745 ±10 °C) 1:1 compound with solid solution extending on both sides of the equimolar composition. This interpretation was necessitated by the melting point data which indicated that a sharp inflection occurred in the liquidus curve at about the 1:1 composition. An alternate interpretation might be a continuous region of solid solution with a minimum close to the 65:35 composition.

The subject of a compound occurring with solid solution on both sides is amply discussed by Zernike [8]. An example of this type of phenomenon was reported by Bowen et al., [9] in the system, Fe_2SiO_4–Ca_2SiO_4. It should be noted that if a compound occurs in the middle of a solid solution region, a plot of some intensive property versus composition should show a sharp change in slope at the composition of the compound. Several experiments were performed in an attempt to find other changes in intensive properties besides the melting points. Specimen ranging in composition from $54Eu_2O_3$:$46In_2O_3$ to $46Eu_2O_3$:$54In_2O_3$ (in one mole percent increments) were prepared and quenched from 1,650 °C. X-ray analysis showed that specimens containing greater than 50 mole percent Eu_2O_3 were composed of a mixture of phases, 1:1 and B_{ss}. Those containing 50 mole percent or less of Eu_2O_3 were single phase $1:1_{ss}$. The inability to quench in the solid solution on the high Eu_2O_3 portion makes it impossible to observe a sharp change in intensive properties. It is interesting to observe that it is only the melting point data which indicates solid solution of the 1:1 compound at compositions containing greater than 50 mole percent Eu_2O_3. For compositions containing less than 50 mole percent Eu_2O_3, it is the solid state data which gives this indication. This observation, in a sense, would suggest a sharp change in intensive properties. The solid solution areas on either side of Eu_2O_3·In_2O_3 in figure 1 are labeled as $1:1_{ss(I)}$ and $1:1_{ss(II)}$ in order to delineate the expected change in intensive properties.

The single phase 1:1 solid solution areas extend from about 31 to 50 mole percent In_2O_3 and from 50 to about 71 mole percent In_2O_3 at the solidus. Apparently exsolution was extensive. Solid solution of Eu_2O_3 in the 1:1 compound amounts to less than one mole percent at room temperature.

The X-ray pattern of Eu_2O_3·In_2O_3 is given in table 3 along with the patterns of the 1:1 mixtures of Gd_2O_3–In_2O_3 and Dy_2O_3–In_2O_3[2]. All three of these phases appear to be isostructural. The structure-type has not been previously reported. The latter two phases were prepared from equimolar mixtures which had been heat treated at 1,600 °C in sealed Pt tubes.

[2] The purity of the Gd_2O_3 and Dy_2O_3 used was greater than 99.9 percent. Complete analyses are given elsewhere [2].

TABLE 2. *Melting characteristics of the* Eu_2O_3–In_2O_3 *system* [1]

Composition			Results			Composition			Results		
Eu_2O_3	In_2O_3	Temp.	No melting	Partial melting	Complete melting	Eu_2O_3	In_2O_3	Temp.	No melting	Partial melting	Complete melting
Mole %	*Mole %*	*°C*				*Mole %*	*Mole %*	*°C*			
100	0	2,110	X			60	40	1,745	X		
		2,175	X					1,775		X	
		2,235	X					1,800		X	
		2,245			X			1,805		X	
		2,280			X			1,825		X	
		2,330			X			1,840		X	
90	10	2,105	X					1,860		X	
		2,145	X					1,880		X	
		2,170		X				1,910		X	
		2,190		X				1,940			X
80	20	1,920	X			55	45	1,740	X		
		1,960	X					1,755		X	
		1,970	X					1,780		X	
		1,990	X					1,810		X	
		2,010	X					1,830		X	
		2,050	X					1,855			X
		2,065		X				1,880			X
		2,095		X				1,915			X
		2,130		X		50	50	1,730	X		
		2,170		X				1,740	X		
		2,185		X				1,750			X
		2,215			X			1,760			X
		2,230			X			1,765			X
77.5	22.5	1,940	X					1,780			X
		2,020	X			45	55	1,735	X		
		2,035		X				1,745			X
		2,110		X		40	60	1,715	X		
75	25	1,905	X					1,725	X		
		1,965	X					1,735		X	
		1,975	X					1,750			X
		2,000		X				1,795			X
		2,030		X		35	65	1,725	X		
		2,040		X				1,745			X
		2,045		X		30	70	1,680	X		
		2,055		X				1,695	X		
		2,060		X				1,705	X		
		2,085		X				1,720	X		
		2,115		X				1,725	X		
72.5	27.5	1,860	X					1,730	X		
		1,920	X					1,735		X	
		1,945		X				1,740			X
		1,955		X				1,745			X
		1,970		X				1,755			X
		1,985		X				1,780			X
		2,010		X				1,810			X
		2,025		X				1,840			X
		2,040		X		25	75	1,675	X		
		2,070		X				1,735		X	
		2,090		X				1,755			X
		2,110			X			1,770			X
70	30	1,810	X					1,780			X
		1,825	X					1,795			X
		1,840	X					1,805			X
		1,895	X					1,845			X
		1,900	X					1,855			X
		1,915	X			20	80	1,730	X		
		1,940	X					1,745		X	
		1,950		X				1,800			X
		1,965		X		15	85	1,735	X		
		1,970		X				1,765		X	
		1,975		X				1,800		X	
		2,000		X				1,825			X
		2,030		X		10	90	1,805	X		
		2,070			X			1,825		X	
65	35	1,805	X					1,860			X
		1,820	X			0	100	1,820	X		
		1,840		X				1,905	X		
		1,850		X				1,915			X
		1,855		X				1,985			(2)
		1,870		X				2,000			(2)
		1,880		X							
		1,885		X							
		1,930		X							
		1,955			X						

[1] Specimens calcined at 800 °C for 20 hr and 1350 °C for 6 hr prior to melting point determination.
[2] Specimens completely vaporized.

After further heat treatment, at 1,650 °C, only the 1:1 Dy_2O_3–In_2O_3 specimen decomposed to a mixture of B-type and C-type solid solutions. With the exception of one diffraction peak (d=1.9317A), the pattern of $Eu_2O_3 \cdot In_2O_3$ was indexed on a hexagonal basis with a_H and c_H equal to 3.69 A and 12.38 A, respectively. The other two listed patterns could not be similarly indexed with the same degree of agreement between observed and calculated $1/d^2$ values. The marked difference between the patterns of 1:1 Gd_2O_3–In_2O_3 and 1:1 Dy_2O_3–In_2O_3, and that of $Eu_2O_3 \cdot In_2O_3$ is that the corresponding 101 and 202 reflections of the former are doublets. However, the unindexed peak (d=1.9317A) of the $Eu_2O_3 \cdot In_2O_3$ pattern is present in the other two patterns. Apparently all three phases possess a lower symmetry than hexagonal. The listed parameters of $Eu_2O_3 \cdot In_2O_3$ are therefore based on a pseudocell.

TABLE 3. *X-ray diffraction powder data for Eu_2O_3-In_2O_3 and equimolar mixtures of Gd_2O_3–In_2O_3 and Dy_2O_3–In_2O_3 (CuK_α radiation)*

Eu_2O_3-In_2O_3					1:1 Gd_2O_3-In_2O_3		1:1 Dy_2O_3-In_2O_3	
hkl[a]	d[b]	$1/d^2$ obs	$1/d^2$ cal[c]	I/I_0[d]	d[b]	I/I_0[d]	d[b]	I/I_0[d]
	A				A		A	
100	3.1963	0.0979	0.0979	13	3.1739	16	3.1443	12
101	3.0940	.1045	.1044	100	3.0847	55	3.0701	30
					3.0732	60	3.0475	73
102	2.8383	.1241	.1240	100	2.8219	100	2.8004	100
103	2.5258	.1567	.1566	12	2.5135	18	2.4953	13
104	2.2222	.2025	.2022	7	2.2139	15	2.1968	12
105	1.9560	.2614	.2610	8	1.9489	20	1.9371	15
(e)	1.9317	.2680	------	3	1.9270	7	1.9178	6
110	1.8461	.2934	.2937	41	1.8332	35	1.8171	30
106	1.7338	.3326	.3326	17	1.7278	20	1.7172	21
201	1.5855	.3978	.3982	24	1.5759	26	1.5642	33
202	1.5475	.4176	.4177	17	1.5424	10	1.5335	7
					1.5384	19	1.5018	12

[a] Pseudo hexagonal Miller indices.
[b] Interplanar spacing.
[c] Based on the unit-cell parameters, a_H=3.69 A, c_H=12.38 A.
[d] Relative intensity.
[e] This peak does not fit pseudo hexagonal cell.

The occurrence of a perovskite-type compound (orthorhombic) was prevalent in mixtures that contained greater than 50 mole percent In_2O_3. Extended heat treatment of the 55 and 60 mole percent In_2O_3 specimens caused the complete disappearance of the perovskite-type compound, thus suggesting that it was metastable having no equilibrium position on the phase diagram. However, for specimens higher in In_2O_3 content than 60 mole percent, the perovskite-type phase was never completely eliminated, only reduced in amount. Failure to eliminate the perovskite phase in these specimens arose from experimental difficulties. A phase transformation of Eu_2O_3·In_2O_3 to the perovskite-type structure is not considered probable, although this must be considered as a possibility. Throughout the entire temperature range studied for the 1:1 mixture, this perovskite structure was never identified in the X-ray patterns of the various specimens.

The formation of the perovskite-type structure was not unexpected. This structure occurs in the Sm_2O_3–In_2O_3 system [10] as a stable 1:1 phase. Samarium sesquioxide (Sm_2O_3) has just slightly larger unit cell dimensions than Eu_2O_3. Evidently Sm^{+3} is the smallest rare earth ion that will form a stable perovskite-type structure with In^{+3}.

Because of experimental difficulties, all attempts to locate the exact limits of the two phase area $1{:}1_{ss(II)}+C_{ss}$ (In_2O_{3ss}) by solid state reaction were unsuccessful. It is estimated from melting point data to extend from about 71 to 81 mole percent In_2O_3 at the solidus. The eutectic occurs at 1,730 °C and about 73 mole percent In_2O_3.

The melting point of In_2O_3 was determined to be 1,910±10 °C. X-ray patterns of In_2O_3 heated to 1,905 °C and 1,915 °C showed only the diffraction peaks identifiable with cubic In_2O_3. Specimens heated to 1,985 °C and 2,000 °C completely vaporized.

5. Summary

The equilibrium phase diagram for the Eu_2O_3-In_2O_3 system was determined from a study of solid state reactions and melting point relations. The quenching technique was employed for subsolidus experiments. An inductively heated iridium crucible was used exclusively for the determination of solidus and liquidus temperatures. Phases were identified by examination of X-ray diffraction patterns.

Eu_2O_3 and In_2O_3 were found to melt at 2,240 ±10 °C and 1,910 ±10 °C respectively. The presence of extraneous diffraction peaks in X-ray patterns of several specimens containing Eu_2O_3 solid solutions indicated that Eu_2O_3 may have a metastable polymorph of the A-type rare earth oxide structure.

A sharp inflection in the liquidus curve suggested that a Eu_2O_3·In_2O_3 compound exists in the system with solid solution extending on both sides of the equimolar composition. The compound melts congruently at 1,745 ±10 °C. Its X-ray pattern was indexed on the basis of a pseudo-hexagonal cell with a_H=3.69 A and c_H=12.38 A. Isostructural phases have been found at the equimolar mixtures in the Gd_2O_3-In_2O_3 and Dy_2O_3-In_2O_3 systems. A eutectic occurs in the Eu_2O_3-In_2O_3 system at 1,730 °C and about 73 mole percent In_2O_3.

Thanks to R. S. Roth, E. M. Levin, and C. R. Robbins for their many helpful suggestions.

6. References

[1] R. S. Roth and S. J. Schneider, Pt. I, J. Research NBS **64A**, 309–316 (1960).
[2] S. J. Schneider and R. S. Roth, Pt. II, J. Research NBS **64A**, 317–332 (1960).
[3] L. G. Wisnyi and S. Pijanowski, U.S. Atomic Energy Comm. Report, KAPL-1564 (1956); G. L. Ploetz, C. W. Krystyniak and H. E. Dumas, J. Am. Ceram. Soc. **41**, 551–554 (1958).
[4] L. Brewer, Chem. Rev. **52**, 1–76 (1953).
[5] Handbook of Chemistry and Physics, 40th ed., 585, Chem. Rubber Publ. Co., Cleveland (1958).
[6] V. M. Goldschmidt, T. Barth, and G. Lunde, Skrifter Norske Videnskaps-Akad. Mat. Natur. Kl. No. 7, **28** (1925).
[7] D. T. Cromer, J. Phys. Chem. **61**, 753 (1957).
[8] J. Zernike, Chemical Phase Theory, 227–228, Kluwer's Publ. Co., Deventer-Netherlands (1955).
[9] N. L. Bowen, J. F. Schairer, and E. Posnjak, Am. J. Sci., 5th Ser. **25**, 273–297 (1933).
[10] R. S. Roth, J. Research NBS **58**, 75–88 (1957) RP2736.

(Paper 65A5–123)

JOURNAL OF RESEARCH of the National Bureau of Standards—A. Physics and Chemistry
Vol. 65A, No. 5, September–October 1961

Heats of Hydrolysis and Formation of Dimethoxychloroborane

Marthada V. Kilday, Walter H. Johnson, and Edward J. Prosen

(June 7, 1961)

The heat of hydrolysis of dimethoxychloroborane has been measured; for the reaction,
$(CH_3O)_2BCl(liq)+3H_2O(liq)=H_3BO_3(c)+2CH_3OH(liq)+HCl(g)$
$\Delta H(25\ °C)=-26.6\pm0.8$ kj/mole
$=-6.4\pm0.2$ kcal/mole.
From this, we have calculated the heat of formation of dimethoxychloroborane: for the liquid, $\Delta Hf°(25\ °C)=-782.1\pm1.8$ kj/mole (-186.9 ± 0.4 kcal/mole), and for the gas, $\Delta Hf°(25\ °C)=-747.9\pm2.2$ kj/mole (-178.8 ± 0.5 kcal/mole).

1. Introduction

Heats of formation for the three ethoxy derivatives of boron trichloride have been determined [1, 2];[1] however, in the series of methoxy derivatives, the heat of formation of only trimethoxyborane (or methyl borate) has been reported [1]. As part of the program at the National Bureau of Standards for determining thermochemical properties of boron-containing compounds, we have measured the heat of hydrolysis of liquid dimethoxychloroborane. From this, we have calculated values for the heats of formation of liquid and of gaseous dimethoxychloroborane; we have also estimated a value for the heat of formation of gaseous methoxydichloroborane.

2. Materials and Apparatus

The sample of dimethoxychloroborane (DMCB) was purified by fractional crystallization.[2] Freezing-point measurements indicated a purity of about 95 percent DMCB.[2]

Trimethoxyborane (or methyl borate) is believed to be the principal impurity in the sample for three reasons. First, its boiling point, 68.7 °C [3], is near that of dimethoxychloroborane, 74.7 °C [3], and the two might distill simultaneously. The boiling point of methoxydichloroborane, 58 °C, is sufficiently removed that distillation should provide a satisfactory separation. Second, the sample was probably the product of reaction between boron trichloride and methyl alcohol where methoxy substitution for one, two, or three chlorine atoms occurs depending on the mole ratios of the reactants [3]; therefore, methyl borate might be present in small amounts. The third reason is that titrations of the product of hydrolysis of the sample in water indicate an average of 99.5 percent by weight of the boron and only 92.6 percent by weight of the chlorine expected if the sample were pure DMCB. Thus, the impurity contained approximately the same amount of boron per gram as DMCB and essentially no chlorine; this is true of methyl borate. If the 5 mole percent impurity found from freezing-point measurements were methyl borate, the analysis would be 100.2 percent of boron and 95.2 percent of chlorine.

Further information about the composition of the impurity was sought and two methods for determining carbon in the sample were employed. In the first method, a DMCB sample was burned in an oxygen bomb; the CO_2 in the combustion products was absorbed by Ascarite and weighed. In the second method, a C-H ratio was determined from combustion in a tube furnace.[3] Unfortunately, the results of both methods were inconclusive because of the limitations and uncertainties imposed by the presence of chlorine and boron in the sample, and by the fact that the amount of impurity was small.

The sample used in determining the heat of solution of crystalline boric acid was obtained by the recrystallization from aqueous solution of analytical-grade boric acid. The sample was air-dried at room temperature and placed in spherical Pyrex-glass bulbs which were then evacuated at approximately 10^{-5} mm of Hg pressure and room temperature for 6 hr to remove surface moisture before sealing. It is interesting to note that this long exposure to reduced pressure apparently did not cause decomposition of the H_3BO_3, since the ratios of the weight of H_3BO_3 titrated in the final calorimetric solutions to the weight of sample were 0.997, 1.005, 0.993, and 0.997.

Glass ampoules are generally desirable sample containers in solution calorimetry, but they were unsatisfactory for the DMCB samples because the reaction became so violent upon breaking the ampoule that the calorimetric solution was spattered and the gaseous products were lost before being dissolved. Even when only the capillary tip of the ampoule was broken, enough water was drawn into the bulb by the partial vacuum to produce an explosion.

[1] Figures in brackets indicate the literature references at the end of this paper.
[2] Pure Substances Section of the Chemistry Division.
[3] Analytical Chemistry Section of the Chemistry Division.

A satisfactory reaction rate was achieved when the sample was enclosed in a monel cylinder (capsule) with a diaphragm of Mylar [4] film closing both ends. The reaction started when the film was pierced with a nichrome needle.

The capsule which contained the samples during calorimetric experiments is shown in figure 1. The capsule, capsule-holder, and lower end of the puncture-rod were made of Monel to resist attack by hydrochloric acid formed in the reaction of the DMCB with water. The upper end of the puncture-rod was made of polystyrene to minimize heat leakage from the calorimeter. The lower end of the Monel rod was cut at an angle of 30° and the edge was sharp for cutting the Mylar diaphragms. A nichrome needle, 1-mm diam, was attached at the center of the lower end of the Monel rod; vertical grooves in the rod permitted the displacement of liquid as the rod entered the capsule. The Monel plate, or cap, at each end of the cylindrical capsule was held in place by three Monel screws. A Mylar diaphragm, 0.025-mm thickness, and a polyethylene gasket, 0.13-mm thickness, closed the cylinder at each end; the cylinder was sealed when the screws were tightened. The lower end of the capsule-holder was threaded so that the capsule could be attached to it easily and securely; several holes in the walls of the holder permitted circulation of the calorimetric solution.

[4] Trademark.

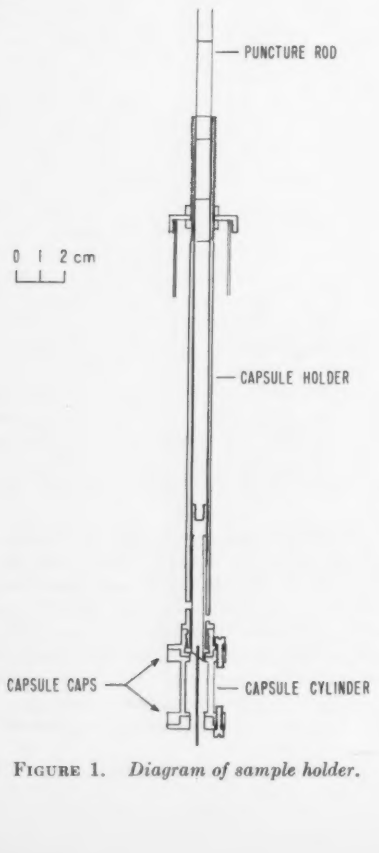

FIGURE 1. *Diagram of sample holder.*

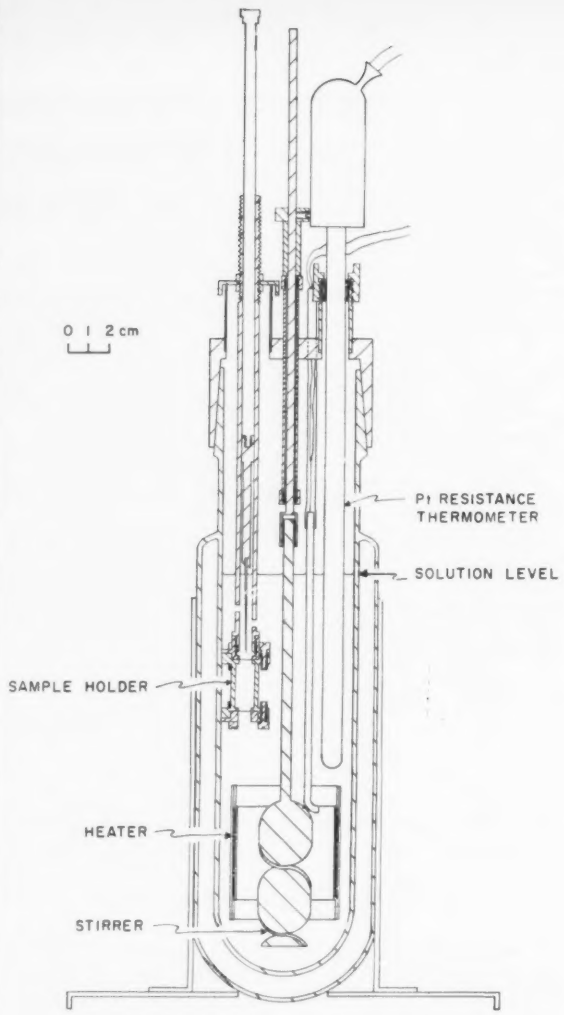

FIGURE 2. *Diagram of solution calorimeter.*

The solution calorimeter is shown in figure 2. The body of the vessel is Pyrex glass with a standard-taper, ground-glass joint at the top and a silvered vacuum-jacket. The cap is nickel-plated brass with gas-tight fittings for a stirrer, a platinum resistance thermometer, a capsule-holder, two heater-leads, and a gas exit-tube (not shown). The stirrer-support and shaft are stainless steel with two Teflon bearings, and the portion of the stirrer in contact with the solution is Pyrex glass. The stirrer was driven by a motor at approximately 500 rpm.

The brass case for the calorimeter heater consisted of an inner cylinder with ⅛-inch tubes for leads welded inside on opposite sides of the cylinder (only one lead-tube is shown), and an outer-cylinder which was a tight fit over the inner cylinder; the walls of the case are approximately ¼-mm thickness. The lacquered manganin heater wire, No. 36 B and S

gage, of 121-ohm resistance was non-inductively wound over a thin sheet of mica covering the depression on the inner cylinder, and a second sheet of mica was placed between the wire and the outer cylinder. The two rims of the case were soft-soldered and flashed with copper; then the entire assembly, including the two lead-tubes, was plated with gold to a minimum thickness of 0.08 mm. Above the solution level the lead-tubes were attached to glass tubing with a DeKhotinsky cement. A pair of copper leads, for current and potential measurements, extended from each lead-tube.

The calorimeter was immersed in a water bath in which the temperature, approximately 26.8 °C, varied by not more than ±0.002 °C during an experiment. The bath, temperature controls, and method of measuring electrical energy during calibrations have been described previously [4,5].

Measurements of the current and voltage across the heater were made alternately with a Wenner potentiometer at 2-min intervals; i.e., the current was measured on the first minute, the voltage on the second, etc. Temperature measurements were made with a calibrated platinum resistance thermometer which was enclosed in a glass sheath and had a resistance at 0 °C of 25.473 ohms; the resistance was measured with a Leeds and Northrup G-2 bridge in conjunction with a high-sensitivity galvanometer.

3. Experimental Procedures

Portions, weighing 1.0 to 1.5 g, of the DMCB sample were distilled under vacuum into glass ampoules which were then sealed and stored at −15 °C. These ampoules were made of Pyrex-glass tubing, 7-mm diam and 100-mm long, with a scratch around the middle to facilitate breaking later. The sample occupied about one-third of the total volume of the ampoule.

Before a calorimetric experiment, a sample was transferred from a glass ampoule to the Monel capsule (fig. 1). All parts of the capsule including the diaphragms and gaskets were carefully weighed before placing them in a dry box containing a helium atmosphere.[5] The top gasket, diaphragm, cap, and screws were assembled; then the capsule was inverted and screwed onto a support which facilitated subsequent manipulations. The glass ampoule containing the sample was broken at the scratch, and the sample was poured through a funnel into the cylinder. The second diaphragm, gasket, and cap were assembled, and the screws were tightened sealing the capsule.

A minimum time elapsed between removing the capsule from the dry box and weighing it, to reduce errors resulting from exchange of helium and air through the Mylar diaphragms. When the capsule contained a sample of DMCB, there was a gain in weight of about 0.2 mg during the first hour, and 0.1 mg or less during the second hour; the balance case was saturated with water vapor at 25 °C. However, when the capsule contained liquid water, and the atmosphere of the balance was dried by anhydrous magnesium perchlorate, no change in weight was observed during a period of more than 2 hr. Therefore, we concluded that the Mylar diaphragms were, for the requirements of this work, impervious to moisture. The gain in weight observed when the capsule contained the sample, was apparently the result of exchanging helium with air and of adsorption of moisture on the capsule after removing it from the dry box. The weighing errors involved were less than 0.1 percent of the sample weight.

For the hydrolysis of the DMCB the calorimeter contained 450 g of distilled water (25 moles). An electrical calibration preceded each chemical reaction. Each experiment included a 20-min equilibration period, a 20-min initial rating period, a 20-min calibration period which included 9 min of electrical heating, a 20-min middle rating period, a 20-min chemical reaction period, and a 20-min final rating period. Temperatures were recorded at 2-min intervals during the three rating periods, and at 1-min intervals during the calibration and chemical reaction periods.

Five marks on the upper end of the puncture-rod (fig. 1) indicated various fixed positions used during the calorimetric experiments. The lowest mark was at the initial position where the needle was not in contact with the capsule. To start the reaction, only the top diaphragm was pierced with the nichrome needle. After 1 min the puncture-rod was pushed down to the point where the needle punctured the bottom diaphragm. On the third minute the rod was withdrawn to the initial position, and the following minute both diaphragms were again pierced and the needle again withdrawn to the initial position. On the fifth minute the top diaphragm was cut out by the sharp edges on the Monel puncture-rod; the bottom diaphragm was cut out on the sixth minute. Thus, when the rod was returned to its initial position, the calorimetric solution was free to circulate through the capsule. Most of the reaction occurred as the bottom diaphragm was first punctured with the needle, but the reactions were never as violent as when the samples were contained in glass ampoules.

The final calorimetric solutions were titrated with 0.1*N* sodium hydroxide solution to determine the amounts of hydrochloric acid and of boric acid. End points were taken from curves obtained by plotting the volume of standard alkali solution versus *p*H as measured on a Beckmann *p*H meter. The first end point, occurring at *p*H 5.6, indicated the volume of sodium hydroxide equivalent to the HCl. D-Mannitol was then added to the solution forming a complex with the boric acid and increasing its acidity; a second titration curve was obtained with an end point at *p*H 7.6 which indicated the volume of alkali equivalent to the boric acid.

[5] The helium atmosphere was used only because of its availability at the time; a nitrogen atmosphere would have eliminated the small errors resulting from exchange of gases through the Mylar film.

4. Data and Discussion

Results of the dimethoxychloroborane (DMCB) hydrolysis experiments are given in table 1. E_a is the energy equivalent of the initial system as determined in an electrical calibration which preceded the chemical reaction. ΔRc is the temperature rise measured during the chemical reaction period and corrected for cooling and stirring energies as described by Prosen [6]. In the 4th column are the weights *in vacuo* of the DMCB samples; the buoyancy factor was calculated using 1.2 g/ml as the density of the samples. This density is an approximation obtained from weights of samples contained in spherical glass bulbs of known volumes; it is believed to be within 10 percent of the correct value.

The number of moles of HCl and of H_3BO_3 given in the table were obtained from the titrations of the DMCB hydrolysis solutions. In DMCB the chlorine and boron are equiatomic, but the titrations indicated about 7 mole percent less HCl than H_3BO_3. To eliminate loss of chlorine by evaporation as a possible cause for the low value obtained in the titrations, the following experiment was performed. A sample of DMCB in a thin glass bulb, 150 ml of water, and a monel weight for crushing the bulb were placed in a bomb ordinarily used for oxygen combustions. The bomb was tightly closed, then shaken vigorously to break the bulb and to dissolve the gaseous products in the water. The resulting solution was titrated immediately. Two such experiments yielded 0.0212 mole HCl and 0.0226 mole H_3BO_3, and 0.0162 mole HCl and 0.0175 mole H_3BO_3, respectively; the HCl was 6 and 7 mole percent less than the H_3BO_3. Therefore, the chlorine deficiency in the products of hydrolysis was assumed to result from an impurity in the DMCB sample.

As mentioned previously, we have reason to suspect that the principal impurity was methyl borate. It fulfills the above requirements of a lower chlorine content than DMCB, and almost the same molecular weight, and has a slightly lower boiling point than DMCB. There is some evidence of fractionation of the sample as may be seen by inspection of table 1. The Sample Number indicates the order in which the calorimetric samples were distilled from the main sample. (Samples 4 and 5 were two small samples which were combined for one calorimetric experiment.) The weight percents given in the table are the ratios of the weight of the element found in titration to the weight of the sample. The weight percent of chlorine tends to increase with each sample while the weight percent of boron remains constant; this we would expect as a greater proportion of the more volatile impurity is transferred in the first portions distilled.

Reduction of the data from the calorimetric experiments given in table 1 was made with the following assumptions:

1. Methyl borate was the only impurity in the samples.
2. The number of moles of methyl borate was equal to the difference between the number of moles of HCl and the number of moles H_3BO_3 titrated in the hydrolysis solutions.
3. The number of moles of DMCB was equal to the number of moles of HCl found by titration of the hydrolysis solutions.

For conversion to the thermochemical calorie the relation, 1 thermochemical calorie=4.1840 joules was used. The atomic weights used are from the 1957 International Table of Atomic Weights [7].

The heat contributed by the methyl borate impurity, q_{MB}, is the product of the number of moles of methyl borate and the heat of hydrolysis of methyl borate, 18.01 kj/mole, measured by Charnley, Skinner, and Smith [1]. The following equation was used to obtain the heats of reaction:

$$\Delta H(26.8\ ^\circ\mathrm{C})=\frac{E_a(\Delta Rc)-q_{MB}}{\text{HCl titrated}\times 1000}.$$

No correction was made for the energy required to break the Mylar diaphragms because it was found to be of the order of 0.2 joule which was near the limit of detection.

The mean value for the heat of reaction, ΔH(26.8 °C)=−94.77 kj/mole or −22.65 kcal/mole, has been converted to 25 °C by use of $\Delta Cp=51$ cal/mole °C obtained from the following estimated heat capacity and apparent molal heat capacities: $(CH_3O)_2BCl$ (liq), 40 cal/mole °C; H_3BO_3 in final solution, 30 cal/mole °C; HCl in final solution, −27 cal/mole °C; and CH_3OH in final solution, 20 cal/mole °C. Thus for the reaction,

TABLE 1. *Data for the dimethoxychloroborane hydrolysis experiments*

Expt. no.	E_a	ΔRc	Wt. of sample	HCl titrated	H_3BO_3 titrated	Sample no.	Cl	B	Methyl borate	q_{MB}	$-\Delta H$(26.8 °C)
	j/ohm	*Ohm*	*g*	*Mole*	*Mole*		*wt. %* (Theor., 32.72)	*wt. %* (Theor., 9.99)	*Mole*	*j*	*kj/mole*
1	21,200.6	0.023544	0.59815	0.005187	0.005520	10	30.75	9.99	0.000333	5.99	95.08
2	21,224.2	.040068	1.04074	.008906	.009572	6	30.34	9.95	.000666	11.99	94.14
3	21,229.7	.034277	0.88547	.007502	.008182	7	30.04	10.00	.000680	12.24	95.37
5	21,232.5	.039942	1.05143	.008847	.009640	4–5	29.83	9.92	.000793	14.28	94.25
6	21,238.6	.030793	0.78938	.006817	.007174	8	30.62	9.83	.000357	6.43	94.99
Mean											94.77
Standard deviation of the mean											±0.24

$$(CH_3O)_2BCl(liq)+3H_2O(liq)=[H_3BO_3+HCl+2CH_3OH](3000H_2O)$$

$$\Delta H(25\ °C)=-94.39\pm0.75\ kj/mole$$

$$=-22.56\pm0.18\ kcal/mole. \quad (1)$$

The uncertainty of about 1 percent was assigned to this value to include the experimental reproducibility and analytical errors as well as the uncertainties introduced by unidentified impurities and possible polymerization products.

To derive the heat of formation of DMCB from the heat of hydrolysis, it is necessary to know the heats of formation of CH_3OH, H_3BO_3, H_2O, and HCl and to employ the heats of three auxiliary reactions: (1) the heat of solution of crystalline boric acid, (2) the heat of solution of HCl gas in boric acid solution, and (3) the heat of solution of methyl alcohol in the solution of boric acid and hydrochloric acid.

The heat of solution of crystalline boric acid has been measured in several laboratories [8, 9, 10, 11, 12]; as there is disagreement in the results reported, we made four determinations at 25 °C. The data for these experiments are given in table 2, where the number of moles of H_3BO_3 was calculated from the titration of the final solutions. Thus we obtain for the reaction:

$$H_3BO_3(c)=H_3BO_3(1900\ H_2O)$$

$$\Delta H(25\ °C)=+21.94\ \pm0.16\ kj/mole$$

$$=\ +5.24\ \pm0.04\ kcal/mole.^6 \quad (2)$$

TABLE 2. *Data for the boric acid solution experiments*

Experiment	ΔRc	$-Q^*$	H_3BO_3	$\Delta H(25\ °C)$
	Ohm	*j*	*Mole*	*kj/mole*
1	−0.011518	243.95	0.011223	21.737
2	−.013709	290.36	.013133	22.109
3	−.015882	336.38	.015347	21.918
4	−.014360	304.14	.013830	21.991
Mean				21.939
Standard deviation of the mean				±0.078

*Electrical energy equivalent = 21,180 j/ohm.

The uncertainty is taken as twice the standard deviation of the mean of the experimental values.

The heat of solution of gaseous hydrochloric acid in boric acid solution was not determined. However, the heat of dilution of concentrated hydrochloric acid (37.39% HCl) in $0.014M$ H_3BO_3 solution was measured in four experiments. The result was the same as for comparable dilution in water. We, therefore, assumed that the heat of solution of gaseous hydrochloric acid in 0.019M H_3BO_3 solution is equal to the heat of solution of gaseous hydrochloric acid in water [13] as follows:

$$HCl(g)+H_3BO_3(3000\ H_2O)=[HCl+H_3BO_3]\ (3000\ H_2O)$$

$$\Delta H(25\ °C)=-17.95\ kcal/mole. \quad (3)$$

The heat of solution of methyl alcohol in a solution $0.014M$ in boric acid and $0.012M$ in HCl was also measured and found to be equal to the heat of solution of methyl alcohol in water at infinite dilution [13]. Thus, we assume

$$2CH_3OH(liq)+[H_3BO_3+HCl](3000\ H_2O)=[H_3BO_3+HCl+2CH_3OH](3000\ H_2O)$$

$$\Delta H°(25\ °C)=-3.50\ kcal/mole. \quad (4)$$

By subtracting the sum of eqs (2, 3, and 4) from eq (1), we obtain

$$(CH_3O)_2BCl\ (liq)+3H_2O\ (liq)=H_3BO_3(c)+2CH_3OH\ (liq)+HCl(g)$$

$$\Delta H°(25\ °C)=-26.57\pm0.79\ kj/mole$$

$$=-\ 6.35\pm0.19\ kcal/mole. \quad (5)$$

The uncertainty assigned to this value is taken as the square root of the sum of the squares of the individual uncertainties involved in the calculations. Estimated uncertainties of ±0.02 kcal/mole were assigned to reactions 3 and 4.

To calculate the heat of formation of DMCB we used for crystalline boric acid, $\Delta Hf°(25\ °C)=-262.16$ kcal/mole derived from the value for the heat of formation of boric oxide based on crystalline boron obtained by Prosen, Johnson, and Pergiel [4]. The heats of formation at 25 °C of the other compounds were taken from [13]: CH_3OH(liq), −57.02 kcal/mole; HCl(g), −22.019 kcal/mole; and H_2O (liq), −68.317 kcal/mole. Combining these with the heat of reaction (5) we obtained for the heat of formation of liquid dimethoxychloroborane

$$\Delta Hf°(25\ °C)=-782.07\ \pm1.84\ kj/mole$$

$$=-186.92\ \pm0.44\ kcal/mole.$$

The uncertainties considered here include that of reaction (5), ±0.32 kcal/mole for the boric acid, ±0.1 kcal/mole for the methyl alcohol, ±0.02 kcal/mole for the hydrochloric acid, and ±0.010 kcal/mole for the water. The uncertainty given is the square root of the sum of the squares of the individual uncertainties.

The heat of vaporization at 25 °C was calculated from the data of Wiberg and Sutterlin [3] as 8.17± 0.30 kcal/mole. This leads to the following value for the heat of formation of gaseous dimethoxychloroborane;

$$\Delta Hf°(25\ °C)=-747.89\ \pm2.18\ kj/mole$$

$$=-178.75\ \pm0.52\ kcal/mole.$$

[6] Smisko and Mason [10] found no significant change in the heat of dilution between 500 and 5000 moles of water per mole of boric acid; therefore, we assume the value given in equation (2) is the same as for the dilution, 3000 H_2O per mole of H_3BO_3.

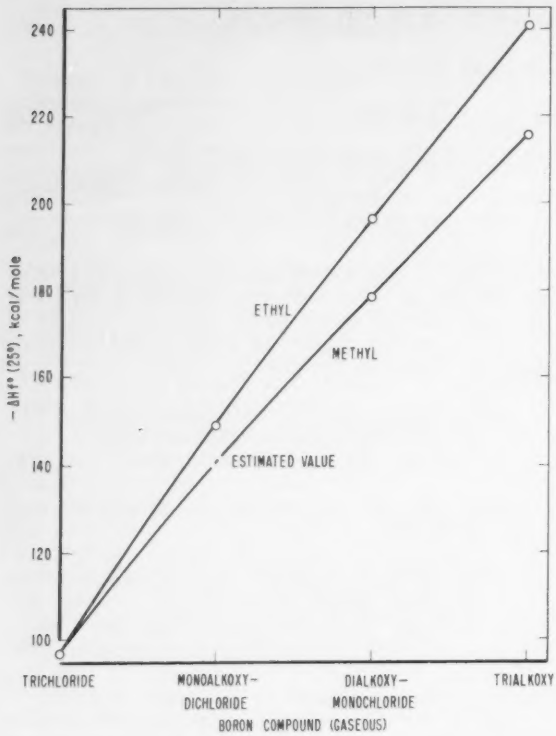

FIGURE 3. *Heats of formation of gaseous alkoxy derivatives of boron trichloride.*

TABLE 3. *Heats of formation of some of the gaseous alkoxy derivatives of boron trichloride*

Compound	$-\Delta Hf°$ (25 °C) (gas)
	kcal/mole
BCl_3	97. 11 [14]
$(CH_3O)BCl_2$	(141. 0)*
$(CH_3O)_2BCl$	178. 8 ±0.5
$(CH_3O)_3B$	215. 7 [1]
$(C_2H_5O)BCl_2$	149. 6 [2]
$(C_2H_5O)_2BCl$	196. 4 [2]
$(C_2H_5O)_3B$	240. 8 [1]

*The value in parentheses is an estimate.

5. Conclusions

Since no value for the heat of formation of dimethoxychloroborane has been reported previously, we can only compare our value with those for other compounds in the same family; i.e., the methoxy and ethoxy derivatives of boron trichloride. These values are given in table 3 and plotted in figure 3. The differences between the ethoxy and the methoxy substitutions are reasonably consistent. One-third of the difference between the values for the trialkoxy derivatives is 8.4 kcal/mole, and one-half of the difference between the values for the dialkoxy derivatives is 8.8 kcal/mole. The difference between the values for the monoalkoxy derivatives is therefore taken as 8.6 kcal/mole. This yields 141.0 kcal/mole for the heat of formation at 25 °C of gaseous methoxydichloroborane.

We wish to acknowledge the fine machine work done on the metal parts of this calorimeter by Herbert B. Lowey.

6. References

[1] T. Charnley, H. A. Skinner, and N. B. Smith, J. Chem. Soc. **1952,** 2288.
[2] H. A. Skinner and N. B. Smith, J. Chem. Soc. **1954**, 3930.
[3] E. Wiberg and W. Sutterlin, Z. anorg. u. allgem. Chem. **202,** 1 (1931).
[4] E. J. Prosen, W. H. Johnson, and F. Y. Pergiel, J. Research NBS **62,** 43 (1959) RP2927.
[5] W. H. Johnson, A. A. Gilliland, and E. J. Prosen, J. Research NBS **63A,** 161 (1959).
[6] E. J. Prosen, Chapter 6, F. D. Rossini, ed., Experimental thermochemistry (Interscience Publishers, Inc., New York, N.Y., 1956).
[7] E. Wichers, J. Am. Chem. Soc. **80,** 4121 (1958).
[8] W. A. Roth and E. Börger, Ber. **70B,** 48 (1937); W. A. Roth, E. Börger, and A. Bertram, Ber. **70B,** 971 (1937).
[9] W. A. Roth, Z. Naturforsch. **1,** 574 (1946).
[10] J. Smisko and L. S. Mason, J. Am. Chem. Soc. **72,** 3679 (1950).
[11] E. R. Van Artsdalen and K. P. Anderson, J. Am. Chem. Soc. **73,** 579 (1951).
[12] M. von Stackelberg, F. Quatram, and J. Dressel, Z. Elektrochem. **43,** 14 (1937).
[13] F. D. Rossini, D. D. Wagman, W. H. Evans, S. Levine, and I. Jaffe, Selected values of chemical thermodynamic properties, NBS Circular 500 (U.S. Government Printing Office, Washington 25, D.C., 1952).
[14] W. H. Johnson, R. G. Miller, and E. J. Prosen, J. Research NBS **62,** 213 (1959) RP2956.

(Paper 65A5—124)

JOURNAL OF RESEARCH of the National Bureau of Standards—A. Physics and Chemistry
Vol. 65A, No. 5, September–October 1961

Tritium-Labeled Compounds VII. Isotope Effects in the Oxidation of D-Mannitols-C^{14} and D-Mannitols-*t* to D-Fructoses[1]

Lorna T. Sniegoski,[2] Harriet L. Frush, and Horace S. Isbell

(May 17, 1961)

D-Mannitols, labeled either with carbon-14 at C1, C2, or C3, or with tritium attached to C1, C2, or C3, were prepared. After oxidation by *Acetobacter suboxydans*, the distribution of radioactivity in each of the resulting labeled D-fructoses was determined. Labeled D-mannitol is unique among the hexitols in that it may be oxidized by *A. suboxydans* in either the labeled or the unlabeled part of the molecule. Except in the oxidation of D-mannitol-*2-t*, the competing reactions result in the formation of a mixture of D-fructoses, each having radioactivity in one of two different positions. Hence, the isotope effect, k^*/k, (where k^* and k are, respectively, the rate constants for oxidation in the labeled and in the unlabeled part of the labeled D-mannitol molecule) is the ratio of the activities at the two positions of the product, D-fructose.

The following isotope effects were found for the bacterial oxidation of labeled D-mannitols: (1) for D-mannitol-*2*-C^{14}, $k^*/k=0.93$; (2) for D-mannitol-*2-t*, $k^*/k=0.23$; and (3) for D-mannitol-*3-t*, $k^*/k=0.70$. For D-mannitols labeled at other positions, no isotope effect was detected, since k^*/k was unity. The large isotope-effect for D-mannitol-*2-t* is indicative of rupture of the C2—H bond in the rate-determining process. It is suggested that the secondary isotope-effect for tritium at C3 indicates hyperconjugation of the C3 hydrogen atom in the activated enzyme—substrate complex; the lack of such effect for tritium at C1 may be due to unfavorable steric conditions for hyperconjugation of the C1 hydrogen atoms in the complex.

The following substances were prepared and their isotopic distributions determined: D-fructose-*1,6*-C^{14} and D-fructose-*1,6-t* (from 1-labeled D-mannitols); D-fructose-*2,5*-C^{14} and D-fructose-*5-t* (from 2-labeled D-mannitols); and D-fructose-*3,4*-C^{14} and D-fructose-*3,4-t* (from 3-labeled D-mannitols). A procedure, employing D-fructose-*1,6*-C^{14} as an internal standard, was devised for the analysis of D-fructose-*3,4-t*.

1. Introduction and Discussion

The burgeoning use of radioisotopes as tracers for studying chemical and biological reactions makes desirable the determination of differences in the behavior of radioactive and nonradioactive atoms. Although the chemical properties of isotopes are essentially the same, certain differences in *rates* of reaction are found, especially when the isotope is directly involved in a rate-determining step [1].[3] The ratio of the rates of reaction of the labeled and the unlabeled molecules, the isotope effect, is associated with the differences in mass. Carbon-14, the most useful and versatile radioisotope for the study of organic reactions, has a mass 1.167 times that of carbon-12. Isotope effects in the reactions of C^{14}-labeled materials are small, and are frequently neglected. However, the radioisotope tritium, having a mass about three times that of hydrogen, produces isotope effects of considerably greater magnitude. Such effects may lead to errors if ignored; nevertheless, they provide a valuable means for studying reaction mechanisms, by indicating whether or not a tritium bond is involved in the rate-determining step of a reaction.

The oxidation of D-mannitol (I) to D-fructose by *Acetobacter suboxydans* is particularly suitable for the study of isotope effects. *A. suboxydans* is highly specific for the oxidation of the penultimate hydroxyl group of any compound having the structure

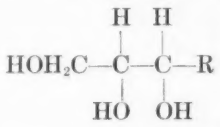

in the D-series [2]. D-Mannitol is unique among the hexitols, because each of the two identical three-carbon portions of the molecule is in the

[1] Part of a project on the production of radioactive carbohydrates, sponsored by the Division of Research of the Atomic Energy Commission.
[2] Abstracted from a thesis submitted by Lorna T. Sniegoski to the University of Maryland in June 1960, in partial fulfillment of the requirements for the degree of Doctor of Philosophy. The authors are indebted to the late Professor Nathan L. Drake for helpful advice and discussions. Portions of this work were presented before the 138th National Meeting of the American Chemical Society, New York, N.Y., September 1960, and at a symposium on The Detection and Use of Tritium, held by the International Atomic Energy Agency, Vienna, Austria, May 1961.
[3] Figures in brackets indicate the literature references at the end of this paper.

requisite steric arrangement for oxidation by *A. suboxydans*. Thus, in the unlabeled molecule, oxidation can take place equally well at C2 or C5. When one three-carbon portion of the molecule is labeled with either carbon-14 or tritium in any of its three positions, the organism can attack either the labeled or the unlabeled portion. If there is no isotope effect, the product will be an equimolecular mixture of the D-fructoses (II) and (III)[4], with the radioactivity in the mixture equally divided between two positions. However, if the presence of the radioisotope affects the rate of oxidation, there will be unequal distribution of the radioactivity, a result which can be used for quantitatively evaluating the isotope effect.

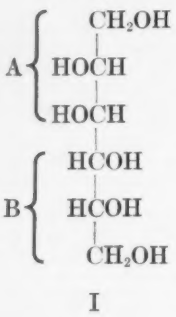

I

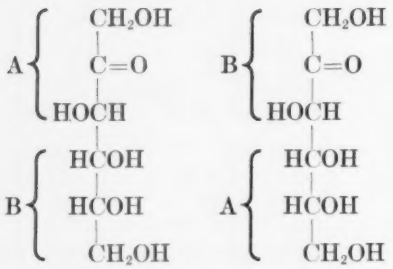

II III

Previously, D-mannitol-*1-C*^{14} had been oxidized by *A. suboxydans* to D-fructose-*1,6-C*^{14} [3], and the isotopic distribution in the latter compound had been determined [4].[5] In the present study, D-mannitols labeled either with carbon-14 at C1, C2, or C3, or with tritium attached to C1, C2, or C3, were prepared and were then oxidized by *A. suboxydans*. The resulting labeled D-fructoses were isolated, the isotopic distributions were determined, and the isotope effects were calculated. In the course of the work, methods were developed for determining isotopic distribution; these methods include the use of D-fructose-*1,6-C*^{14} as an internal standard in the assay of tritium-labeled D-fructoses.

[4] Unit A in formulas II and III is derived from the same part of the D-mannitol molecule; the same is true of unit B.

[5] In previous papers from this laboratory, the alternative designation of the position of the label in a labeled D-mannitol was given in parentheses, e.g., D-mannitol-*1(6)-C*^{14}. In this and subsequent papers in the series, the parenthetical number will be omitted. The oxidation product of D-mannitol-*1-C*^{14} contains two singly-labeled species, namely, D-fructose-*1-C*^{14} and D-fructose-*6-C*^{14}, and is designated D-fructose-*1,6-C*^{14} (see formulas I, II, and III).

Tables 1 and 2 summarize the isotope effects determined for the bacterial oxidation of C^{14}- and tritium-labeled D-mannitols. It is evident that, in the oxidation of D-mannitols labeled at C2, tritium causes a large isotope effect and carbon-14 a small one. There is also an isotope effect for tritium attached to C3; it is relatively small compared to that at C2, but is larger than the effect of carbon-14 at C2. The oxidation of the remaining three alditols was unaffected by the presence of the isotope. Thus, although *A. suboxydans* has specific steric requirements for the groups attached to a chain of three carbon atoms, an isotope effect is detectable only when carbon-14 is at C2 or when tritium is attached to either C2 or C3.

Although the biological oxidation may be a complicated process, the high yield of a single product suggests an oxidation step that is relatively simple. If the cleavage of the C2—H bond is rate-determining,

TABLE 1. *Isotope effect in the bacterial oxidation of five position-labeled* D-*mannitols; analysis of isotopic distribution in the resulting* D-*fructoses*

	Carbon atoms of original D-fructose [a]	Average fraction of the activity of original D-fructose, %	Isotope effect, k^*/k, in D-mannitol oxidation
D-Mannitol-*1-C*^{14}			
D-Fructose-*1,6-C*^{14}	1*, 2, 3, 4, 5, 6		
↓	1, 2, 3, 4, 5, 6*		
D-"Glucose" phenylosotriazole (IV)	1*, 2, 3, 4, 5, 6	100.0	
↓	1, 2, 3, 4, 5, 6*		
4-Formyl-2-phenylosotriazole (V)	1*, 2, 3	49.8	0.99
Formaldehyde-dimedon compound (VII)	6*	50.1	
D-Mannitol-*2-C*^{14}			
D-Fructose-*2,5-C*^{14}	1, 2*, 3, 4, 5, 6		
↓	1, 2, 3, 4, 5*, 6		
D-"Glucose" phenylosotriazole	1, 2*, 3, 4, 5, 6	100.0	
↓	1, 2, 3, 4, 5*, 6		
4-Formyl-2-phenylosotriazole	1, 2*, 3	48.4	
Potassium D-arabonate-*1,4-C*^{14} (VI)	2*, 3, 4, 5, 6		
↓	2, 3, 4, 5*, 6		
Benzimidazole from D-arabonic-*1,4-C*^{14} acid (VIII)	2*, 3, 4, 5, 6	(100.0)	0.93
	2, 3, 4, 5*, 6		
D-Erythritol-*3-C*^{14} (IX)	3, 4, 5*, 6	52.1	
↓			
D-Erythritol-*3-C*^{14} tetrabenzoate	3, 4, 5*, 6		
D-Mannitol-*3-C*^{14}			
D-Fructose-*3,4-C*^{14}	1, 2, 3*, 4, 5, 6		
↓	1, 2, 3, 4*, 5, 6		
D-"Glucose" phenylosotriazole	1, 2, 3*, 4, 5, 6	100.0	0.99
↓	1, 2, 3, 4*, 5, 6		
4-Formyl-2-phenylosotriazole	1, 2, 3*	49.7	
D-Mannitol-*1-t*			
D-Fructose-*1,6-t*	1*, 2, 3, 4, 5, 6	100.0	1.02
↓	1, 2, 3, 4, 5, 6*		
Potassium D-arabonate-*5-t*	2, 3, 4, 5, 6*	49.5	
D-Mannitol-*2-t*			
D-Mannitol-*2-t*	1, 2*, 3, 4, 5, 6	100.0	0.23
↓	1, 2, 3, 4, 5*, 6		
D-Fructose-*5-t*	1, 2, 3, 4, 5*, 6	81.6	

[a] Position of radioactive atom indicated by *.

TABLE 2. *Isotope effect in the bacterial oxidation of* D-*mannitol-3-t; use of the "double-label" technique in the analysis of isotopic distribution in* D-*fructose-3,4-t*

Compound analyzed	Radioactivity after successive recrystallizations		Ratio t/C^{14}	Isotope effect, k^*/k, in D-mannitol oxidation [a]
	t	C^{14}		
D-Fructose-*3,4-t-1,6-*C^{14}	$\mu c/mg$ 0.0210 0.0207	$\mu c/mg$ 0.00278 0.00281		
Avg	0.0209	0.00280	7.46	0.70
D-Erythrono-1,4-lactone-*2,4-*C^{14} (X)	0.0253 0.0258	0.00296 0.00288		
Avg	0.0256	0.00292	8.76	

[a] $k^*/k=(2\rho^\circ-\rho)/\rho$.

a large isotope-effect would be expected in the oxidation of D-mannitol-*2-t*, and a smaller one in the oxidation of D-mannitol-*2-*C^{14}. The observed effects are in accordance with this expectation.

The secondary isotope-effect found for tritium at C3 is relatively large, and shows that the C3—H bond is involved, in some manner, in the rate-determining step. The effect may be attributed to hyperconjugation similar to that postulated to explain the effect of β-deuterium atoms on the rate of solvolysis of certain deuterated alkyl compounds [5, 6, 7]. Thus, if the C3—H bond of the activated enzyme–substrate complex had partial "no-bond" character, the labeled and unlabeled complexes would differ in the extent of stabilization arising from hyperconjugation. Because a carbon–tritium bond is stronger than a carbon–hydrogen bond, the enzyme–substrate complex labeled with tritium at C3 of the alditol would be less stabilized by hyperconjugation and have greater energy of activation than its unlabeled counterpart. Therefore, in accordance with the experimental results, the rate of reaction would be lower for the labeled than for the unlabeled complex.

Solely on the basis of the above mechanism, there should also be an isotope effect for tritium at C1; this should be less than that at C3, because C1, with tritium attached, bears a hydrogen atom also. The absence of such an effect is surprising and may be indicative of a heretofore unrecognized steric factor in the reaction mechanism. Evidence has been advanced by others that the extent of hyperconjugation depends, to some degree, on the orientation of the C—H bond [7]. Inasmuch as the atoms in the activated enzyme–substrate complex are, presumably, oriented in a definite conformation, it seems possible that steric conditions are favorable for hyperconjugation of the hydrogen atom at C3, but unfavorable at C1.

2. Evaluation of the Isotope Effect in the Bacterial Oxidation of Labeled D-Mannitols to Labeled D-Fructoses

The isotope effect causes changes in the isotopic composition of both substrate and product as a reaction proceeds [1, 8]. Evaluation of the effect is complicated by the dependence of the isotopic composition on the extent of the reaction. Labeled molecules of D-mannitol contain *two* possible sites which will compete in the bacterial oxidation; at (or near) one of these sites there is an isotopic atom. Thus, in labeled D-mannitol, the isotope effect is manifested in two different ways, namely, (a) by intermolecular differences in the overall oxidation rates of labeled and unlabeled molecules, and (b) by intramolecular competition for oxidation. The latter isotope effect can be formulated, somewhat arbitrarily, as the ratio k^*/k, where k^* and k are, respectively, the overall rate constants for oxidation of the labeled and unlabeled portions of the labeled molecules of D-mannitol. (See page 47 of ref 1.) This ratio is constant during the reaction and independent of changes in isotopic composition caused by the intermolecular effect.

Because the labeled substrate simultaneously forms two products by competitive reactions, it follows from the law of mass action that

$$P_A/P_B=k^*/k \tag{1}$$

where P_A and P_B are, respectively, the amounts (in millimoles) of the labeled products, D-fructose (II) and D-fructose (III), formed by oxidation at C2 and C5, respectively, of the labeled molecules of D-mannitol. If n millimoles of total D-fructose are formed, then (except in the oxidation of D-mannitol-*2-t*)

$$[A]_A=P_A\phi/n \tag{2}$$

where $[A]_A$ is the amount of radioactivity of C1, C2, or C3 per millimole of the total product, and ϕ is the amount of radioactivity of one milliatom of tritium or carbon-14. Similarly,

$$[A]_B=P_B\phi/n \tag{3}$$

where $[A]_B$ is the amount of radioactivity of C4, C5, or C6 per millimole of the total product. It follows from eqs (1), (2), and (3) that

$$[A]_A/[A]_B=P_A/P_B=k^*/k. \tag{4}$$

In the oxidation of D-mannitols labeled with carbon-14 at C1, C2, or C3, or with tritium attached to C1 or C3, the isotope effect, k^*/k, was calculated, by means of eq (4), from values of $[A]_A$ and $[A]_B$ determined from the distribution analysis.

In the oxidation of D-mannitol-*2-t*, the tritium is removed when oxidation occurs at C2, and the products of the oxidation are nonradioactive D-fructose and D-fructose-*5-t*. If $[A]_M$ is the amount of radioactivity per millimole of D-mannitol-*2-t*, then the molar activity *lost* at C2 (which is a measure of the oxidation at this point) is $[A]_M-[A]_B$. Hence, from eq (4),

$$\frac{[A]_M-[A]_B}{[A]_B}=P_A/P_B=k^*/k. \tag{5}$$

The isotope effect in the oxidation of D-mannitol-*2-t* was calculated by means of eq(5)[6] from the molar activities of D-mannitol-*2-t* and D-fructose-*5-t*.

3. Methods for Determining Isotopic Distribution in Labeled D-Fructoses

The procedures devised for the isotopic analysis of the three C^{14}-labeled D-fructoses are given in table 1. The general method, common to all three analyses, involves the cleavage of the molecule between C3 and C4. D-Fructose was converted to D-"glucose" phenylosotriazole (IV) which, by oxidation, yielded 4-formyl-2-phenylosotriazole (V), formic acid, and formaldehyde. The molar activity of V is that of the portion of D-fructose including C1, C2, and C3, and the difference between the molar activities of IV and V is the molar activity of the portion including C4, C5, and C6. This method was supplemented by the analysis of C6 of D-fructose-*1,6-*C^{14}, and of compounds formed from fragments of D-fructose-*2,5-*C^{14}.

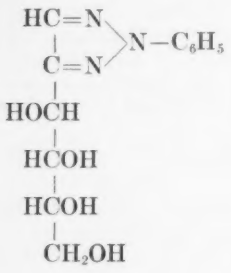

IV

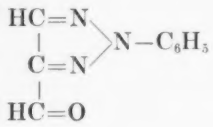

V

The carbon-14 in D-fructose-*1,6-*C^{14} prepared by the method used here was previously reported by Frush and Isbell [4] to be equally and exclusively distributed between C1 and C6. Their analysis was based on the molar radioactivities of D-fructose-*1,6-*C^{14} and of two oxidation products, namely, potassium D-arabonate-*5-*C^{14} (VI) and formaldehyde-C^{14}; the latter was derived from C5 of the potassium D-arabonate-*5-*C^{14} and isolated as the dimedon compound (VII). The isotopic distribution of D-fructose-*1,6-*C^{14}, determined in the present study by the method given in table 1, is in accord with the previous conclusion.[7]

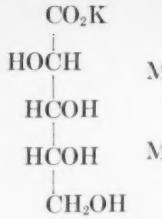

VI

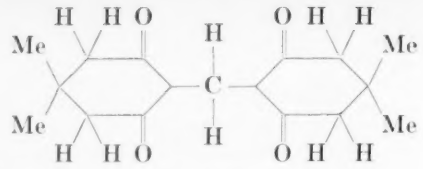

VII

D-Fructose-*2,5-*C^{14} was analyzed by the general method, supplemented by additional procedures given in table 1.[8] The sugar was degraded to potassium D-arabonate-*1,4-*C^{14}, the assay of which was confirmed by that of the corresponding benzimidazole (VIII). Potassium D-arabonate-*1,4-*C^{14} was also degraded to D-erythrose-*3-*C^{14}, which was analyzed both as the reduction product, D-erythritol-*3-*C^{14} (IX),[9] and the corresponding tetrabenzoate.

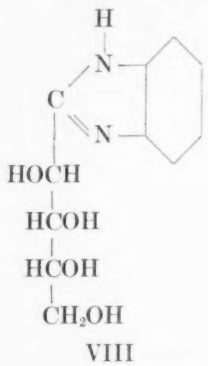

VIII

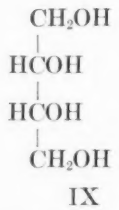

IX

D-Fructose-*3,4-*C^{14} was assayed only by the general method, which determines the radioactivity collectively at the unit of C1, C2, and C3, and at the unit of C4, C5, and C6. This assay was considered adequate, because the prior analysis [4] of D-fructose-*1,6-*C^{14} had shown that there is no redistribution of radioactivity in the molecule by fragmentation and resynthesis.

The procedures used for the isotopic analysis of the three tritium-labeled D-fructoses are outlined in tables 1 and 2. The distribution of tritium in D-fructose-*1,6-t* was determined from the radioassay of this substance and that of the potassium D-arabonate-*5-t* derived from it. The isotope effect in the oxidation of D-mannitol-*2-t* was calculated by means of eq (5) from the relationship between the activity of the D-mannitol-*2-t* and that of the oxidation product, D-fructose-*5-t*.

The isotopic analysis of D-fructose-*3,4-t* required the following reactions: oxidation of D-fructose-*3,4-t* to potassium D-arabonate-*2,3-t;* degradation of this to D-erythrose-*1,2-t;* and oxidation of D-erythrose-*1,2-t* to D-erythrono-1,4-lactone-*2-t* (X), the product

---

[6] The isotope effect in the oxidation of five of the six labeled D-mannitols used in this study can be determined from the ratio of the activity at two positions in the total product. However, during the oxidation of D-mannitol-*2-t*, the intermolecular isotope effect causes alteration in the activity of the D-fructose-*5-t* because of the more rapid oxidation of the unlabeled D-mannitol. Therefore, eq (5) applies only at the completion of the reaction, at which time the intermolecular isotope-effect disappears.

[7] Brice and Perlin [9], also, have studied the distribution of carbon-14 in D-fructose-*1,6-*C^{14} and have found "no significant contamination of the inactive carbon atoms with C^{14}."

[8] A brief summary of the analysis of D-fructose-*1,6-*C^{14} and D-fructose-*2,5-*C^{14} is given in ref 10.

[9] This erythritol is asymmetric because of the isotope at C3.

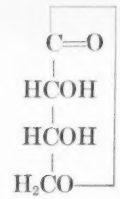

X

analyzed. Because the yield from this series of reactions was low, a new technique was devised for facilitating the analysis. D-Fructose-*1,6-*C^{14} (which is *equally labeled* at C1 and C6) was added to the D-fructose-*3,4-t*, and this mixture was recrystallized and treated as described above. The isotopic distribution in the D-fructose-*3,4-t* was calculated by the following method.

If the D-fructose-*3,4-t-1,6-*C^{14} contains P_A+P_B millimoles of tritium-labeled D-fructose, the activity due to tritium is $P_A\phi_t+P_B\phi_t$; where ϕ_t is the activity of a milliatom of tritium. The activity due to carbon-14 is $2P_F\phi_C$, where P_F is the amount (in millimoles) of *either* D-fructose-*1-*C^{14} or D-fructose-*6-*C^{14}, and ϕ_C is the activity of a milliatom of carbon-14. In the corresponding D-erythrono-1,4-lactone-*2-t-4-*C^{14}, the activity due to tritium is $P_B\phi_t$, and the activity due to carbon-14 is $P_F\phi_C$. Then

$$\rho^\circ=\frac{P_A\phi_t+P_B\phi_t}{2P_F\phi_C} \tag{6}$$

and

$$\rho=\frac{P_B\phi_t}{P_F\phi_C} \tag{7}$$

where ρ° and ρ are, respectively, the tritium–carbon-14 ratios in the D-fructose and the corresponding D-erythrono-1,4-lactone. It follows from eqs (6) and (7) that

$$P_A/P_B=(2\rho^\circ-\rho)/\rho=k^*/k. \tag{8}$$

The isotope effect in the oxidation of D-mannitol-*3-t* was calculated from the analytical data by means of eq (8). This method permits the use of a nonradioactive carrier at any step in the analysis, because the calculation depends only on the *ratios* of tritium to carbon-14.

4. Experimental Procedures

4.1. Preparation of Labeled D-Mannitols

D-Mannitol-*1-*C^{14} and D-mannitol-*2-*C^{14} were prepared by the sodium borohydride reduction [11] of D-mannono-1,4-lactone-*1-*C^{14} [12] and D-mannono-1,4-lactone-*2-*C^{14} [13], respectively. D-Mannitol-*1-t* and D-mannitol-*2-t* were prepared by the reduction of D-mannono-1,4-lactone and D-fructose, respectively, with tritiated lithium borohydride [14]. D-Mannitol-*3-*C^{14} was prepared from D-glycerose by three successive cyanohydrin syntheses, in the first of which, sodium cyanide-C^{14} was used. The D-erythrono-1,4-lactone-*1-*C^{14} obtained in the first step was converted to D-erythrose-*1-*C^{14} by catalytic reduction of tri-*O*-acetyl-D-erythronyl-*1-*C^{14} chloride [15, 16] and subsequent deacetylation. By methods analogous to those devised for the synthesis of D-mannono-1,4-lactone-*2-*C^{14}, D-erythrose-*1-*C^{14} was converted to D-arabinose-*2-*C^{14}, and this, in turn, to D-mannono-1,4-lactone-*3-*C^{14}. Finally, the lactone was reduced to D-mannitol-*3-*C^{14} [11].

D-Mannitol-*3-t* was prepared by the following series of reactions: D-Arabonic acid $\xrightarrow[(V_2O_5+NaClO_3)]{\text{oxidation [17]}}$ D-*erythro*-pentulosonic acid (2-keto-D-arabonic acid) $\xrightarrow[(LiBH_4\text{-}t)]{\text{reduction}}$ {D-arabonic-*2-t* acid, D-ribonic-*2-t* acid} $\longrightarrow$ D-arabono-1,4-lactone-*2-t* $\xrightarrow[(NaHg_x)]{\text{reduction}}$ D-arabinose-*2-t* $\xrightarrow[(NaCN)]{\text{cyanohydrin synthesis}}$ D-mannono-1,4-lactone-*3-t* $\xrightarrow[(NaBH_4)]{\text{reduction}}$ D-mannitol-*3-t*.

The experimental details for the preparation of D-mannitol-*3-*C^{14} and D-mannitol-*3-t* will be published in subsequent papers from this laboratory.

4.2. Bacterial Oxidation of Labeled D-Mannitols and Preparation of Labeled D-Fructoses

The labeled D-mannitols were oxidized with a culture of *Acetobacter suboxydans*[10] which was maintained as follows: Agar slants were prepared from 10-ml aliquots of an aqueous solution containing, by weight, 0.5 percent of yeast extract, 0.3 percent of peptone, 1.5 percent of agar, and 5.0 percent of D-mannitol. After being sterilized and cooled, these slants were streaked with *A. suboxydans* and kept at 30 °C for 24 to 48 hr; if not used at once, the organism was stored at 5 to 10 °C and transferred about once a month.

Inoculum for the oxidations was prepared from a broth containing 1 g of yeast extract, 0.6 g of potassium dihydrogen phosphate, and 3.64 g of D-mannitol in 200 ml of aqueous solution. Portions (25 ml) of the broth were measured into 125-ml Erlenmeyer flasks and sterilized. *A. suboxydans* was introduced from a slant, and the flasks were kept at 30 °C. After 48 hr, a satisfactory growth had occurred, and the inoculum was ready for use.

All oxidations of D-mannitol were conducted in 50-ml Erlenmeyer flasks, each containing 1 mmole of D-mannitol, 50 mg of yeast extract, 30 mg of potassium dihydrogen phosphate, and 10 ml of water. The solutions were sterilized and cooled. Five drops of inoculum were added to each solution with a sterile pipet, and the cultures, after gentle mixing, were kept at 30 °C in an incubator.

[10] Obtained from Dr. N. K. Richtmyer, National Institutes of Health, Bethesda, Md.

Oxidations were performed first with unlabeled D-mannitol under the conditions just described, in order to determine the time required for optimal yields of D-fructose. At suitable time-intervals, the preparations were deproteinized [18] by the addition of 1 ml of a 0.7-*M* aqueous solution of zinc sulfate, and neutralization (to the phenolphthalein end-point) with a saturated aqueous solution of barium hydroxide. The precipitate was removed by filtration through a layer of paper pulp and purified diatomaceous earth, the filtrate was diluted to 100 ml in a volumetric flask, and 1-ml aliquots were analyzed for total reducing-substance[11] by the Somogyi method [19].

Oxidations of the *labeled* D-mannitols were then conducted by the above procedure. Simultaneously with a labeled material, nonradioactive controls were oxidized, and the progress of the oxidation was followed by analysis of the controls. When the total reducing-substance in the controls was approximately the same as the maximum found previously, the product from the labeled D-mannitol was deproteinized, filtered, de-ionized by passage through mixed cation- and anion-exchange resins,[12] and finally freeze-dried. The residue was dissolved in 2 ml of anhydrous methanol containing a drop of acetic acid, and the solution was filtered through decolorizing carbon into a standard-tapered test tube and concentrated at 30 °C under diminished pressure.[13] Addition of methanol and evaporation were repeated several times; finally, the sirup was dissolved in methanol, 2-propanol was added to incipient turbidity, and the solution was nucleated with crystalline D-fructose. Additional 2-propanol was added from time to time, as the crystallization proceeded. The mother liquor was removed from the crystals with a capillary pipet, and the crystals were washed with a mixture of methanol and 2-propanol and dried in a vacuum desiccator. The labeled D-fructose was recrystallized from methanol by the addition of 2-propanol. Additional crops were obtained from the mother liquor by the use of nonradioactive D-fructose as a carrier. The total radiochemical yield was 70 to 75 percent.

In the oxidation of D-mannitol-*2-t*, it was necessary to avoid the introduction of unlabeled D-mannitol with the inoculum, and also to isolate and purify the D-fructose-*5-t* without carrier, because the isotopic distribution was determined from the relative molar activities of these two labeled compounds. For this oxidation, the inoculum was treated as follows: A 25-ml portion was centrifuged, and the supernatant liquor was decanted from the precipitated bacteria. The precipitate was mixed with 10 ml of a sterile, 0.15-*M* aqueous solution of potassium chloride, and the suspension was centrifuged. The liquid was again decanted, and the rinsing process was repeated. Finally, the bacteria were suspended in 20 ml of the potassium chloride solution, and each of the solutions containing D-mannitol-*2-t* was inoculated with five drops of this suspension. The remainder of the procedure was the same as that used with the other labeled D-mannitols.

Before analysis, the D-fructoses were chromatographically pure, as indicated by radioautographs or scans of chromatograms developed in 1-butanol–acetic acid–water (4:1:5 v/v, upper phase) and in 2-butanone–acetic acid–water saturated with boric acid (9:1:1) [20]. Each labeled D-fructose except D-fructose-*5-t* was diluted with nonradioactive D-fructose to a specific activity convenient for the analysis, and the mixture was recrystallized. The C^{14}-labeled D-fructoses used for analysis had activities of about 0.01 μc/mg, and the tritium-labeled D-fructoses, 0.2 to 0.3 μc/mg. For the isotopic analysis of D-fructose-*3,4-t*, a mixture of this compound and D-fructose-*1,6-C*^{14} was prepared, recrystallized, and analyzed for both tritium and carbon-14 (see table 2 and section 3).

4.3. Preparation of Compounds Used in the Isotopic Analysis of Labeled D-Fructoses

4.3.1. "D-Glucose" Phenylosotriazole (IV) [21, 22]

A solution of the labeled D-fructose (250 mg, 1.39 mmole) in 10 ml of water, contained in a 50-ml, round-bottomed flask, was treated with one drop of acetic acid and 0.45 ml (4.56 mmole) of phenylhydrazine, and allowed to stand at room temperature for 20 min. Sodium acetate trihydrate (250 mg) and acetic acid (0.5 ml) were then added, and the solution was heated in a boiling-water bath for 30 min, treated with 5 ml of water, and kept at about 5 to 10 °C for 2 hr. Crystalline D-glucose phenylosazone was remove by filtration and washed with a little water. The osazone, transferred to a 200-ml round-bottomed flask, was refluxed for 1 hr with 30 ml of 2-propanol and a solution of 1 ml of 6-*N* sulfuric acid and 1.5 g of copper sulfate pentahydrate in 45 ml of water. The hot mixture was filtered through a layer of purified diatomaceous earth and decolorizing carbon, and the filtrate was concentrated under diminished pressure to about 15 ml. The triazole, which crystallized readily, was separated by filtration, washed with water, and dried in a vacuum desiccator; the yield was about 75 mg (20%). After three or four recrystallizations from ethanol,[14] the radioactivity was constant; the molecular radioactivity serves as a check on that of the original labeled D-fructose.

4.3.2. 4-Formyl-2-phenylosotriazole (V) [21]

Labeled D-glucose phenylosotriazole (80 mg, 0.30 mmole) and sodium metaperiodate (277 mg, 1.3

[11] In their preparation of D-fructose-*1,6-C*^{14}, Isbell and Karabinos [3] determined both the total reducing-substance and the D-fructose (the latter by polarization at two temperatures). They showed that the maxima for the two occur at approximately the same time. In the present study, oxidations were stopped when the total reducing-substance was at a maximum (80 percent). The time required for the oxidation was usually about 45 hr.

[12] Amberlite IR 120-H, Rohm and Haas Co., Philadelphia, Pa., and Duolite A4, Chemical Process Co., Redwood City, Calif. The effluent was tested for ionic impurities by means of a conductivity meter (supplied by Barnstead Still and Sterilizer Co., Boston, Mass).

[13] Evaporations in test tubes are conveniently carried out in a Rotary Evapomix, a product of Buchler Instruments, New York, N.Y.

[14] The semimicro recrystallizations carried out in this study were conducted in small test-tubes. In some cases, the mother liquor was removed, and the crystals were washed, in place, by means of a capillary pipet.

mmole) in 12 ml of water, in a glass-stoppered test-tube, were mechanically shaken for 24 hr, during which time the appearance of the crystals changed. The crystalline product, 4-formyl-2-phenylosotriazole, was separated and dissolved in the minimal amount of warm ethanol; after filtration through decolorizing carbon, the solution was concentrated to a small volume under a stream of nitrogen, and treated with water to incipient turbidity. When crystallization was complete, the compound was separated, washed with ice water, and dried in a desiccator. The yield, after two recrystallizations from warm ethanol by the addition of water, was 65 to 70 percent, and the specific radioactivity was constant.

4.3.3. Potassium D-Arabonate (VI) [4]

A solution of labeled D-fructose (360 mg, 2 mmoles) in 10 ml of water was frozen on one part of the wall of a heavy-walled flask, and 10 ml of 2-*M*, aqueous potassium hydroxide was frozen on another part. The flask was immediately attached to a Parr apparatus, evacuated, filled with oxygen at a pressure of 10 psi, and shaken for 24 hr at room temperature. The solution was then diluted with 300 ml of methanol, nucleated with a minute quantity of crystalline potassium D-arabonate, and stored in the refrigerator for 24 hr. The mother liquor was decanted from the crystals, which adhered to the wall of the flask, and the crystals were washed with methanol and dissolved in a few milliliters of water. The solution was filtered into a standard-tapered test-tube, concentrated in a stream of nitrogen to about 3 ml, and diluted with methanol to incipient turbidity. After crystallization was complete, about 260 mg, or 64 percent, of potassium D-arabonate had separated. This was slowly recrystallized several times by storing an aqueous solution of the material in a desiccator containing anhydrous calcium sulfate and a beaker of methanol. Large, pure crystals separated in the course of 1 or 2 days. The activity was constant after three recrystallizations. The molar activity was checked by the preparation and assay of the derived benzimidazole.

4.3.4. Benzimidazole From D-Arabonic Acid (VIII) [23]

Potassium D-arabonate (90 mg, 0.44 mmole) was combined in a test-tube with *o*-phenylenediamine hydrochloride (80 mg, 0.44 mmole), and 0.3 ml of a solution prepared from 4 ml of water, 1 ml of ethanol, and 0.85 ml of concentrated hydrochloric acid. The mixture was heated in an oil bath at 135 °C for 2 hr; during the first hour, 50-percent aqueous ethanol was added, at intervals, in order to prevent evaporation to dryness. Finally, the residue was dissolved in 0.5 ml of water, and the solution was filtered through decolorizing carbon. When the filtrate and washings were diluted with water to about 1.5 ml and made just alkaline with dilute ammonium hydroxide, crystallization of the derivative occurred. The crystals were separated and washed, successively, with ethanol, acetone, and ether. The benzimidazole derivative (about 92 mg or 87%) was recrystallized once from hot methyl Cellosolve (2-methoxyethanol) and once from 50-percent aqueous ethanol.

4.3.5. D-Erythritol-3-C^{14} (IX)

Potassium D-arabonate-*1,4*-C^{14} (300 mg, 1.47 mmoles, prepared from D-fructose-*2,5*-C^{14}) was dissolved in 7.5 ml of water, and 0.3 ml of an aqueous solution of barium acetate (9 g/100 ml), 0.3 ml of an aqueous solution of ferrous sulfate (9.2 g of heptahydrate/100 ml), and 0.15 ml of 30-percent hydrogen peroxide were added [24]. The mixture was kept at 45 °C for 90 min, again treated with 0.15 ml of hydrogen peroxide, and allowed to stand at 45 °C for another hour. The mixture was then filtered through a small amount of decolorizing carbon, and the filtrate was passed through 15 ml of mixed cation- and anion-exchange resins. The effluent, containing D-erythrose-*3*-C^{14}, was concentrated under diminished pressure to a sirup.

A solution of the sirup in 15 ml of water was cooled in an ice bath and stirred with a magnetic stirrer. Freshly prepared, 0.3-*M*, aqueous sodium borohydride (30 ml) was added dropwise from a buret, and stirring of the ice-cold solution was continued for 90 min. A small amount of cation-exchange resin was then added, and the solution was passed through a column containing 15 ml of the resin; the effluent was concentrated under diminished pressure to a thin sirup. In order to remove boric acid as methyl borate, the sirup was dissolved in methanol, and the solvent was distilled under diminished pressure; after this process had been repeated several times, the sirup crystallized. The yield of crude D-erythritol-*3*-C^{14} was 124 mg (69%).

A solution of the crude material in ethanol and water was filtered through decolorizing carbon and concentrated under diminished pressure to a sirup. The D-erythritol-*3*-C^{14} was then recrystallized to constant activity from the minimal amount of hot ethanol by the addition of 2-propanol to incipient turbidity. The molar radioactivity was checked by the preparation and radioassay of D-erythritol-*3*-C^{14} tetrabenzoate.

4.3.6. D-Erythritol-3-C^{14} Tetrabenzoate

A solution of D-erythritol-*3*-C^{14} (80 mg, 0.66 mmole) in 2 ml of pyridine, contained in a 50-ml flask having a magnetic stirrer, was cooled in an ice bath. Benzoyl chloride (1 ml, 8.6 mmoles) was added, and the mixture was stirred in the ice bath for several hours, allowed to stand overnight at room temperature, and treated with ice water which precipitated a sirup; this was successively washed with water, 5-percent aqueous sodium carbonate, and water. Upon addition of ethanol, the sirup crystallized; the crystals were separated and recrystallized to constant radioactivity from methyl Cellosolve.

4.3.7. Formaldehyde–Dimedon Compound (VII) [4]

A mother liquor, that remained after a preparation of 4-formyl-2-phenylosotriazole from D-fructose-*1*,

6-C^{14} by the method of section 4.3.2, theoretically contained about 0.5 mmole of C^{14}-labeled formaldehyde in 20 ml of water. An aqueous solution of sodium bisulfite was added dropwise to this solution, in an amount just sufficient to remove the iodine that first appeared. (As the end-point was approached, a dilute solution of the bisulfite was used.) The mixture was then neutralized (to the end-point of methyl orange) by the dropwise addition of a solution of sodium bicarbonate. To the reaction mixture was added 5 ml of an aqueous solution containing 182 mg of sodium bicarbonate and 182 mg (1.30 mmole) of dimedon (5,5-dimethyl-1, 3-cyclohexanedione). The formaldehyde–dimedon compound crystallized readily; it was separated, washed with water, and recrystallized by dissolving it in the minimal amount of hot methyl Cellosolve, filtering the solution through decolorizing carbon, and adding an equal volume of water. Recrystallization was repeated until the specific radioactivity was constant.

4.3.8. D-Erythrono-1,4-Lactone-*2-t-4*-C^{14} (X)

D-Fructose-*3,4*-t-*1,6*-C^{14} (181 mg, 1.0 mmole having a tritium/carbon-14 ratio of 7.46) was degraded by the procedure described in section 4.3.3 to yield 144 mg (70.2%) of potassium D-arabonate-*2,3-t-5*-C^{14}. A 133-mg sample of this compound was degraded to D-erythrose-*1,2-t-4*-C^{14} by the procedure of section 4.3.5. The sirupy D-erythrose (39 mg, 0.33 mmole) so obtained was dissolved in 1.5 ml of water, and the solution was cooled in an ice bath. Barium benzoate dihydrate (215 mg, 0.52 mmole) and bromine (0.020 ml, 0.39 mmole) were added, and the mixture was shaken until all of the bromine had dissolved; it was then allowed to stand overnight at room temperature [25]. Excess bromine was removed by the addition of a small amount of decolorizing carbon, and the mixture was filtered. To the filtrate was added 122 mg (0.30 mmole) of nonradioactive barium D-erythronate. An aqueous solution of silver sulfate (156 mg, 0.5 mmole) was added, and the precipitate of silver bromide and barium sulfate was removed by filtration. The solution was then passed through a column of cation-exchange resin (10 ml), the effluent extracted with chloroform, and the aqueous solution concentrated under reduced pressure to a sirup. Absolute ethanol was added, and the solution was again concentrated; this process was repeated several times. Finally, the sirup was moistened with absolute ethanol, nucleated with D-erythrono-1,4-lactone, and stored in a desiccator for several days, during which time, crystallization of D-erythrono-1,4-lactone-*2-t-4*-C^{14} occurred. The compound (74 mg) was recrystallized from absolute ethanol.

In order to obtain D-fructose-*3,4-t-1,6*-C^{14} at a level of activity suitable for radioassay, a portion of the D-fructose-*3,4-t-1,6*-C^{14} used in the oxidative degradation was diluted with the unlabeled compound and recrystallized. Both the D-fructose-*3,4-t-1,6*-C^{14} and the D-erythrono-1,4-lactone-*2-t-4*-C^{14} were analyzed by the method described in section 4.4, and, from the tritium/carbon-14 ratios (ρ° and ρ, respectively), k^*/k was calculated by eq (8). The results are given in table 2.

4.4 Radioassay of Carbon-14 and Tritium

All measurements of radioactivity were made with a windowless, gas-flow, proportional counter by methods described in prior publications from this laboratory. The same procedures, equipment, and reagents were used in the determination of the molar activities of any group of compounds which were to be compared.

Samples containing carbon-14 (only) were dissolved in formamide, *N,N*-dimethylformamide, or ethylene glycol, and counted from a layer of solution that was "infinitely thick" to the radiation [26]; in each individual assay, the sample was counted to at least 10,000 counts. The activities of the C^{14}-labeled compounds were calculated from the relationship:

$$A = amk \qquad (9)$$

where A is the activity, in microcuries, of the sample counted; a, the observed counts per second (cps) corrected for background; m, the combined weight, in grams, of the solute and solvent; and k, an empirically determined constant, which, with the equipment used, was 2.39×10^{-3} μc cps^{-1} g^{-1}. The calculation is illustrated by the following: A 9.625-mg sample of a compound having a molecular weight of 265.3 was dissolved in 1 ml (1.133 g) of formamide; the solution gave 31.48 cps. The activity in the sample was $31.48\times1.143\times2.39\times10^{-3}$, or 0.0860 μc, corresponding to $(0.0860/9.625)\times265.3$ or 2.37 μc/mmole.

Samples containing tritium (only) were assayed in the proportional counter in films that were infinitely thick to the radiation [27]. In each assay, five films, from aliquots of the same solution, were prepared on planchets; each film was counted to at least 10,000 counts, and the average value was used. Activities of tritium-labeled compounds were also calculated by means of eq (9). For these compounds, A is the activity, in microcuries, of the film; a is the observed cps; m is the weight, in milligrams, of the film; and k, with the equipment used, is 4.45×10^{-5} μc cps^{-1} mg^{-1}. Thus, a 0.5060-mg sample of a compound with a molecular weight of 182.2, in a film weighing 20.22 mg, gave 123.27 cps. The activity in the sample was $123.27\times20.22\times4.45\times10^{-5}$, or 0.1109 μc; this corresponds to $(0.1109/0.5060)\times182.2$, or 39.9 μc/mmole.

Samples containing *both* tritium and carbon-14 were also assayed in films [28]. The films were counted both with and without a screen of 1/4-mil, double-aluminized Mylar,[15] which completely stops the radiation from tritium, but admits a portion of that from carbon-14 to the sensitive area of the counting chamber. By means of empirically determined counting-efficiencies, the amount of carbon-14

[15] Supplied by Hastings and Co., Inc., Philadelphia, Pa.

was calculated from the difference between the counts without and with the screen.

The activity of carbon-14 in the sample is given by the relationship:

$$A_C = \frac{a'}{3.7 \times 10^4 E'_m} \tag{10}$$

where A_C is the radioactivity, in microcuries, of the carbon-14 in a film of weight m, and E'_m and a', respectively, are the counting efficiency of carbon-14 and the cps observed, both with the screen in place; 3.7×10^4 is the disintegration rate (in. dps) per microcurie. The activity of tritium in the sample is calculated from the following relationship, in which allowance is made for the radiation of carbon-14:

$$A_t = mk[a - (a' E_m / E'_m]. \tag{11}$$

A_t is the radioactivity, in microcuries, of the tritium in the film; m is the weight, in milligrams, of the film; k is an empirically determined constant (1.90×10^{-4} μc cps^{-1} mg^{-1}); and E_m and a, respectively, are the counting efficiency of carbon-14 and the cps observed, both without the screen in place.

The calculation of the two activities in the mixture is illustrated by the use of typical data on the assay of D-fructose-*3,4-t-1,6-C*^{14}. A 1.985-mg sample in a film-forming solution gave a film weighing 4.93 mg, for which a' was 37.59 cps, a was 124.51 cps, E'_m was 0.184, and E_m was 0.395. $A_C = 37.59/(3.7 \times 10^4 \times 0.184) = 0.00552$ μc. The specific activity with respect to carbon-14 is $0.00552/1.985 = 0.00278$ μc/mg. $A_t = 4.93 \times 1.90 \times 10^{-4}[124.51 - 37.59\ (0.395/0.184)] = 0.0409$ μc. The specific activity with respect to tritium is $0.0409/1.985 = 0.0206$ μc/mg.

(Paper 65A5–125)

5. References

[1] L. Melander, Isotope effects on reaction rates (Ronald Press Co., New York, N.Y., 1960).
[2] R. M. Hann, E. B. Tilden, and C. S. Hudson, J. Am. Chem. Soc. **60,** 1201 (1938).
[3] H. S. Isbell and J. V. Karabinos, J. Research NBS **48,** 438 (1952) RP2334.
[4] H. L. Frush and H. S. Isbell, J. Research NBS **51,** 167 (1953) RP2446.
[5] A. Streitwieser, Jr., R. H. Jagow, R. C. Fahey, and S. Suzuki, J. Am. Chem. Soc. **80,** 2326 (1958).
[6] E. S. Lewis, Tetrahedron **5,** 143 (1959).
[7] V. J. Shiner, Jr., Tetrahedron **5,** 243 (1959).
[8] G. A. Ropp, J. Am. Chem. Soc. **82,** 842 (1960).
[9] C. Brice and A. S. Perlin, Can. J. Biochem. Physiol. **35,** 7 (1957).
[10] H. L. Frush and L. J. Tregoning, Science **128,** 597 (1958).
[11] H. L. Frush and H. S. Isbell, J. Am. Chem. Soc. **78,** 2844 (1956).
[12] H. S. Isbell, H. L. Frush, N. B. Holt, A. Schwebel, and T. T. Galkowski, J. Research NBS **48,** 163 (1952) RP2301.
[13] H. S. Isbell, H. L. Frush, and R. Schaffer, J. Research NBS **54,** 201 (1955) RP2581.
[14] H. L. Frush, H. S. Isbell, and A. J. Fatiadi, J. Research NBS **64A,** 433 (1960).
[15] K. W. Rosenmund, Ber. deut. chem. Ges. **51,** 585 (1918).
[16] E. W. Cook and R. T. Major, J. Am. Chem. Soc. **58,** 2410 (1936).
[17] R. Pasternack and P. P. Regna, U.S. Patent 2,188,777 (1940).
[18] M. Somogyi, J. Biol. Chem. **160,** 69 (1945).
[19] M. Somogyi, J. Biol. Chem. **160,** 61 (1945).
[20] W. R. Rees and T. Reynolds, Nature **181,** 767 (1958).
[21] R. M. Hann and C. S. Hudson, J. Am. Chem. Soc. **66,** 735 (1944).
[22] N. D. Cheronis, Micro and semimicro methods, Vol. VI of Technique of organic chemistry, A. Weissberger, ed. (Interscience Publishers, Inc., New York, N.Y., 1954, p. 533).
[23] N. K. Richtmyer, Advances in Carbohydrate Chem. **6,** 182 (1951).
[24] R. C. Hockett and C. S. Hudson, J. Am. Chem. Soc. **56,** 1632 (1934).
[25] C. S. Hudson and H. S. Isbell, BS J. Research **3,** 57 (1929) RP82.
[26] A. Schwebel, H. S. Isbell, and J. D. Moyer, J. Research NBS **53,** 221 (1954) RP2537.
[27] H. S. Isbell, H. L. Frush, and R. A. Peterson, J. Research NBS **63A,** 171 (1959).
[28] H. S. Isbell, H. L. Frush, and N. B. Holt, J. Research NBS **64A,** 363 (1960).

JOURNAL OF RESEARCH of the National Bureau of Standards—A. Physics and Chemistry
Vol. 65A, No. 5, September–October 1961

Franck-Condon Factors to High Vibrational Quantum Numbers I: N_2 and N_2^+

R. W. Nicholls [1]

(June 5, 1961)

Franck-Condon factor arrays have been computed numerically to high vibrational quantum numbers for the band systems

N_2:	$C^3\Pi - B^3\Pi$	(Second Positive)
N_2:	$B^3\Pi - A^3\Sigma$	(First Positive)
N_2:	$A^3\Sigma - X^1\Sigma$	(Vegard Kaplan)
N_2:	$a^1\Pi - X^1\Sigma$	(Lyman-Birge-Hopfield)
N_2^+:	$A^2\Pi - X^2\Sigma$	(Meinel)
N_2^+:	$B^2\Sigma - X^2\Sigma$	(First Negative)

and for the following ionization transitions

$N_2\ X^1\Sigma \rightarrow N_2^+ X^2\Sigma$
$N_2\ X^1\Sigma \rightarrow N_2^+ A^2\Pi$
$N_2\ X^1\Sigma \rightarrow N_2^+ B^2\Sigma$

1. Introduction

The intensity $I_{v'v''}$ in emission of the (v', v'') molecular band is given by Nicholls (1958)

$$I_{v'v''} = KN_{v'}E^4_{v'v''}R^2_e(\bar{r}_{v'v''})q_{v'v''} \tag{1}$$

where K is a constant which contains the effects of geometry and units, $N_{v'}$ is the population in the level v', $E_{v'v''}$ is the energy quantum of the v', v'' transition, $R_e(r)$ is the electronic transition moment. r is the internuclear separation and $\bar{r}_{v'v''}$ is the r-centroid (Nicholls and Jarmain, 1956, 1959) of the transition and $q_{v'v''}$ is the Franck-Condon factor (Bates, 1952; Nicholls, 1958). $R_e(r)$, $\bar{r}_{v'v''}$ and $q_{v'v''}$ are respectively defined by:

$$R_e(r) = \int \psi'_e{}^* M \psi''_e \, d\tau_e \tag{2}$$

$$\bar{r}_{v'v''} = \int \psi_{v'}\psi_{v''} r dr \Big/ \int \psi_{v'}\psi_{v''} dr \tag{3}$$

$$q_{v'v''} = \left| \int \psi_{v'}\psi_{v''} dr \right|^2 \tag{4}$$

where ψ'_e, ψ''_e are respectively electronic wave functions of the upper and lower states involved, M is the multipole moment of the transition, $d\tau_e$ is the element of configuration space of electronic wave function, r is the internuclear separation, and $\psi_{v'}$, $\psi_{v''}$ are the vibrational wave functions of the upper (v') level and lower (v'') level, respectively.

[1] Department of Physics, University of Western Ontario, London, Ontario. Consultant in Heat Division, National Bureau of Standards, 1959–60.

The Franck-Condon factor $(q_{v'v''})$ is governed by the overlap of the vibrational wave functions of the two levels which are concerned in the v', v'' transition. It is sometimes called, somewhat clumsily, the vibrational overlap integral square and can vary over two or three orders of magnitude for the significant bands of a system. For many band systems, although the variation from band to band of $N_{v'}$, $E^4_{v'v''}$ and $R_e(r)$ is significant, their combined effect is often not more than one or two orders of magnitude. E does not change very much over a band system of relatively small wavelength extension (e.g., $\Delta E^4/E^4 = 14$ percent between 2000 and 6000A and few band systems are so extensive). $N_{v'}$ is of course controlled by excitation conditions. For a number of band systems which have been studied, a significant variation $R_e(r)$ with r has been measured, (Turner and Nicholls, 1954a, b; Wallace and Nicholls, 1955; Nicholls 1956; Dixon and Nicholls, 1958; Robinson and Nicholls, 1958, 1960; Hebert and Nicholls, 1961). It is however seldom as much as an order of magnitude. Thus the Franck-Condon factor exerts dominant effect upon the intensity variation from band to band across a system.

Since the pioneering work of Hutchisson (1930, 1931) who used an analytic method to evaluate the vibrational overlap integral for homonuclear molecules (harmonic and anharmonic oscillators), and its extension by Dunham (1932) to heteronuclear molecules, a number of authors have used a wide variety of methods and have produced a number of $q_{v'v''}$ arrays of varying extent. This work may be summarized as follows:

Gaydon and Pearse (1939) proposed a method by which wave functions of a simple harmonic oscillator are linearly distorted to fit an equivalent Morse

Potential. They compared Franck-Condon factors calculated in this way with their experimental results on RbH. Pillow (1949, 1950, 1951, 1952, 1953a,b, 1954, 1955) has improved and applied the method to a large number of transitions (Pillow and Rowlatt, 1960). Nicholls (1950), Montgomery and Nicholls (1951) and Turner and Nicholls (1951) also used the method.

The basis of the distortion method was criticized by Wu (1952) who suggested two further analytic methods for Morse molecules. One of these methods which is based on the WKB approximation has been used by Wyller (1953, 1958). Bates (1952) has published a very useful double entry table based upon modifications of Hutchisson's formulas, from which Franck-Condon factors for any transition may be read $v'=0-2$: $v''=0-2$.

Prior to the general availability of digital computers, the extreme tedium of direct numerical integration, such as has been carried out by Bates (1949) and Jarmain and Nicholls (1954) for Morse molecules, forced most workers to resort to analytic approximations to overlap integrals. Most of these approximations are valid for small quantum numbers. An example is the analytic method of Fraser and Jarmain (Fraser and Jarmain, 1953; Jarmain and Fraser, 1953; Fraser, 1954) which has been applied to a wide variety of band systems (Jarmain, Fraser, and Nicholls, 1953, 1955; Fraser, Jarmain, and Nicholls, 1954; Nicholls, Fraser, and Jarmain, 1959; Nicholls, Fraser, and Jarmain, and McEachran, 1960; Jarmain, Ebisuzaki, and Nicholls, 1960; Ortenberg, 1960).

Biberman and Yakubov (1960) have recently proposed a WKB method of evaluating Franck-Condon factors analytically at high vibrational quantum numbers. The method has been applied by Yakubov (1960). Nevertheless, with the current availability of large capacity electronic computers, direct numerical integration to high quantum numbers is straightforward, and there seems to be little point in developing further approximate analytic methods. The only limitation of this method is the realism (particularly at high quantum numbers) of the empirical potentials used.

Losev (1958) used a small capacity computer for direct evaluation of overlap integrals. The capacity of the machine was not, however, sufficient to accommodate the severe cancellation.

Ideally, Franck-Condon factor arrays computed to as high vibrational quantum numbers v' and v'' as are physically reasonable from observed spectra are required for all important molecular band systems. This implies good knowledge of molecular potentials so that the wave functions used are appropriate to 'real' rather than empirical potentials. Most of the Franck-Condon factor tables currently in the literature have been calculated for empirical (e.g., simple harmonic or Morse oscillator) potentials.

However recent work of Jarmain (1959, 1960) and Vanderslice et al. (Vanderslice, Mason and Maisch, 1959, 1960a, 1960b; Tobias, Fallon, and Vanderslice, 1960; Fallon, Tobias, and Vanderslice, 1961) has provided, by a WKB-Klein-Dunham method, numerical information on 'real' molecular potentials. It is therefore planned to program a numerical solution of the Schrodinger equation appropriate to such numerical potentials to provide numerical wave functions from which more realistic Franck-Condon factor arrays can be determined.

2. Method

In the meantime the results reported in this paper represent an interim step. Morse potentials have been assumed and a program for the numerical integration of the overlap integrals has been written for the electronic digital 704 computer at the National Bureau of Standards. The input data are ω_e, $\omega_e x_e$, r_e, μ_A, v_{max} for both of the electronic states involved. Each member of the two families of wave functions ψ_i' $(i=0-v'_{max})$, $\psi_j''(j=0-v''_{max})$ is computed at 0.01A intervals, overlap integrals between all pairs of them are computed and squared. The program has been applied to a number of transitions and results are presented here for transitions in N_2 and N_2^+.

The basis of the method is as follows: The zeroth vibrational wave function of a Morse molecule is (Morse 1929).

$$\psi_0(r)=\left(\frac{\alpha}{\Gamma(K-1)}\right)^{1/2}[K\exp(-\alpha\overline{r-r_e})]^{1/2(K-1)}\exp\left[-\frac{K}{2}\exp(-\alpha\overline{r-r_e})\right] \quad (5)$$

where $K=\dfrac{\omega_e}{\omega_e x_e}$

$$\alpha=0.243534\,(\mu_A\omega_e x_e)^{1/2} \qquad A^{-1}$$

r_e=equilibrium internuclear separation (A)

Thus the input data for point by point computation of $\psi_0(r)$ at a series of values of r is $\omega_e, \omega_e x_e, r_e, \mu_A$. The symbolism is standard (Herzberg, 1950). The gamma function may be evaluated through Stirling's formula:

$$\Gamma(x)=\left(\frac{2\pi}{x}\right)^{1/2}x^x\exp(-x)\left\{1+\frac{1}{12x}+\frac{1}{288x^2}+\cdots\right\} \quad (6)$$

Once the zeroth wave function is tabulated the complete family of wave functions can be built up one at a time by the relationships

$$\left(\frac{\psi_v}{\psi_{v-1}}\right)=\left(\frac{C_v}{C_{v-1}}\right)\frac{1}{Z}\left(\frac{L_v}{L_{v-1}}\right) \quad (7)$$

$$=\left[\frac{(K-v)(K-2v-1)}{v(K-2v+1)}\right]^{1/2}\times\frac{1}{K\exp(-\alpha\overline{r-r_e})}\left(\frac{L_v}{L_{v-1}}\right) \quad (8)$$

$$C_0=\left(\frac{\alpha}{\Gamma(K-1)}\right)^{1/2} \quad (9)$$

The wave functions ψ_v of higher quantum number than zero contain, as is seen in eq (7), ratios of associated Laguerre functions L_v of the form:

$$L_v = L^{K-2v-1}_{K-v-1}(Z) = Z^v - v(K-v-1)Z^{v-1} + \frac{v(v-1)}{2}(K-v-1)(K-v-2)Z^{v-2} + \ldots + (-1)^v\{(K-v-1)(K-v-2)\ldots(K-2r)\} \quad (10)$$

where the number of terms in the vth polynomial is $(v+1)$; $L_0 = L^{K-1}_{K-1}(Z) = 1$; $Z = K\exp(-\alpha\overline{r-r_e})$. For the lowest quantum numbers, eq (10) may be used in the evaluation of L_v. At higher values of v loss of significant figures through cancellation between positive and negative terms forces the use of the recursion relation

$$L_v(Z) = ZL_{v-1} - (K-2v)\sum_{r=0}^{v-1}\binom{v-1}{r}\frac{(2r)!}{(r+1)!}L_{v-r-1} \quad (11)$$

(Fraser, Jarmain, and Henderson, 1959). If in the use of eq (8) L_{v-1} should vanish at some value of r, the alternative relation

$$\left(\frac{\psi_v}{\psi_{v-2}}\right) = \left(\frac{C_v}{C_{v-2}}\right)\left(\frac{1}{Z^2}\right)\left(\frac{L_r}{L_{v-2}}\right) \quad (12)$$

can be used.

Prior to numerical integration, each wave function is evaluated at 0.01A intervals over its significant range of r. This significant range may be estimated by recalling that the width $r_2 - r_1$ of a Morse potential in the region of energy U is given by

$$r_2 - r_1 = \frac{1}{\alpha}\log_e\left[\frac{1+\left(\frac{U}{D}\right)^{1/2}}{1-\left(\frac{U}{D}\right)^{1/2}}\right] = \frac{1}{\alpha}\log_e\left[\frac{1+2(V-V^2)^{1/2}}{1-2(V-V^2)^{1/2}}\right] \text{ at level } v \text{ where } V = x_e(v+1/2). \quad (13)$$

Rough rules of thumb for the total range in r to be treated are for many electronic states

$v_{max} \sim 6$ Add 50% to $r_2 - r_1$: 40% of total range should be less than r_e

$v_{max} \sim 12$ Add 40% to $r_2 - r_1$: 40% of range should be less than r_e

$v_{max} \sim 18$ Add 30% to $r_2 - r_1$: 35% of range should be less than r_e.

Beyond these ranges the amplitudes of wave functions are negligible.

Provision has been made for storage on magnetic tape of the vibrational wave functions involved in the NBS computer center, for future users. Checks were of course applied for normality of the wave functions i.e., $\int(\psi_v)^2\,dr = 1$ and the overlap integrals between all possible pairs of wave functions of a transition were evaluated. The overlap integrals were squared and values checked by applying the sum rules $\Sigma_{v'}q_{v'v''} = 1 = \Sigma_{v''}q_{v'v''}$. It may be noted in passing that computation of r-centroids was also made. These will be discussed independently elsewhere.

3. Basic Data and Results

Franck-Condon factor arrays have been computed for the following radiative transitions

N_2:	$C^3\Pi_u - B^3\Pi_g$	Second Positive
	$B^3\Pi_g - A^3\Sigma_u^+$	First Positive
	$A^3\Sigma_u^+ - X^1\Sigma_g^+$	Vegard-Kaplan
	$a^1\Pi_g - X^1\Sigma_g^+$	Lyman-Birge-Hopfield
N_2^+:	$A^2\Pi_u - X^2\Sigma_g^+$	Meinel
	$B^2\Sigma_u^+ - X^2\Sigma_g^+$	First Negative

and also for the following ionization transitions

$$N_2(X^1\Sigma_g^+, v=0) \rightarrow N_2^+ X^2\Sigma(v=0-21)$$

$$N_2(X^1\Sigma_g^+, v=0) \rightarrow N_2^+ A^2\Pi(v=0-5)$$

$$N_2(X^1\Sigma_g^+, v=0) \rightarrow N_2^+ B^2\Sigma(v=0-29)$$

Wave functions were computed in all cases on the basis of a Morse model for as many levels as were known spectroscopically and a rectangular $q_{v'v''}$ array of $(v'_{max}+1)(v''_{max}+1)$ members were then evaluated for each transition. In such arrays data was of course calculated for many bands which were not usually spectroscopically observed.

The input data (ω_e, $\omega_e x_e$, r_e, μ_A, v_{max}) used for each of the states is listed in table 1 and was taken in large part from the compilation of Mulliken (1959) and the original papers of analysis of the band systems.

The nine arrays of Franck-Condon factors are presented in tables 2 to 10 inclusive.

TABLE 1. *Basic Data*

State	ω_e(cm^{-1})×10^{-3}	$\omega_e x_e$(cm^{-1})×10^{-1}	r_e(A)	μ_A	v_{max}
$N_2X^1\Sigma$	2.35807	1.419	1.0976	7.00377	27
$a^1\Pi$	1.6937	1.383	1.220	7.00377	16
$A^3\Sigma$	1.46037	1.3891	1.293	7.00377	16
$B^3\Pi$	1.73411	1.447	1.2123	7.00377	21
$C^3\Pi$	2.0351	1.708	1.1482	7.00377	4
$N_2^+X^2\Sigma$	2.20719	1.614	1.118	7.00363	21
$A^2\Pi$	1.90284	1.491	1.177	7.00363	5
$B^2\Sigma$	2.41984	2.319	1.075	7.00363	29

TABLE 2. *Franck-Condon factors to high vibrational quantum numbers for the N_2 second positive ($C^3\Pi - B^3\Pi$) band system*

v' \ v''	0	1	2	3	4	5	6	7	8	9	10	11
0	*4.4929-1*	*3.2870-1*	1.4691-1	5.2258-2	1.6345-2	4.7260-3	1.2999-3	3.4632-4	9.0427-5	2.3327-5	5.9777-6	1.5275-6
1	3.8986-1	1.8685-2	*2.0376-1*	*2.0027-1*	1.1238-1	4.8391-2	1.7904-2	6.0242-3	1.9045-3	5.7747-4	1.7024-4	4.9252-5
2	1.3494-1	*3.2232-1*	3.2988-2	5.9570-2	*1.6138-1*	*1.4274-1*	8.3030-2	3.8599-2	1.5642-2	5.7932-3	2.0181-3	6.7377-4
3	2.3630-2	2.5146-1	1.6304-1	*1.1812-1*	1.8410-3	8.8906-2	*1.3450-1*	*1.0024-1*	6.1610-2	2.9799-2	1.2816-2	5.0889-3
4	2.1905-3	6.9566-2	*3.0342-1*	*4.7625-2*	*1.5698-1*	1.4160-2	2.9388-2	9.9550-2	*1.1050-1*	*8.0226-2*	4.6144-2	2.2924-2

v' \ v''	12	13	14	15	16	17	18	19	20	21
0	3.9014-7	9.9745-8	2.5539-8	6.5466-9	1.6780-9	4.2921-10	1.0925-10	2.7561-11	6.8697-12	1.6833-12
1	1.4075-5	3.9912-6	1.1265-6	3.1711-7	8.9119-8	2.5012-8	7.0058-9	1.9548-9	5.4183-10	1.4846-10
2	2.1835-4	6.9311-5	2.1688-5	6.7206-6	2.0690-6	6.3413-7	1.9374-7	5.9029-8	1.7929-8	5.4207-9
3	1.9106.3	6.8923-4	2.4164-4	8.3002-5	2.8101-6	9.4178-6	3.1341-6	1.0378-6	3.4236-7	1.1258-7
4	1.0317-2	4.3321-3	1.7309-3	6.6710-4	2.5045-4	9.2257-5	3.3524-5	1.2065-5	4.3127-6	1.5344-6

4. Discussion

The most obvious feature of the double entry tables of Franck-Condon factors is, as indicated on them, the family of well defined loci on the v' v'' plane of maximum values of the factors. The loci, which have the general appearance of co-axial parabolas correlate well with the occurrence of observed bands. These primary and subsidiary 'Condon Parabolas', as the loci are called, pass through those v', v'' for which the largest contribution to each overlap integral arises from the strong overlap in r between *one* antinode *of each* of the wave functions $\psi_{v'}$ and $\psi_{v''}$.

The wave function $\psi_v(r)$ has $v+1$ antinodes of which the general one is $r_i^{(v)}$. $r_1^{(v)}$ and $r_{v+1}^{(v)}$ are the terminal antinodes and $r_1^{(v)} < r_e < r_{v+1}^{(v)}$. The primary Condon parabolas arise, as is well known, from overlap of the terminal antinodes of $\psi_{v'}$ and $\psi_{v''}$. The two branches of the parabola are determined by the conditions

$$\left.\begin{aligned} r_{v'+1}^{(v')} &= r_{v''+1}^{(v'')} \\ r_1^{(v')} &= r_1^{(v'')} \end{aligned}\right\} \tag{14}$$

The secondary parabolas are determined by overlap of the terminal antinode of one wave function and the next-to-terminal antinode of the other, that is:

$$\left.\begin{aligned} r_{v'}^{(v')} &= r_{v''+1}^{(v'')} \\ r_1^{(v')} &= r_2^{(v'')}. \end{aligned}\right\} \tag{15}$$

The conditions for the ith subsidiary parabola are then:

$$\left.\begin{aligned} r_{v'+2-i}^{(v')} &= r_{v''+1}^{(v'')} \\ r_1^{(v')} &= r_i^{(v'')}. \end{aligned}\right\} \tag{16}$$

The geometry of the parabolas has been studied for a variety of potentials by applying the conditions of eqs (14), (15), and (16) and is discussed in detail elsewhere (Nicholls, 1961). In this work the dominating influence of Δr_e upon the shape of the 'Parabolas' is shown analytically. The loci are only true parabolas for simple harmonic potentials as Condon (1926) pointed out for the primary parabola. For Morse Potentials the primary 'parabola' is actually a quartic.

The following qualitative statements may be made upon the dominant influence of Δr_e upon the shape of the loci in particular and upon the form of the three dimensional Franck-Condon factor surface in general.

For band systems in which Δr_e is quite small, that is, the potentials lie essentially one above the other, the primary parabola is very narrow, appears to lie along the prime diagonal $v'=v''$ in the v', v'' plane and has its maximum value at the (0,0) band. In a three dimensional representation when Δr_e is small ($\sim$0.01A) the $q_{v'v''}$ surface is often a descending diagonal ridge along $v'=v''$.

When Δr_e is a little larger ($\sim$0.05A) the ridge widens into a very narrow parabolic ridge with an axial valley. This situation occurs for the N_2^+ First Negative band system.

As Δr_e is further increased, the primary parabola widens, its vertex moves down the prime diagonal away from (0,0), and subsidiary parabolas appear. At relatively large ($\sim$0.4A) values of Δr_e (e.g., 0_2 Schumann-Runge and N_2 Vegard-Kaplan systems) the band system is quite extended in wavelength and the oscillator strength of the whole system is spread over many more bands than for systems having a smaller Δr_e. Thus the intensity per band is decreased.

In an extreme case, the primary parabola lies along the $v'=0$ and $v''=0$ progressions at large v'' and v' respectively and avoids the (0,0) region entirely.

Examples of these general remarks are seen in the tables. The N_2^+ First Negative system having a small Δr_e (0.043A) exhibits a very narrow primary

TABLE 3. *Franck-Condon factors to high vibrational quantum numbers for the N_2 first positive ($B^3\Pi$—$A^3\Sigma$) band system*

v' \ v''	0	1	2	3	4	5	6	7	8
0	3.3816-1	*3.2480-1*	*1.8996-1*	8.8567-2	3.6486-2	1.3990-2	5.1465-3	1.8513-3	6.5953-4
1	*4.0645-1*	2.3100-3	1.0321-1	*1.7820-1*	*1.4502-1*	8.6473-2	4.3670-2	1.9997-2	8.6259-3
2	1.9746-1	2.1203-1	*1.1380-1*	1.2048-3	7.7240-2	*1.2750-1*	*1.1871-1*	7.4955-2	4.2471-2
3	5.0143-2	*2.9871-1*	3.8683-2	*1.6230-1*	3.2267-2	9.0504-3	6.9100-2	*1.0094-1*	*9.0789-2*
4	7.1905-3	1.3180-1	*2.7381-1*	1.8065-3	*1.1388-1*	*8.8227-2*	5.2273-3	1.7977-2	6.3607-2
5	5.8713-4	2.7286-2	2.1065-1	1.8081-1	4.7796-2	4.2616-2	*1.0567-1*	3.8289-2	1.2298-6
6	2.6156-5	2.9248-3	6.1481-2	*2.6054-1*	8.3053-2	*1.0404-1*	3.1711-3	*8.0781-2*	*6.9671-2*
7	5.6982-7	1.6132-4	8.4620-3	1.0650-1	*2.7061-1*	1.9163-2	*1.2905-1*	6.7482-3	3.9461-2
8	4.7221-9	4.1737-6	5.6752-4	1.8566-2	1.5609-1	*2.4380-1*	2.7659-5	*1.1586-1*	3.6330-2
9	6.5075-12	3.9626-8	1.7188-5	1.4947-3	3.4197-2	2.0292-1	1.9185-1	1.6939-2	*7.8622-2*
10	2.7802-15	6.0552-11	1.8482-7	5.2408-5	3.2741-3	5.5689-2	*2.4021-1*	1.2991-1	5.2188-2
11	8.1140-16	3.3224-14	3.0349-10	6.3216-7	1.3176-4	6.2985-3	8.2650-2	*2.6301-1*	7.2055-2
12	2.5148-16	5.0349-16	2.1376-13	1.1012-9	1.7690-6	2.8895-4	1.0992-2	1.1398-1	*2.6878-1*
13	5.9625-17	1.6620-16	4.3337-16	1.0512-12	3.2357-9	4.2896-6	5.7172-4	1.7773-2	1.4799-1
14	3.4245-16	4.4756-17	4.5421-16	9.7232-16	4.0476-12	8.1628. 9	9.3348-6	1.0436-3	2.7016-2
15	1.7005-16	2.5344-16	2.7160-17	4.1387-16	2.8052-15	1.2846-11	1.8385-8	1.8657-5	1.7849-3
16	5.1720-18	7.4160-17	2 2234-16	4.9038-17	6.3948-17	4.5515-14	3.4427-11	3.7813-8	3.4803-5
17	2.0782-16	1.5676-17	2.1122-16	5.4009-16	2.1696-15	2.4366-15	2.1664-13	8.5321-11	7.2030-8
18	1.8889-16	1.2423-16	2.4354-17	9.1758-17	1.2590-16	3.5970-16	3.0869-17	4.8996-13	1.9965-10
19	1.0678-17	1.1379-16	1.9019-17	2.6078-16	9.9179-16	3.8594-15	4.2273-15	8.3215-15	1.2193-12
20	7.5363-17	2.8873-18	3.7751-16	2.6077-16	9.2651-17	9.5416-17	9.2691-16	1.7885-15	1.2898-14
21	1.7325-16	2.6683-17	4.2656-16	4.0688-18	4.6754-16	3.5655-15	3.9524-15	2.1349-15	9.2663-17

v' \ v''	9	10	11	12	13	14	15	16
0	2.3477-4	8.4031-5	3.0383-5	1.1135-5	4.1473-6	1.5729-6	6.0831-7	2.4019-7
1	3.5891-3	1.4631-3	5.9070-4	2.3802-4	9.6271-5	3.9251-5	1.6185-5	6.7658-6
2	2.1815-2	1.0529-2	4.8845-3	2.2119-3	9.8835-4	4.3920-4	1.9525-4	8.7217-5
3	6.4061-2	3.9171-2	2.1871-2	1.1508-2	5.8243-3	2.8759-3	1.3995-3	6.7625-4
4	*8.5488-2*	*7.5106-2*	5.5103-2	3.5667-2	2.1275-2	1.2016-2	6.5431-3	3.4791-3
5	2.4543-2	5.8198-2	*7.0564-2*	*6.3384-2*	4.7949-2	3.2525-2	2.0514-2	1.2313-2
6	1.2893-2	2.4600-3	2.8099-2	5.2611-2	*6.0394-2*	*5.4340-2*	4.2250-2	2.9867-2
7	*7.7327-2*	3.8328-2	2.7384-3	6.4003-3	2.9121-2	4.7031-2	*5.2119-2*	*4.7183-2*
8	8.3601-3	*6.0770-2*	*5.7211-2*	1.8520-2	8.6772-5	9.5049-3	2.8339-2	4.1643-2
9	*6.7727-2*	3.1940-4	3.3048-2	*5.9448-2*	3.7289-2	7.9625-3	3.6806-4	1.1202-2
10	3.7645-2	*8.3700-2*	1.3068-2	9.5758-3	*4.6033-2*	*4.8138-2*	2.2815-2	3.0276-3
11	*8.7792-2*	9.0118-3	*7.8960-2*	3.5274-2	6.6872-5	2.5442-2	*4.0325-2*	*3.5706-2*
12	2.8566-2	*1.1080-1*	2.6171-5	*5.8457-2*	*5.4227-2*	5.7104-3	7.8299-3	3.3974-2
13	*2.5751-1*	4.6872-3	*1.1561-1*	9.3424-3	3.2354-2	*6.1513-2*	2.0820-2	1.3633-4
14	1.8258-1	*2.3145-1*	7.7329-4	*1.0292-1*	2.9820-2	1.0861-2	*5.5208-2*	3.6818-2
15	3.9015-2	2.1544-1	1.9452-1	1.3301-2	*7.8290-2*	*5.2860-2*	5.5460-4	*3.9360-2*
16	2.8927-3	5.3947-2	*2.4432-1*	1.5158-1	3.6337-2	4.9346-2	*6.8075-2*	2.9424-3
17	6.1314-5	4.4801-3	7.1852-2	*2.0718-1*	1.0776-1	6.3088-2	2.3488-2	*7.4348-2*
18	1.2872-7	1.0294-4	6.6745-3	9.2613-2	*2.8243-1*	6.7723-2	8.7269-2	6.1701-3
19	4.3255-10	2.1785. 7	1.6584. 4	9.6153-3	1.1595-1	*2.8900-1*	3.5244-2	*1.0409-1*
20	3.1035-12	8.8458-10	3.5155-7	2.5781-4	1.3450-2	1.4143-1	*2.8644-1*	1.2813-2
21	3.1514-14	7.4958-12	1.7175-9	5.4388-7	3.8848-4	1.8331-2	1.6845-1	*2.7497-1*

TABLE 4. *Franck-Condon factors to high vibrational quantum numbers for the N_2 Vegard-Kaplan ($A^3\Sigma_u^+ - X^1\Sigma_g^+$) band system*

v' \ v''	0	1	2	3	4	5	6	7	8	9	10	11	12	13	14
0	5.9004-4	5.3372-3	2.2858-2	6.1668-2	1.1764-1	*1.6884-1*	*1.8941-1*	*1.7036-1*	*1.2501-1*	7.5777-2	3.8279-2	1.6212-2	5.7795-3	1.7379-3	4.4108-4
1	3.3186-3	2.2781-2	6.9190-2	*1.1951-1*	*1.2164-1*	6.3828-2	6.2561-3	1.3953-2	7.8661-2	*1.3698-1*	*1.4493-1*	*1.0997-1*	6.4036-2	2.9626-2	1.1103-2
2	9.9751-3	5.0849-2	*1.0348-1*	9.7316-2	2.9217-2	2.1608-3	5.4725-2	8.9237-2	*4.6160-2*	8.8402-4	2.9551-2	1.0011-1	*1.3776-1*	*1.1956-1*	7.4723-2
3	2.1326-2	7.8496-2	9.7675-2	3.3262-2	2.5390-3	5.6172-2	*6.3910-2*	8.5635-3	1.6968-2	*7.3178-2*	*6.1805-2*	7.6001-3	1.5200-2	8.3825-2	*1.3146-1*
4	3.6417-2	*9.3276-2*	5.9979-2	3.7143-4	4.1074-2	*5.7583-2*	4.6254-3	2.5535-2	6.3308-2	1.9160-2	7.1270-3	*6.2758-2*	*6.3144-2*	9.3831-3	1.3789-2
5	5.2901-2	8.9624-2	2.0109-2	1.4649-2	*5.8682-2*	1.2234-2	1.6881-2	*5.4617-2*	1.0645-2	1.6426-2	*5.8712-2*	2.0156-2	6.5852-3	*6.1432-2*	*5.8318-2*
6	6.7985-2	7.0820-2	8.3805-4	4.2328-2	3.4003-2	2.6303-3	4.7678-2	1.6412-2	1.1626-2	*5.0081-2*	9.7430-3	1.7291-2	*5.5788-2*	1.4565-2	1.1314-2
7	7.9391-2	4.5385-2	5.2638-3	*5.1543-2*	5.4018-3	2.8049-2	3.2372-2	1.7097-3	*4.3075-2*	1.3077-2	1.4090-2	*4.6348-2*	4.7851-3	2.4469-2	*5.1703-2*
8	8.5879-2	2.2052-2	2.2306-2	3.8028-2	1.9331-3	4.2032-2	4.1846-3	2.7007-2	2.5721-2	4.0727-3	*4.1475-2*	6.2965-3	2.1849-2	*4.0018-2*	3.6001-4
9	*8.7302-2*	6.4345-3	3.8377-2	1.6510-2	1.8150-2	2.8901-2	3.7627-3	*5.6963-2*	8.8547-4	*5.1093-2*	1.5917-2	1.0832-2	*5.7647-2*	6.3259-4	*5.2836-2*
10	8.4340-2	2.0527-4	*4.5272-2*	2.2543-3	3.3488-2	8.0539-3	2.2423-2	1.8373-2	9.7438-3	3.0255-2	5.2910-4	*5.4748-2*	5.3800-3	2.2182-2	2.7567-2
11	7.8120-2	2.0154-3	4.1796-2	9.8901-4	*3.5296-2*	1.6839-5	*3.2569-2*	1.2430-3	*2.8347-2*	7.1660-3	1.9634-2	1.8916-2	7.2235-3	*5.1974-2*	5.8293-6
12	6.9875-2	9.0148-3	3.1413-2	9.4229-3	2.4925-2	7.4255-3	2.4781-2	4.2046-3	2.7191-2	9.8545-4	*2.9624-2*	2.5973-4	*2.8530-2*	5.8720-3	2.0159-2
13	6.0710-2	1.8172-2	1.8992-2	2.0605-2	1.1159-2	2.0029-2	9.6300-3	1.8092-2	1.1135-2	1.4768-2	1.5191-2	9.7822-3	2.1516-2	3.7907-3	*2.8305-2*
14	5.1488-2	2.7067-2	8.4944-3	2.8700-2	1.9247-3	*2.7519-2*	5.6975-4	*2.6054-2*	4.3335-4	*2.5269-2*	9.6076-4	*2.4365-2*	2.8265-3	2.2085-2	7.4375-3
15	4.2800-2	3.4179-2	2.0378-3	*3.1063-2*	2.8713-4	2.5598-2	2.2123-3	2.1912-2	3.6225-3	2.0405-2	3.8253-3	2.0855-2	2.8517-3	*2.2876-2*	1.1484-3
16	3.4994-2	*3.8232-2*	8.7146-8	2.8014-2	4.8324-3	1.7543-2	*1.0459-2*	1.1142-2	*1.3917-2*	7.9106-3	*1.5617-2*	6.8300-3	*1.6040-2*	7.4514-3	*1.5229-2*

v' \ v''	15	16	17	18	19	20	21	22	23	24	25	26	27
0	9.4399-5	1.6998-5	2.5662-6	3.2317-7	3.3706-8	2.8836-9	2.0060-10	1.1235-11	4.9590-13	1.9734-14	1.2528-16	2.0799-16	6.0389-16
1	3.4093-3	8.6291-4	1.8051-4	3.1206-5	4.4467-6	5.1967-7	4.9422-8	3.7943-9	2.3417-10	1.1095-11	3.4235-13	1.7361-14	1.8362-15
2	3.5672-2	1.3418-2	4.0462-3	9.8770-4	1.9604-4	3.1660-5	4.1495-6	4.3901-7	3.7194-8	2.4953-9	1.2993-10	5.0766-12	1.6469-13
3	*1.1966-1*	7.5428-2	3.5429-2	1.2869-2	3.6898-3	8.4423-4	1.5491-4	2.2805-5	2.6846-6	2.5109-7	1.8463-8	1.0484-9	4.4781-11
4	8.2940-2	*1.2990-1*	*1.1518-1*	6.9607-2	3.0949-2	1.0519-2	2.7898-3	5.8366-4	9.6722-5	1.2687-5	1.3110-6	1.0569-7	6.5395-9
5	5.9053-3	1.9816-2	9.2101-2	*1.3044-1*	*1.0655-1*	5.9379-2	2.4233-2	7.5072-3	1.7991-3	3.3659-4	4.9287-5	5.6330-6	4.9852-7
6	*6.5313-2*	*4.8253-2*	1.1414-3	3.3656-2	1.0676-1	*1.2893-1*	9.3406-2	4.6616-2	1.7039-2	4.7060-3	9.9785-4	1.6352-4	2.0707-5
7	6.1426-3	2.2266-2	*6.8871-2*	3.2748-2	8.2227-4	5.5913-2	*1.2159-1*	*1.2168-1*	7.6253-2	3.3343-2	1.0698-2	2.5833-3	4.7525-4
8	*3.6103-2*	*4.2274-2*	2.6210-4	*5.9363-2*	*6.5671-2*	1.4629-2	1.1143-2	8.4197-2	*1.3048-1*	1.0693-1	5.7008-2	2.1469-2	5.9411-3
9	2.8104-2	2.2605-3	*4.7481-2*	2.6029-2	3.7874-3	*5.7749-2*	*5.1100-2*	1.5156-3	3.5628-2	*1.1196-1*	*1.2836-1*	8.5750-2	3.8429-2
10	1.9442-3	*4.1368-2*	1.2208-2	1.4639-2	*5.0441-2*	8.0584-3	2.0857-2	*6.7486-2*	2.7168-2	3.6116-3	7.1407-2	*1.3023-1*	*1.1361-1*
11	*3.3332-2*	1.2354-2	1.3818-2	*5.9436-2*	8.0111-4	*3.4402-2*	*3.8620-2*	3.0367-5	*4.6607-2*	*5.9145-2*	5.2553-3	2.7301-2	1.0818-1
12	1.9080-2	5.9996-3	*3.5262-2*	8.7432-4	*3.1374-2*	2.3384-2	4.6994-3	*4.8807-2*	1.6185-2	1.2230-2	*6.5677-2*	3.3467-2	1.8068-3
13	2.4929-5	*3.0804-2*	4.9631-3	*2.1798-2*	2.2934-2	4.3865-3	*4.0537-2*	5.0635-3	2.5210-2	*4.3736-2*	5.0077-4	*4.1055-2*	*6.1736-2*
14	1.6863-2	1.6090-2	8.2915-3	2.7504-2	5.7058-4	*3.3945-2*	5.1767-3	2.3053-2	*3.0040-2*	1.4968-3	*4.6125-2*	2.0152-2	9.6071-3
15	*2.5634-2*	1.2963-6	*2.7191-2*	2.1633-3	*2.4151-2*	1.1404-2	1.3699-2	2.7986-2	1.2270-3	*3.8910-2*	8.1905-3	2.1206-2	*4.5013-2*
16	9.9016-3	*1.2818-2*	1.4642-2	8.4316-3	2.1752-2	2.8302-3	*2.9246-2*	6.9650-5	*3.0929-2*	8.5040-3	*1.8791-2*	*3.2031-2*	8.2402-4

parabola. The N_2^+ Meinel and N_2 Second Positive systems have nearly equal Δr_e values (0.061A, 0.064A, respectively) and exhibit somewhat wider primary parabolas and the start of a secondary parabola. The N_2 First Positive system exhibits one primary and two subsidiary parabolas all of which are relatively narrow as Δr_e=0.081A for this system. Four wider subsidiary parabolas and one wider primary parabola whose vertex just avoids the (0,0) band are possessed by the N_2 Lyman-Birge-Hopfield system (Δr_e=0.13A). The extreme pattern of behavior (for Δr_e=0.196A) is shown by the N_2 Vegard-Kaplan system which possesses six very wide subsidiary parabolas and one wide primary parabola.

A steady diminution in Franck-Condon factors with increasing v' is seen in the tables for the N_2 $X^1\Sigma$, N_2^+ $X^2\Sigma$, N_2^+ $A^2\Pi$, N_2^+ $B^2\Sigma$ ionization excitations.

The author's sincere thanks are due to Miss I. Stegun and Miss R. Zucker of the NBS Computation Laboratory for writing and testing the program, and to Mr. W. R. Jarmain for providing details of the method of computation in a form suitable for programing.

TABLE 5. *Franck-Condon factors to high vibrational quantum numbers for bands of the N_2 Lyman-Birge-Hopfield ($a^1\Pi_g - X^1\Sigma_g^+$) system*

v' \ v''	0	1	2	3	4	5	6	7	8	9	10	11	12	13
0	4.3147-2	1.5170-1	2.4766-1	2.4924-1	1.7313-1	8.8079-2	3.3993-2	1.0171-2	2.3917-3	4.4536-4	6.5886-5	7.7400-6	7.1926-7	5.2477-8
1	1.1623-1	1.9315-1	8.0487-2	4.0177-4	8.7320-2	1.8508-1	1.7516-1	1.0324-1	4.2495-2	1.2894-2	2.9684-3	5.2658-4	7.2502-5	7.7577-6
2	1.7128-1	9.6767-2	3.2760-3	1.0744-1	8.5983-2	8.5541.4	6.4509-2	1.6401-1	1.6142-1	9.4062-2	3.7178-2	1.0603-2	2.2534-3	3.6286-4
3	1.8348-1	1.2119-2	7.5543-2	6.9313-2	3.6061-3	9.5107-3	6.5801-2	1.4814-4	7.8397-2	1.6324-1	1.4506-1	7.5175-2	2.6753-2	6.8242-3
4	1.6026-1	6.3914-3	9.6609-2	5.8118-4	7.7442-2	3.7353-2	1.6885-2	9.6672-3	3.6152-2	9.1675-3	1.0847-1	1.6260-1	1.1787-1	5.3039-2
5	1.2140-1	7.7060-2	4.6680-2	3.3922-2	5.6701-2	8.3644-3	7.8822-3	7.9121-3	4.6748-2	8.5363-2	7.9576-3	3.9113-2	1.4016-1	1.4985-1
6	8.2871-2	8.5419-2	4.5383-3	7.2885-2	2.7951-3	6.3473-2	1.4846-2	4.0420-2	5.5021-3	2.0104-3	7.8737-2	5.1442-2	1.6276-3	8.7172-2
7	5.2304-2	9.9714-2	5.7959-3	5.6582-2	1.7174-2	4.6938-2	1.2779-2	5.7309-2	1.0399-3	6.7550-2	1.5376-2	3.2095-2	8.3544-2	1.1954-2
8	3.1090-2	9.2157-2	3.3721-2	1.8257-2	5.3397-2	4.2086-3	5.4396-2	4.7475-3	5.0309-2	1.7512-2	3.1436-2	5.5586-2	1.0426-3	7.3166-2
9	1.7644-2	7.3457-2	6.1052-2	1.3142-4	5.4846-2	9.2341-3	3.9713-2	1.5872-2	3.8686-2	1.1738-2	5.0739-2	1.2464-3	6.3084-2	1.2393-2
10	9.6608-3	5.2852-2	7.3781-2	9.7471-3	2.7952-2	3.9179-2	5.0804-3	4.7431-2	9.4200-4	4.9335-2	1.8431-3	4.9046-2	1.1514-2	3.5553-2
11	5.1456-3	3.5298-2	7.1626-2	3.2004-2	4.5490-3	4.9179-2	4.9041-3	3.4460-2	1.7415-2	2.5184-2	2.2571-2	2.6982-2	1.8394-2	4.0959-2
12	2.6837-3	2.2297-2	6.0437-2	5.1009-2	1.1577-3	3.2993-2	2.8601-2	5.8283-3	4.1688-2	2.1007-5	4.3320-2	5.4143-4	4.5667-2	6.3378-5
13	1.3780-3	1.3502-2	4.6253-2	5.3538-2	1.3977-2	1.0905-2	4.2574-2	2.3212-3	3.0711-2	1.7579-2	1.6377-2	2.8647-2	1.0683-2	3.3026-2
14	6.9962-4	7.9172-3	3.2962-2	5.7972-2	3.1418-2	2.5375-4	3.4721-2	2.0400-2	6.6949-3	3.6796-2	1.3573-4	3.6255-2	4.5241-3	5.3505-2
15	3.5254-4	4.5299-3	2.2268-2	5.0057-2	4.4474-2	4.2788-3	1.6705-2	3.5353-2	7.8834-4	2.8085-2	1.6663-2	1.1055-2	3.0416-2	2.8417-3
16	1.7686-4	2.5446-3	1.4443-2	3.9684-2	4.9779-2	1.6781-2	3.0392-3	3.4144-2	1.3841-2	7.8066-3	3.2518-2	3.9481-4	3.0054-2	8.7665-3

v' \ v''	14	15	16	17	18	19	20	21	22	23	24	25	26	27
0	2.9709-9	1.2832-10	4.1106-12	9.9345-14	3.3615-15	3.0101-17	4.3574-16	4.8245-16	1.0952-16	1.1648-15	2.7283-16	6.6761-16	1.8359-15	2.0131-16
1	6.4253-7	4.0808-8	1.9606-9	7.0520-11	1.8302-12	2.3676-14	4.1986-16	8.6253-16	4.5937-16	1.5854-16	9.8175-16	2.1260-16	2.0687-16	4.9335-16
2	4.4589-5	4.1814-6	2.9740-7	1.5857-8	6.2259-10	1.7511-11	3.5988-13	1.8946-15	8.4255-17	6.9250-16	9.1179-17	1.7731-18	1.1287-17	2.1375-16
3	1.2847-3	1.8106-4	1.9191-5	1.5250-6	8.9997-8	3.8880-9	1.1838-10	2.3433-12	3.3098-14	3.4689-16	1.1776-15	2.3464-16	1.0360-15	1.2129-15
4	1.6319-2	3.5966-3	5.8124-4	6.9568-5	6.1694-6	4.0236-7	1.9017-8	6.3003-10	1.3674-11	2.6901-13	5.5744-15	7.6479-16	4.3130-16	2.2953-16
5	8.7152-2	3.2616-2	8.4426-3	1.5660-3	2.1160-4	2.0924-5	1.5064-6	7.7871-8	2.8156-9	6.8393-11	1.2525-12	8.1166-15	1.5217-15	1.7040-15
6	1.5686-1	1.2213-1	5.6318-2	1.7212-2	3.6717-3	5.6045-4	6.1776-5	4.9073-6	2.7756-7	1.0921-8	2.8774-10	5.2210-12	5.7443-14	3.3133-15
7	3.1952-2	1.3391-1	1.4800-1	8.5723-2	3.1173-2	7.6735-3	1.3248-3	1.6284-4	1.4270-5	8.8267-7	3.7741-8	1.0816-9	2.0109-11	1.5562-13
8	4.9484-2	1.9439-3	8.9062-2	1.5540-1	1.1640-1	5.0917-2	1.4532-2	2.8438-3	3.9011-4	3.7718-5	2.5518-6	1.1851-7	3.6551-9	6.9987-11
9	3.4393-2	7.8477-2	7.5768-3	4.0354-2	1.4013-1	1.4178-1	7.5755-2	2.5231-2	5.6135-3	8.6061-4	9.1860-5	6.7969-6	3.4248-7	1.1363-8
10	4.4981-2	3.7797-3	7.6180-2	3.7765-2	7.2487-3	1.0525-1	1.5492-1	1.0330-1	4.0497-2	1.0285-2	1.7656-3	2.0824-4	1.6856-5	9.2168-7
11	5.2590-3	6.1266-2	4.7036-3	4.6677-2	6.8721-2	1.1699-3	6.1404-2	1.5085-1	1.2947-1	6.0438-2	1.7612-2	3.3944-3	4.4294-4	3.9248-5
12	5.0482-2	3.2684-3	4.6130-2	3.0377-2	1.3531-2	7.9458-2	2.0142-2	2.2846-2	1.2880-1	1.4915-1	8.4181-2	2.8335-2	6.1512-3	8.8962-4
13	1.2956-2	3.0547-2	2.6337-2	1.6466-2	5.4613-2	8.1207-7	6.4021-2	5.0336-2	1.9290-3	9.3245-2	1.5734-1	1.0964-1	4.2991-2	1.0555-2
14	7.7462-3	7.6321-2	5.5526-3	4.6588-2	2.0058-4	5.6134-2	1.2476-2	3.3442-2	7.9625-2	3.9385-3	5.3209-2	1.5075-1	1.3557-1	6.1671-2
15	3.6895-2	9.0014-4	4.0821-2	1.7892-3	4.3017-2	9.5126-3	3.4975-2	3.8010-2	7.2387-3	7.7082-2	2.4771-2	1.9622-2	1.2914-1	1.5192-1
16	2.1658-2	1.7875-2	1.7293-2	2.2493-2	1.9805-2	2.0646-2	3.2328-2	9.6230-3	5.5729-2	5.1842-4	5.9387-2	5.2688-2	1.6734-3	9.6082-2

TABLE 6.—*Franck-Condon factors to high vibrational quantum numbers for the N_2^+ Meinel ($A^2\Pi - X^2\Sigma$) band system*

v' \ v''	0	1	2	3	4	5	6	7	8	9	10
0	*4.7507-1*	*3.7976-1*	1.2261-1	2.0552-2	1.9140-3	9.8223-5	2.5730-6	2.8280-8	7.1881-11	1.3034-14	1.3712-16
1	3.2551-1	3.1147-2	*3.3577-1*	*2.3675-1*	6.2361-2	7.9463-3	5.1634-4	1.6252-5	2.0531-7	5.6007-10	1.7873-13
2	1.3597-1	*2.2454-1*	2.1360-2	1.8509-1	*2.9463-1*	1.1706-1	1.9723-2	1.5814-3	5.8634-5	8.3781-7	2.4027-9
3	4.5258-2	1.9900-1	7.9737-2	1.0485-1	6.2736-2	*2.9286-1*	1.7382-1	3.7932-2	3.6854-3	1.5859-4	2.5305-6
4	1.3290-2	1.0318-1	*1.7446-1*	7.1951-3	*1.5584-1*	5.8075-3	*2.4791-1*	*2.2299-1*	6.2282-2	7.2377-3	3.5730-4
5	3.6240-3	4.1446-2	1.3947-1	*1.0776-1*	6.9178-3	*1.5087-1*	5.6092-3	1.8156-1	*2.5782-1*	9.1651-2	1.2619-2

v' \ v''	11	12	13	14	15	16	17	18	19	20	21
0	2.7562-18	1.4459-16	1.0180-16	9.5982-17	6.8800-16	9.3860-17	4.4501-16	1.0922-15	1.5305-16	4.8250-16	1.4032-15
1	4.6499-15	2.7039-16	7.7745-16	5.7731-16	5.1409-17	4.8211-16	1.5310-16	2.8998-17	1.4699-16	1.5527-17	3.4885-17
2	1.2992-12	3.4067-15	9.4675-16	6.8119-18	9.2846-17	2.6601-18	5.3240-17	6.4896-18	7.2136-19	3.6857-19	3.3878-17
3	7.5480-9	6.1950-12	6.6985-15	5.2723-15	3.0122-16	8.5199-16	2.3340-16	4.6723-16	3.4614-16	1.6626-16	6.1908-16
4	6.3015-6	1.9287-8	2.2829-11	6.3533-15	4.6511-15	3.5759-15	1.4709-16	1.5949-15	7.9021-16	1.9054-16	6.2021-16
5	7.0813-4	1.3686-5	4.2478-8	7.2533-11	1.2025-14	1.1015-14	1.3299-15	1.9820-16	3.6896-16	1.1160-15	3.3943-16

TABLE 7. *Franck-Condon factor array to large vibrational quantum numbers for the N_2^+ first negative ($B^2\Sigma - X^2\Sigma$) band system*

v' \ v''	0	1	2	3	4	5	6	7	8	9	10
0	*6.5094-1*	*2.5883-1*	7.0162-2	1.5997-2	3.2972-3	6.3420-4	1.1549-4	1.9998-5	3.2805-6	5.0335-7	7.0274-8
1	3.0144-1	2.2260-1	*2.8598-1*	1.3242-1	4.2726-2	1.1403-2	2.6998-3	5.8613-4	1.1849-4	2.2393-5	3.9313-6
2	4.5371-2	*4.0599-1*	5.0646-2	*2.2901-1*	*1.6535-1*	7.1133-2	2.3623-2	6.6908-3	1.6951-3	3.9336-4	8.4449-5
3	2.2475-3	1.0562-1	*4.1372-1*	2.1005-3	1.5566-1	*1.7060-1*	9.4514-2	3.8008-2	1.2612-2	3.6675-3	9.6386-4
4	1.4521-5	6.9353-3	1.6604-1	*3.7922-1*	6.7256-3	9.2901-2	*1.5692-1*	1.0964-1	5.2363-2	2.0033-2	6.5985-3
5	4.6340-7	3.9858-5	1.3395-2	2.2051-1	3.3100-1	2.9248-2	4.8153-2	*1.3527-1*	*1.1606-1*	6.4883-2	2.8257-2
6	9.4819-9	3.0877-6	5.7286-5	2.0691-2	*2.6731-1*	2.8304-1	5.3307-2	2.0444-2	1.0647-1	*1.1489-1*	7.4424-2
7	6.4377-10	3.4169-8	1.1319-5	4.9298-5	2.7894-2	*3.0677-1*	2.4145-1	7.2364-2	5.9387-3	8.0835-2	*1.0837-1*
8	4.1998-13	5.7552-9	4.9506-8	3.0055-5	1.8070-5	3.4188-2	*3.4009.1*	2.0830-1	8.4684-2	4.7434-4	5.8649-2
9	1.2746-12	3.8766-12	2.6591-8	1.7424-8	6.4203-5	1.0666-6	3.8904-2	*3.6856-1*	1.8373-1	9.0654-2	5.5515-4
10	3.9487-14	1.0275-11	1.7096-10	8.3563-8	3.2950-8	1.1610-4	8.0941-5	4.1527-2	*3.8526-1*	1.6717-1	9.1407-2
11	2.8767-16	6.9997-13	3.8767-11	1.6762-9	1.9686-7	6.7150-7	1.8230-4	3.8725-4	4.1704-2	*4.1493-1*	1.5792-1
12	5.2594-16	2.4906-15	5.5598-12	7.8486-11	9.1842-9	3.5933-7	3.5224-6	2.5089-4	1.0871-3	3.9276-2	*4.5379-1*
13	7.4212-20	9.9105-16	1.0091-13	2.7547-11	5.7016-11	3.5189-8	4.9932-7	1.1720-5	3.0102-4	2.3614-3	3.4320-2
14	1.7188-16	9.8952-17	1.3821-15	9.9713-13	9.4783-11	1.3391-11	1.0410-7	4.7645-7	3.0048-5	3.0712-4	4.3643-3
15	1.8407-16	4.0381-17	2.6642-15	3.0960-15	7.6533-12	2.2485-10	1.1384-9	2.4797-7	2.0416-7	6.3998-5	2.4992-4
16	1.8159-17	5.4575-18	2.8290-15	6.5616-15	2.0529-14	3.6688-11	3.6122-10	8.9261-9	4.8200-7	1.5601-8	1.1714-4
17	9.5257-17	1.3459-16	1.3306-15	1.5689-15	5.3219-14	1.1348-12	1.2484-10	2.8360-10	3.8957-8	7.5533-7	1.3451-6
18	3.2282-16	6.4620-16	2.7374-17	3.0826-15	7.6808-15	4.8177-14	8.8436-12	3.2815-10	2.0518-15	1.2246-7	9.0082-7
19	3.0466-16	6.7846-16	1.1417-16	2.9053-15	3.1337-17	7.9994-14	3.1504-14	4.3885-11	6.1538-10	1.8661-9	3.0166-7
20	6.8290-17	1.0853-16	4.7800-17	1.3187-16	1.9387-16	1.0090-14	1.0265-13	1.2416-12	1.6333-10	7.0155-10	1.6088-8
21	2.0275-17	6.9310-17	2.1950-17	1.2681-15	2.4681-15	7.4429-16	7.4978-14	6.1713-14	1.2370-11	4.3238-10	2.3013-10
22	1.6131-16	5.1946-16	2.1950-17	2.0731-15	1.1194-15	1.1293-15	1.8187-14	1.0151-13	8.6085-15	6.8228-11	8.3364-10
23	3.0806-16	7.5001-16	1.8879-18	5.7561-16	2.8680-16	5.7740-16	8.7811-18	5.5815-14	2.4374-13	3.2389-12	2.4321-10
24	2.6276-16	4.0819-16	2.2567-16	3.9537-17	2.8615-15	3.7123-15	2.7915-15	2.7967-14	8.7905-14	7.2159-14	3.0774-11
25	7.3746-17	7.2516-17	5.2749-16	3.2663-16	2.1827-15	1.4253-15	3.9308-16	4.4983-15	1.0689-14	2.0665-13	1.5994-12
26	2.6573-18	1.4601-17	4.5026-16	2.0016-16	5.8352-17	3.0164-16	2.0010-15	1.9069-15	5.6924-16	7.6241-15	6.6945-17
27	1.0392-16	1.4208-16	8.1945-17	6.7362-18	8.7095-16	2.7341-15	4.5872-15	1.1201-14	2.1936-15	6.4900-14	3.8017-14
28	2.6226-16	2.7250-16	3.3132-17	2.8661-17	1.9786-15	2.3088-15	8.0611-16	1.1309-14	2.8800-14	1.4500-13	4.4470-14
29	2.6659-16	3.2371-16	3.0606-16	2.8421-17	1.0866-15	1.7611-16	1.8939-15	6.6923-15	9.2761-14	9.0932-14	1.4744-13

TABLE 7. *Franck-Condon factor array to large vibrational quantum numbers for the N_2^+ first negative ($B^2\Sigma$—$X^2\Sigma$)bamd system*—Continued

v' \ v''	11	12	13	14	15	16	17	18	19	20	21
0	8.4194-9	7.4706-10	2.7246-11	1.5572-12	5.7438-12	4.0732-12	1.9329-12	7.4934-13	2.4709-13	6.8549-14	1.6424-14
1	6.2862-7	8.7554-8	9.5331-9	5.6580-10	2.7584-13	4.1016-11	3.8757-11	2.1156-11	9.2253-12	3.5745-12	1.2773-12
2	1.6754-5	3.0305-6	4.8313-7	6.2656-8	5.2243-9	5.9097-11	1.2927-10	1.8980-10	1.2444-10	6.0838-11	2.5444-11
3	2.3237-4	5.1559-5	1.0440-5	1.8810-6	2.8382-7	3.0499-8	1.1388-9	1.9308-10	5.9679-10	4.8728-10	2.7405-10
4	1.9422-3	5.2074-4	1.2807-4	2.8771-5	5.7951-6	9.9985-7	1.3165-7	8.8002-9	5.3633-11	1.3336-9	1.4349-9
5	1.0429-2	3.4058-3	1.0071-3	2.7242-4	6.7369-5	1.5032-5	2.9233-6	4.5566-7	4.4113-8	3.8150-10	2.0816-9
6	3.6515-2	1.4962-2	5.3781-3	1.7413-3	5.1455-4	1.3912-4	3.4114-5	7.3925-6	1.3305-6	1.6789-7	6.7916-9
7	8.0508-2	4.4113-2	1.9912-2	7.8225-3	2.7556-3	8.8413-4	2.5973-4	6.9513-5	1.6626-5	3.3928-6	5.2530-7
8	*9.8214-2*	8.3188-2	5.0528-2	2.4953-2	1.0647-2	4.0574-3	1.4059-3	4.4632-4	1.2957-4	3.3924-5	7.7377-6
9	4.0751-2	*8.6284-2*	*8.2879-2*	5.5439-2	2.9771-2	1.3721-2	5.6271-3	2.0953-3	7.1529-4	2.2401-4	6.3751-5
10	3.6040-3	2.7101-2	7.3930-2	*8.0178-2*	5.8721-2	3.4099-2	1.6889-2	7.4191-3	2.9555-3	1.0800-3	3.6310-4
11	8.8180-2	7.8956-3	1.7195-2	6.2084-2	*7.5740-2*	6.0410-2	3.7741-2	1.9994-2	9.3675-3	3.9758-3	1.5488-3
12	1.5540-1	8.2045-2	1.2382-2	1.0343-2	5.1312-2	*7.0185-2*	6.0656-2	4.0577-2	2.2892-2	1.1393-2	5.1321-3
13	*4.4957-1*	1.5933-1	7.3838-2	1.6506-2	5.8379-3	4.1892-2	*6.4044-2*	*5.9684-2*	4.2558-2	2.5466-2	1.3412-2
14	2.7223-2	*4.6145-1*	1.6967-1	6.4180-2	2.0049-2	3.0433-3	3.3901-2	5.7743-2	*5.7746-2*	4.3701-2	2.7626-2
15	7.1648-3	1.8762-2	*4.6808-1*	1.8661-1	5.3547-2	2.3010-2	1.4302-3	2.7284-2	5.1592-2	*5.5097-2*	4.4065-2
16	1.3548-4	1.0676-2	1.0178-2	*4.6761-1*	2.1044-1	4.2359-2	2.5526-2	5.8439-4	2.1907-2	4.5804-2	*5.1972-2*
17	1.8672-4	2.0326-5	1.4586-2	3.2073-3	*4.5788-1*	2.4131-1	3.1069-2	2.7824-2	1.9790-4	1.7599-2	4.0509-2
18	7.5652-6	2.5870-4	3.5495-5	1.8313-2	1.9948-5	*4.3662-1*	2.7903-1	2.0265-2	3.0199-2	5.4549-5	1.4183-2
19	6.8357-7	2.4387-5	3.0557-4	3.9546-4	2.1029-2	3.0089-3	*4.0194-1*	3.2267-1	1.0750-2	*5.2989-2*	1.6955-5
20	5.9409-7	1.3334-7	5.8097-5	2.9260-4	1.3714-3	2.1794-2	1.4370-2	*5.5292-1*	*5.7021-1*	3.5923-3	*5.6642-2*
21	6.9591-8	9.1908-7	3.4595-7	1.1445-4	1.9932-4	3.2078-3	1.9842-2	3.5454-2	2.9044-1	*4.1810-1*	1.2231-4
22	5.0037-10	2.0893-7	1.0338-6	4.6938-6	1.8534-4	5.9069-5	5.9731-3	1.5008-2	6.5937-2	2.1796-1	*4.6109-1*
23	1.0306-9	1.0520-8	4.7806-7	6.4729-7	1.9630-5	2.4734-4	8.0611-6	9.3682-3	8.2444-3	1.0298-1	1.4206-1
24	6.5049-10	3.7077-10	5.8628-8	8.4343-7	2.1043-8	5.3360-5	2.5985-4	3.1278-4	1.2586-2	2.0152-3	1.4068-1
25	1.4345-10	1.1228-9	7.4423-10	2.0164-7	1.0704-6	1.3360-6	1.1017-4	1.8749-4	1.3264-3	1.4378-2	2.1219-4
26	1.4755-11	4.0176-10	8.5840-10	1.6039-8	4.8573-7	7.4719-7	1.0525-5	1.7906-4	5.2861-5	3.3301-3	1.3483-2
27	4.5578-14	4.7793-11	6.8930-10	8.1140-12	8.0276-8	8.1718-7	3.5258-8	3.6910-5	2.2192-4	1.7120-5	6.2372-2
28	2.0445-12	6.7752-13	1.4968-10	1.0541-9	2.5762-9	2.3357-7	8.9840-7	1.3616-6	8.5564-5	1.8547-4	4.3123-4
29	6.2592-12	1.9120-11	7.1972-12	9.0426-10	1.6712-9	2.2423-8	5.1404-7	4.9309-7	1.0523-5	1.4399-4	6.6619-5

TABLE 8. *Franck-Condon Factors for excitation of levels of N_2^+ ($X^2\Sigma_g^+$) from $N_2(X^1\Sigma_g^+, v=0)$*

v' \ v''	0	v' \ v''	0
0	9.0236-1	11	1.9235-11
1	9.0636-2	12	3.4295-12
2	6.5080-3	13	6.5247-13
3	4.5437-4	14	1.3180-13
4	3.5005-5	15	2.6924-14
5	3.1250-6	16	4.5920-15
6	3.2409-7	17	6.9115-16
7	3.8320-8	18	3.8920-16
8	5.0548-9	19	8.9534-16
9	7.3154-10	20	1.5161-15
10	1.1463-10	21	8.5939-16

TABLE 9. *Franck-Condon Factors for the excitation of levels of N_2^+ ($A^2\Pi$) from $N_2(X^1\Sigma_g^+, v=0)$*

v' \ v''	0
0	2.4468-1
1	3.1069-1
2	2.2530-1
3	1.2358-1
4	5.7340-2
5	2.3877-2

TABLE 10. *Franck-Condon Factors for the excitation of levels of $N_2^+(B^2\Sigma_u^+)$ from $N_2(X^1\Sigma_g^+,\ v=0)$*

v' \ v''	0	v' \ v''	0
0	8.9119–1	15	1.7921–17
1	1.0703–1	16	2.8420–20
2	1.7514–3	17	2.9486–17
3	2.6855–5	18	1.0171–16
4	1.7966–6	19	1.3940–16
5	6.5482–8	20	2.0681–17
6	1.0485–9	21	3.5482–17
7	3.3727–10	22	1.7063–16
8	5.2112–12	23	2.6721–16
9	1.8534–13	24	1.3949–16
10	4.9245–14	25	5.5412–19
11	5.0633–17	26	9.7988–17
12	1.0188–15	27	3.1142–16
13	3.3279–16	28	4.3268–16
14	5.4866–17	29	2.8228–16

5. Bibliography

Bates, D. R. (1949), Proc. Roy. Soc. [A] **196,** 217.
Bates, D. R. (1952), Monthly Notices Roy. Astron. Soc. **112,** 614.
Biberman, L. M., and Yakubov, I. T. (1960), Opt. and Spect. **8,** 155.
Condon, E. U. (1926), Phys. Rev. **32,** 858.
Dixon, R. N., and Nicholls, R. W. (1958), Can. J. Phys. **36,** 127.
Dunham, J. L. (1932), Phys. Rev. **41,** 713, 721.
Fallon, R. J., Tobias, R., and Vanderslice, J. T. (1961), J. Chem. Phys. **34,** 167.
Fraser, P. A. (1954), Proc. Phys. Soc. [A] **67,** 939.
Fraser, P. A., and Jarmain, W. R. (1953), Proc. Phys. Soc. [A] **66,** 1145.
Fraser, P. A., Jarmain, W. R., and Henderson, G. P. (1959), Scientific Report No. 2, Contract AF 19 (604)–4560, University of Western Ontario.
Fraser, P. A., Jarmain, W. R., and Nicholls, R. W. (1954), Astrophys. J. **119,** 286.
Gaydon, A. G., and Pearse, R. W. B. (1939), Proc. Roy. Soc. [A] **173,** 37.
Hebert, G. R., and Nicholls, R. W. (1961), Can. J. Phys. (in press).
Herzberg, G. (1950), The Spectra of Diatomic Molecules (D. Van Nostrand Co., Inc., New York, N.Y.).
Hutchisson, E. H. (1930), Phys. Rev. **36,** 410.
Hutchisson, E. H. (1931), Phys. Rev. **37,** 45.
Jarmain, W. R. (1959), J. Chem. Phys. **31,** 1137.
Jarmain, W. R. (1960), Can. J. Phys. **38,** 217.
Jarmain, W. R., and Fraser, P. A. (1953), Proc. Phys. Soc. [A] **66,** 1153.
Jarmain, W. R., and Nicholls, R. W. (1954), Can. J. Phys. **32,** 201.
Jarmain, W. R., and Ebisuzaki, R., and Nicholls, R. W. (1960), Can. J. Phys. **38,** 510.
Jarmain, W. R., Fraser, P. A., and Nicholls, R. W. (1953), Astrophys. J. **118,** 228.
Jarmain, W. R., Fraser, P. A., and Nicholls, R. W. (1955), Astrophys. J. **122,** 55.
Losev, S. A. (1958), Nauk Doklady Vyschei Shkoly, Fis Mat Nauchi **5.**
Montgomery, C. E., and Nicholls, R. W. (1951), Phys. Rev. **82,** 565.
Mulliken, R. S. (1959), The Threshold of Space, p. 169 (Ed. M. Zelikoff, Pergamon Press, Inc., New York, N.Y.).
Morse, P. M. (1929), Phys. Rev. **34,** 57.
Nicholls, R. W. (1950), Phys. Rev. **77,** 421.
Nicholls, R.W. (1956), Proc. Phys. Soc. **69,** 741.
Nicholls, R.W. (1958), Ann. géophys. **14,** 208.
Nicholls, R. W. (1961), unpublished work.
Nicholls, R. W., and Jarmain, W. R. (1956), Proc. Phys. Soc. **69,** 253.
Nicholls, R. W., and Jarmain, W. R. (1959), Proc. Phys. Soc. **74,** 133.
Nicholls, R. W., Fraser, P. A., and Jarmain, W. R. (1959), Combustion and Flame **3,** 13.
Nicholls, R. W., Fraser, P. A., Jarmain, W. R., and McEachran, R. P. (1960), Astrophys. J. **131,** 399.
Ortenberg, F. S. (1960), Opt. and Spect. **9,** 82.
Pillow, M. E. (1949), Proc. Phys. Soc. [A] **62,** 237.
Pillow, M. E. (1950), Proc. Phys. Soc. [A] **63,** 940.
Pillow, M. E. (1951), Proc. Phys. Soc. [A] **64,** 772.
Pillow, M. E. (1952), Proc. Phys. Soc. [A] **65,** 858.
Pillow, M. E. (1953a), Proc. Phys. Soc. [A] **66,** 1064.
Pillow, M. E. (1953b), Mem. Roy. Soc. Liege **13,** 145.
Pillow, M. E. (1954), Proc. Phys. Soc. [A] **67,** 847.
Pillow, M. E. (1955), Proc. Phys. Soc. [A] **68,** 547.
Pillow, M. E., and Rowlatt, A. L. (1960), Proc. Phys. Soc. **75,** 162.
Robinson, D., and Nicholls, R. W. (1958), Proc. Phys. Soc. **71,** 957.
Robinson, D., and Nicholls, R. W. (1960), Proc. Phys. Soc. **75,** 817.
Tobias, R., Fallon, R. J., and Vanderslice, J. T. (1960), J. Chem. Phys. **33,** 1638.
Turner, R. G., and Nicholls, R. W. (1951), Phys. Rev. **82,** 290.
Turner, R. G., and Nicholls, R. W. (1954a), Can. J. Phys. **32,** 468.
Turner, R. G., and Nicholls, R. W. (1954b), Can. J. Phys. **32,** 475.
Vanderslice, J. T., Mason, E. A., and Maisch, W. G. (1960a), J. Chem. Phys. **32,** 515.
Vanderslice, J. T., Mason, E. A., and Maisch, W. G. (1960b), J. Chem. Phys. **33,** 614.
Vanderslice, J. T., Mason, E. A., Maisch, W. G., and Lippincott, E. R. (1959), J. Mol. Spectroscopy **3,** 17.
Vanderslice, J. T., Mason, E. A., Maisch, W. G., and Lippincott, E. R. (1960), J. Mol. Spectroscopy **5,** 83.
Wallace, L. V., and Nicholls, R. W. (1955), J. Atmospheric and Terrest. Phys. **7,** 101.
Wu, T. Y. (1952), Proc. Phys. Soc. [A] **65,** 965.
Wyller, A. (1953), Mem. Roy. Soc. Liege **13,** 917.
Wyller, A. (1958), Astrophys. J. **127,** 763.
Yakubov, I. T. (1960), Opt. and Spect. **9,** 212.

(Paper 65A5–126)

Publications of the National Bureau of Standards

(Including papers in outside journals)

Selected Abstracts

Theory of an accurate intermediary orbit for satellite astronomy, J. P. Vinti, *J. Research NBS* **65B** (*Math. and Math. Phys.*) *No. 3, 169 (July-September 1961) 70 cents.*
This paper derives an accurate intermediary orbit of an artificial satellite of an oblate planet. The drag-free motion takes place under the action of a gravitational potential which fits the even zonal harmonics exactly through the second and approximately through the fourth, in the case of the earth. This potential leads to separability of the Hamilton-Jacobi equation.
Two alternative sets of orbital elements are set forth. The first set is related directly to initial conditions, but requires numerical factoring of a certain quartic to evaluate some of the integrals. The second set, on the other hand, permits exact factoring of both quartics that appear, but is not related directly to initial conditions, so that its members can best be obtained by a least-square fit of the solution over many orbital revolutions.
The final solution is given in terms of certain uniformising variables, whose periodic terms are correct through the second order in the oblateness parameter and whose secular terms are exact, for the intermediary orbit. These exact solutions for the secular terms are expressed by means of certain rapidly converging series, with complete avoidance of elliptic integrals of the third kind.

Prediction of symptoms of cavitation, R. B. Jacobs, *J. Research NBS* **65C** (*Eng. and Instr.*) *No. 3, 147 (July-September 1961) 70 cents.*
An analysis which indicates some of the basic problems in cavitation and which may permit the prediction of cavitation characteristics of hydraulic equipment is presented. Some experimental results are discussed and are compared with the results of the analysis.
It is concluded that the analysis may be applicable to the prediction of symptoms of cavitation (changes in performance characteristics due to the presence of cavitation), but that more information related to metastability, nucleation, and vapor-phase dynamics is required.

On the nature of the crystal field approximation, C. M. Herzfeld and H. Goldberg, *J. Chem. Phys.* **34,** *No. 2, 643–651 (Feb. 1961).*
A new method is developed for the treatment of molecular interactions, and is applied to a system consisting of a hydrogen atom in a $2p$ state and a hydrogen molecule in the ground state. The interaction of these two species is calculated using ordinary crystal field theory and also the new method. A comparison of the results shows some of the shortcomings of the conventional crystal field theory, and provides corrections to it. The new method consists of (1) expanding all electron terms of the total Hamiltonian for the system which involve interactions between the atom and the molecule, thus transforming the interaction Hamiltonian into sums of products of one-electron operators, and (2) of using properly antisymmetrized wave functions made up of products of atom and molecule eigenfunctions. The calculations show the effect of the neglect of overlap and exchange in ordinary crystal field theory.

The electromagnetic fields of a dipole in the presence of a thin plasma sheet, J. R. Wait, *Appl. Sci. Research* **8,** *Sec. B, 397–417 (1960).*
The problem of electric and magnetic dipoles located near a thin planar slab or sheet of ionized material is considered. A constant and uniform magnetic field is impressed on the slab. Under the assumption that the thickness of the slab is very small, expressions for the resultant fields are obtained. As a result of the anisotropy of the sheet it is indicated that the fields are elliptically polarized in general. On carrying out a saddle-point evaluation of the integrals in the formal solution it is shown that the far fields may be split into "radiation" and "surface wave" components. The dependence of the radiation pattern and the surface wave characteristics on electron density, collision frequency, and the impressed magnetic field is illustrated.

Calculation of properties of magnetic deflection systems, S. Penner, *Rev. Sci. Instr.* **32,** *No. 2, 150–160 (Feb. 1961).*
A convenient matrix method for calculating properties of magnetic deflection systems is presented. This method is applicable to particle beams of small spatial and angular extent, and small energy spread. Equations for quadrupole lenses and for deflecting magnets are given. Examples are given to show the procedure for calculating the parameters of magnet systems.

Departures from the Saha equation for ionized helium. I. Condition of detailed balance in the resonance lines, R. N. Thomas and J. B. Zirker, *Astrophys. J.* **133,** *No. 2, 588–595 (Mar. 1961).*
Conditions for the validity of the assumption of detailed balance in the Lyman lines of He II are investigated. An opacity of 10^6 in Lyman-α is required, which implies high opacity in the subordinate lines and resonance continuum. The b_n-factors are computed, including the transfer problem in the subordinate lines and resonance continuum.

Arc source for high temperature gas studies, J. B. Shumaker, Jr., *Rev. Sci. Instr.* **32,** *No. 1, 65–67 (Jan. 1961).*
A wall-stabilized water-cooled copper ring type arc source is described which operates stably in apparently any gas for periods of an hour or more at currents up to 100 Amperes. Arc temperatures obtained spectroscopically by absolute line intensity and line profile methods are given for the arc in nitrogen at 92 Amperes.

Electron diffraction studies on solid α-nitrogen, E. M. Horl and L. Marton, *Acta Crystallographica* **14,** *Pt. I, 11–19 (Jan. 10, 1961).*
A technique was developed for studying thin films of solidified permanent gases by means of electron transmission diffraction. It was applied to the investigation of thin films of solid α-nitrogen at 4° and 20° K. The orientation of the microcrystallites on aluminum and Formvar substrates was investigated as a function of both the temperature of the substrate and the intensity of the molecular nitrogen beam during deposition. Further, the crystal structure and the cell dimensions of α-nitrogen were reinvestigated. Faults in the stacking sequence of (111) planes, detected under certain conditions, were studied in some detail. Preferential crystal growth processes were observed to be induced by electron bombardment. The influence of conditions of deposition on these processes was also investigated.

The absorption spectra of magnesium and manganese atoms in solid rare gas matrices, O. Schnepp, *J. Phys. Chem. Solids* **17,** *Nos. 3/4, 188–195 (1961).*
The absorption spectra of magnesium and of manganese in solid rare gas matrices have been investigated at liquid helium temperature. An absorption system of magnesium near 2850 Å and two for manganese near 4000 Å and 2800 Å have been observed. These absorptions lie very close to the wavelengths of allowed atomic transitions and it is concluded on the basis of the evidence presented here that the absorbing species are atoms which are, in general, trapped at more than one type of site. The crystal field causes the removal of the orbital degeneracy of the excited atomic P states; the splitting energy is observed to be of the order of 300 cm^{-1}. It is proposed that the removal of the degeneracy is due to asymmetric environments of the trapping site. Possible sites are discussed.

Near infrared atmospheric transmission to solar radiation, D. M. Gates, *J. Opt. Soc. Am.* **50,** *No. 12, 1299–1304 (Dec. 1960).*
Near infrared solar spectrum observations taken on October 15, 1954 with a double-pass NaCl prism spectrometer have been analyzed for transmission coefficients for the "selective" absorption factor and for the "continuum" factor. The alalysis was carried out for 59 wavelength positions between 0.872 and 2.537 μ. The monochromatic data fit well the law $^{\circ}nT=c_1(w)^{1/2}$ where w is the amount of water vapor in the optical path. The coefficient c_1 is given as a continuous function of the wavelength. A coefficient of extinction for the "continuum" factor is also given.

Observations on the chemiluminescent reaction of nitric oxide with atomic oxygen, H. P. Broida, H. I. Schiff, and T. M. Sugden, *Trans. Faraday Soc.* **57,** *No. 458, 259–265 (Feb. 1961).*
A comparison of the absorption spectrum of NO_2 with the emission from the reaction of NO and O produced in various ways at pressures of a few mm of Hg, shows that the emitter is NO_2 in a metastable excited electronic state. Measurement of the short wavelength cut-off of the emission spectrum leads to a minimum value for ΔH_0 of $NO_2 \rightarrow NO+O$ of $71{\cdot}2 \pm 0{\cdot}1$ kcal/mole, in fair agreement with thermal data. The loss of discrete structure in the emission from the same reaction in high-temperature flames is ascribed to increasing complexity which could not be resolved.
The data are examined with respect to a system of potential-energy curves based on earlier work on the fluorescence and the spectroscopy of NO_2, and it is concluded that the emission from the interaction of NO and O occurs as a result of a resonance transfer process. The available evidence on the kinetics of the reaction is discussed in the light of a mechanism based on the two excited states NO_2^* involved, and it is shown that the resonance transfer process between them may be rate-determining, both in the emission from NO+O, and in the fluorescence of NO_2. The simple process $NO+O \rightarrow NO_2+h\nu$ is largely discarded, both on spectroscopic and kinetic grounds.

Vacuum ultraviolet photolysis of ethane: Molecular detachment of hydrogen, H. Okabe and J. R. McNesby, *J. Chem. Phys.* **34,** *No. 2, 668–669 (Feb. 1961).*
The primary process of direct ethane photolysis by Xe radiation (1470Å and 1295Å) was studied at room temperature. The hydrogen and methane isotopic compositions from a mixture of C_2H_6–C_2D_6 and from CH_3CD_3 were measured mass-spectrometrically. The results show that, contrary to the previously proposed mechanism, almost all (>95%) of the hydrogen is formed intramolecularly, and preferentially from the same carbon atom. This may be compared with the mercury-sensitized photolysis of ethane where evidence indicates that almost all hydrogen is produced by an atomic process. Methane is also formed by a molecular process. Then the primary processes may be written as

$$C_2H_6 \rightarrow CH_3CH: + H_2 \quad (1), \qquad C_2H_6 \rightarrow C_2H_4 + H_2 \quad (2),$$
$$C_2H_6 \rightarrow CH_4 + CH_2: \quad (3).$$

No ethane-d_6 was found from CH_3CD_3 photolysis indicating that no methyl radicals are formed in a primary process. The effect of ethylene on the composition of hydrogen isotopes from C_2H_6–C_2D_6 mixtures was examined, since any atomic hydrogen produced may be reacting rapidly with ethylene. The sample was purified and very low conversion (0.01%) was made. The result shows almost no change in the composition of the hydrogen isotopes in the products, indicating that the hydrogen forming step is almost all molecular. It is suggested that higher hydrocarbons may be produced by the following reactions

$$CH_3 + C_2H_6 \rightarrow C_3H_8 \quad (4), \qquad CH_3CH: + C_2H_6 \rightarrow C_4H_{10} \quad (5).$$

The effect of solvents of the γ-ray radiolysis of methyl acetate and cetone, P. Ausloos, *J. Am. Chem. Soc.* **13,** *No. 5, 1056–1060 (Mar. 1961).*
The effect of cyclohexane and benzene on the radiolysis of CH_3COOCH_3, CH_3COOCD_3, and mixtures of CH_3COCH_3–CD_3COCD_3 has been investigated at 17°. In the absence of scavengers, cyclohexane markedly reduces the yield of CO whereas, in the presence of scavengers, it produces no effect. Benzene inhibits the decomposition of methyl acetate and acetone. Hydrogen is mostly formed in processes involving "hot" hydrogen atoms. The effect of the solvents on the yields of ethanes and some of the methanes indicates the importance of cage and intercage recombinations and disproportionations of the radicals in the γ-ray track. The radiolysis of a CH_3COCH_3-CD_3COCD_3 mixtures at −195° is discussed briefly.

Intramolecular rearrangements. I. *sec*-butyl acetate and *sec*-butyl formate, R. Borkowski and P. Ausloos, *J. Am. Chem. Soc.* **83,** *No. 5, 1053–1056 (Mar. 1961).*
The photolysis of *sec*-butyl acetate and *sec*-butyl formate in the vapor, liquid, and solid phases has been studied at different temperatures and wavelengths. The distributions of the three butenes produced in the intramolecular-rearrangements were found to vary with temperature in all three phases. In the vapor phase, a change in wavelength has a pronounced effect on the ratios 1-butene/2-butenes and *cis*-2-butene/*trans*-2-butene. Both ratios increased with a decrease in wavelength. In the liquid phase photolysis, however, no dependence on wavelength was observed, but a drastic change of the butene distribution occurred in the short temperature range associated with the formation of the glassy state. A brief study of the pyrolysis of these compounds showed that, at temperatures greater than 300°, the temperature coefficient of the butene distribution was essentially zero.

Hydrogen atom reactions with propene at 77°K. Disproportionation and recombination, R. Klein and M. D. Scheer, *J. Phys. Chem.* **65,** *324–325 (1961).*
The investigation of the reaction products of deuterium atoms with ordinary propene helps to establish the relative importance of the atom addition to the propyl radical with respect to disproportionation of two propyl radicals. The distribution of the isotope species among the propenes and propanes is calculated. It is concluded that the D atom addition to the propyl radical accounts for little, if any, of the propane formed, and the radical disproportionation reaction is the predominant one.

The activation energy for hydrogen atom addition to propylene, M. D. Scheer and R. Klein, *J. Phys. Chem.* **65,** *375–377 (1961).*
The activation energy for $H+CH_2CH-CH_2$ CH_3CHCH_3 has been measured in a study of the solid phase reaction. Hydrogen atoms, formed in the gas by dissociation on a hot tungsten ribbon, were allowed to diffuse through and react with thin dilute films of propylene in the 77 to 90° K temperature range. The activation energy was determined by measuring the rate of propylene depletion as a function of film temperature. A value of 1.5 kcal/mole was obtained. No significant isotope effect was observed when D instead of H atoms were used. A steric factor of 3×10^{-3} is calculated for the gas phase reaction from the 300°K rate constant $\left(2\times10^{11}\frac{\text{cc}}{\text{mole sec}}\right)$ and an H, C_3H_6 collision diameter of 5.5 Å.

Interpretation of the appearance potentials of secondary ions, M. B. Wallenstein and M. Krauss, *J. Chem. Phys.* **34,** *No. 3, 929–936 (Mar. 1961).*
The statistical theory of mass spectra assumes that the excitation energy in a molecule-ion is essentially equipartitioned prior to unimolecular decomposition. Some of the consequences of this assumption have been deduced and the results have been used to interpret the observed appearance potentials of secondary and tertiary ions of neo-pentane, *n*-butane, and *i*-butene. Although the results are not quantitative, it is evident that considerable vibrational energy is removed with the neutral fragment.
The problem of the detailed interpretation of appearance potentials would seem to be complicated by the possibility of considerable fluctuation of the vibrational energy distribution in the products of a decomposition from the most probable distribution, i.e., equipartition. Some general considerations

with regard to determination of minimum-energy decomposition paths and the significance of this study in relation to the statistical theory of mass spectra are also presented.

Determination of crystallite size distributions from X-ray line broadening, A. Bienenstock, *J. Appl. Phys.* **32,** *No. 2, 187–189 (Feb. 1961).*
The broadening of an 00l powder diffraction line due to a distribution of sizes of crystallites is discussed. A function of the intensity, $P(h_3)\sin^2(\pi h_3)$, is derived. Its cosine transform gives the size distribution directly. The first term of a series expansion of this distribution function corresponds to the expression previously obtained by Warren and Averbach. In addition this function gives less weight to the extremes of the diffraction line shape.

The dependence of the melting temperature of bulk homopolymers on the crystallization temperature, L. Mandelkern, *J. Polymer Sci.* **XLVII,** *issue 149, 494–496 (July 1960).*
Based on the hypothesis that during the crystallization from the melt of bulk homopolymers the length of a crystallite in the chain direction does not significantly exceed that of a critical size nucleus, a simple relation is derived between the melting temperature and the crystallization temperature. This relation is found to describe the experimental results of Wood and Bekkedahl on natural rubber, where a marked effect of the crystallization temperature on the melting temperature has been reported.

The interfacial properties of polyesters at glass and water surfaces, R. R. Stromberg, *Soc. Plastic Eng. J.* **15,** *882–886 (Oct. 1959).*
Some interfacial factors related to adhesion were studied. Monomolecular layers of stearic acid and polyesters on liquid subphases are compared. Stearic acid yields a condensed type isotherm, indicating close packing and high cohesion. The monolayer of poly(ethylene adipate) at low surface pressure is the gaseous type, with very low cohesive forces, and at higher pressures, the liquid expanded type. Poly(ethylene succinate) remains in an expanded liquid state up to collapse pressure. Adsorption of polyesters from dilute solutions onto glass, silica, and alumina was also studied. Considerably more polymer was adsorbed from a poor solvent than from a good solvent. A negative temperature coefficient was observed for adsorption from the poor solvent and no temperature effect from the good solvent. This behavior was attributed, in part, to differences in the configuration of the polyester molecule in the two solvents.

Other NBS Publications

Journal of Research 65B (Math. and Math. Phys.) No. 3 (July-September 1961) 75 cents.
Theory of an accurate intermediary orbit for satellite astronomy. J. P. Vinti. (See above abstract.)
Note on the "baffled piston" problem. F. Oberhettinger.
Some results on non-negative matrices. M. Marcus, H. Minc, and B. N. Moyls.
Probability inequalities of the Tchebycheff type. I. R. Savage.

Journal of Research 65C (Engr. and Instr.) No. 3 (July-September 1961) 75 cents.
Prediction of symptoms of cabitation. R. B. Jacobs. (See above abstract.)
Heating and cooling of air flowing through an underground tunnel. B. A. Peavy.
Stress-corrosion cracking of the AZ31B magnesium alloy. H. L. Logan.
Coatings formed on steel by cathodic protection and their evaluation by polarization measurements. W. J. Schwerdtfeger and R. J. Manuele.
Calibration of inductance standards in the Maxwell-Wien bridge circuit. T. L. Zapf.
Calibration of loop antennas at VLF. A. G. Jean, H. E. Taggart, and J. R. Wait.
Location of the plain of best average definition with low contrast resolution patterns. F. E. Washer and W. P. Tayman.
Influence of temperature and relative humidity on the photographic response to Co^{60} gamma radiation. M. Ehrlich.

Journal of Research 65D (Radio Prop.) No. 5 (September-October 1961) 70 cents.
Frequency dependence of *D*-region scattering at VHF. J. C. Blair, R. N. Davis, Jr., and R. C. Kirby.
Theoretical scattering coefficient for near vertical incidence from contour maps. H. S. Hayre and R. K. Moore.
Mutual interference between surface and satellite communication systems. W. J. Hartman and M. T. Decker.
VHF and UHF signal characteristics observed on a long knife-edge diffraction path. A. P. Barsis and R. S. Kirby.
Experimental study of inverted L-, T-, and related transmission-line antennas. S. Prasad and R. W. P. King.
Reflection from a sharply bounded ionosphere for VLF propagation perpendicular to the magnetic meridian. D. D. Crombie.
Resonance of the space between earth and ionosphere. H. Poeverlein.
Observed attenuation rate of ELF (region below 1 kc/s) radio waves. A. G. Jean, A. C. Murphy, J. R. Wait, and D. F. Wasmundt.
A note concerning the excitation of ELF electromagnetic waves. J. R. Wait.
Computation of whistler ray paths. I. Yabroff.
On the analysis of LF ionospheric radio propagation phenomena. J. R. Johler.

Ideal gas thermodynamic functions and isotope exchange functions for the diatomic hydrides, deuterides, and tritides, L. Haar, A. S. Friedman, and C. W. Beckett, NBS Mono. 20 (1961) $2.75.
Bibliography of temperature measurement—January 1953 to June 1960, C. Halpern and R. J. Moffat, NBS Mono. 27 (1961) 15 cents.
Causes of variation in chemical analyses and physical tests of portland cement, B. L. Bean and J. R. Dise, NBS Mono. 28 (1961) 25 cents.
Thermal expansion of technical solids at low temperatures. A compilation from the literature, R. J. Corruccini and J. J. Gniewek, NBS Mono. 29 (1961) 20 cents.
Corrected optical pyrometer readings, D. E. Poland, J. W. Green, and J. L. Margrave, NBS Mono. 30 (1961) 55 cents.
Mean electron density variations of the quiet ionosphere—May 3, 1959, J. W. Wright, L. R. Wescott, and D. J. Brown, NBS TN40–3 (PB151399–3) (1960) $1.50.
A survey of computer programs for chemical information searching, E. C. Marden and H. R. Koller, NBS TN85 (PB161586) (1961) $2.25.
The Franck-Condon factor $(q_{v'v''})$ array to high vibrational quantum numbers for the $O_2(B^3\Sigma_u^- - X^3\Sigma_g^-)$ Schumann-Runge band system, R. W. Nicholls, Can. J. Phys. **38,** 1705–1711 (1960).
NBS—source of American Standards, W. A. Wildhack, ISA J. **8,** No. 2, 45–50 (Feb. 1961).
Ionospheric mapping by numerical methods, W. B. Jones and R. M. Gallet, Telecommun. J. **12,** 260–264 (Dec. 1960).
Titanium (III) chloride and titanium (III) bromide (titanium tricloride and titanium tribromide), J. M. Sherfey, Chapter IVB, Sec. 17, p. 57–61, Book, Inorganic Syntheses, by E. G. Rochow (McGraw-Hill Book Co., New York, N.Y., 1960).
Science news writing, D. M. Gates, J. M. Parker, Science **133,** No. 3447, 211–214 (Jan. 1961).
Integrated starlight over the sky, F. E. Roach and L. R. Megill, Astrophys. J. **133,** No. 1, 228–242 (Jan. 1961).
Elastomers for static seals at cryogenic temperatures, D. H. Weitzel, R. F. Robbins, G. R. Bopp, and W. R. Bjorklund, Rev. Sci. Instr. **31,** No. 12, 1350–1351 (Dec. 1960).
New standards for the space age, A. T. McPherson, Astronautics **6,** No. 1, 24–25; 50–54 (Jan. 1961).
Correlation of visual and subvisual auroras with changes in the outer Van Allen radiation zone, B. J. O'Brien, J. A. Van Allen, F. E. Roach, and C. W. Gartlein, IGY Bull., No. 45, 1–16 (Mar. 1961).

Spiral patterns in geophysics, V. Agy, J. Atmopsheric and Terrest. Phys. **19,** 136–140 (1960).

Iron (99.9+), G. A. Moore and T. R. Shives, Metals Handb. **1,** 1206–1212 (1961).

Ionospheric absorption at times of auroral and magnetic pulsations, W. H. Campbell and H. Leinback, J. Geophys. Research **66,** 25–34 (Jan. 1961).

Some properties of new or modified exictation sources, M. Margoshes, Am. Soc. Testing Materials, Spec. Tech. Publ. 259, 46–58 (1959).

Seasonal and day-to-day changes of the central position of the S_q overhead current system, S. Matsushita, J. Geophys. Research **65,** No. 11, 3835–3839 (Nov. 1960).

Hydrogen sulfide precipitation of the elements from 0.2–0.5 normal hydrochloric acid, J. I. Hoffman, Chemist-Analyst **50,** No. 1, 30 and 32 (Mar. 1961).

The mechanism of electrolytic deposition of titanium from fused salt media, W. E. Reid, J. Electrochem. Soc. **108,** No. 4, 393–394 (Apr. 1961).

Studies of elevated temperature corrosion of type 310 stainless steel by vanadium compounds, H. L. Logan, Corrosion **17,** 109–111 (Apr. 1961).

Deep penetration of radiation, U. Fano and M. J. Berger, Proc. Symp. Appl. Math. **XI,** 43–59 (1961).

Deposition of iron from salts of fluoro-acids, J. H. Connor and V. A. Lamb, Plating **48,** No. 4, 388–389 (Apr. 1961).

A simple low-temperature specimen holder for an X-ray diffractometer, D. K. Smith, Norelco Reporter **VII,** No. 1, 11–12 (Jan.–Feb. 1961).

Stepless variable resistor for high currents, C. R. Yokley and J. B. Shumaker, Jr., Rev. Sci. Instr. **32,** No. 1, 6–8 (Jan. 1961).

Microbalance techniques for high temperature application, R. F. Walker, Book, Vacuum microbalance techniques, edited by M. J. Katz. I, 87–110, (Plenum Press Inc., New York, N.Y., 1961).

Investigation of bond in beam and pull-out specimens with high-yield-strength deformed bars, R. G. Mathey and D. Watstein, J. Am. Concrete Inst. **32,** No. 9, 1071–1090 (Mar. 1961).

Shielding calculations for civil defense, C. Eisenhauer, Health Phys. **4,** No. 2, 129–132 (1960).

A study of auroral coruscations, W. H. Campbell and M. H. Rees, J. Geophys. Research **66,** No. 1, 41–55 (Jan. 1961).

The nature, cause and effect of the porosity in electrodeposits. VII. A microscopic examination of nickel-chromium coatings after atmospheric corrosion, D. W. Ernst and F. Ogburn, Plating **48,** No. 4, 491–497 (May 1961).

Physical quantities proposed for radiation measurements, L. S. Taylor, Proc. IXth Intern. Congress of Radiology, July 23–30, 1959 (Munchen, Germany), 1301–1302 (1960).

Improving rectifier circuits, G. F. Montgomery, Electronics p. 86–87 (April 7, 1961).

Fracture characteristics of notched tensile specimens of titanium and a titanium alloy, G. W. Geil and N. L. Carwile, Materials Research and Standards (Am. Soc. Testing Materials, Philadelphia, Pa.) **1,** No. 1, 16–21 (Jan. 1961).

The robustness of life testing procedures derived from the exponential distribution, M. Zelen and M. C. Dannemiller, Technometrics **3,** No. 1, 29–49 (Feb. 1961).

Absence of an isotope effect in the fractional recrystallization of alpha-D-glucose-1-t, H. S. Isbell, H. L. Frush, and N. B. Holt, Anal. Chem. **33,** 225–226 (Feb. 1961).

Applications of graphs and Boolean matrices to computer programming, R. B. Marimont, SIAM Rev. **2,** No. 4, 259–268 (Oct. 1960).

Comparison of national standards for roentgen measurement, H. O. Wyckoff, IXth Intern. Congress of Radiology, July 23–30, 1959 (Munchen, Germany), 1315–1318 (1960).

Environmental factors in a family-size underground shelter, R. P. Achenbach, Proc. Meeting on Environmental Engineering in protective Shelters, Feb. 8–10, 1960, Natl. Acad. Sci.-Natl. Research Council, Wash. D.C., 69–118 (1961).

How to evaluate accuracy, W. J. Youden, Materials Research and Standards (Am. Soc. Testing Materials, Philadelphia, Pa.) **1,** No. 4, 268–271 (Apr. 1961).

Improved standard for the calibration of vibration pickups, R. R. Bouche, Exp. Mech. 1–6 (Apr. 1961).

Absorption and scattering of photons by holmium and erbium, E. G. Fuller and E. Hayward, Proc. Intern. Conf. Nuclear Structure, 760–766 (Kingston, Canada, 1960).

Introductory remarks, U. Fano, Conf. Coherence Properties of Electromagnetic Radiation, AFOSR–583, Report on Conf., 31–38 (University of Rochester, The Institute of Optics, Rochester, N.Y., Apr. 1961).

Available heat sinks for protected underground installations, B. A. Peavy, Proc. Meeting on Environmental Engineering in Protective Shelters, Feb. 8–10, 1960, Natl. Acad. Sci.-Natl. Research Council, Wash. D.C., 69–118 (1961).

Studies of the low-temperature distillation of hydrogen isotopes, T. M. Flynn, Cryogenics **1,** No. 2, 1–5 (Dec. 1960); Advances Cryogenic Engr. **6,** 236–244 (1961).

Inert enclosed pump for shaped flow of ultraclean solutions, M. W. Barnes and R. H. Noyce, Rev. Sci. Instr. **32,** No. 3, 353 (Mar. 1961).

On some partial differential equations of Brownian motion of a free particle, A. Ghaffari, (Abstract) Proc. Intern. Conf. on Partial Differential Equations and Continuum Mechanics 348–350 (1961) (Univ. of Wisconsin, Madison, Wisc., June 7–15, 1960).

Radiation protection standards, L. S. Taylor, Radiology **74,** 824–831 (May 1960).

Atomic beam frequency standards, R. C. Mockler, R. E. Beehler, and C. S. Snider, IRE Trans. Instrumentation **I–9,** No. 2, 120–132 (Sept. 1960).

The development of more stable gage blocks, M. R. Meyerson, T. R. Young, and W. R. Ney, ASTM Bull. **1,** No. 5, 368–374 (May 1961).

The power spectrum and its importance in precise frequency measurements, J. A. Barnes and R. C. Mockler, IRE Trans. Instrumentation **I–9,** No. 2, 149–155 (Sept. 1960).

VLF phase perturbation associated with meteor shower ionization, C. J. Chilton, J. Geophys. Research **66,** No. 2, 379–383 (Feb. 1961).

Tests for regression coefficients when errors are correlated, M. M. Siddiqui, Annals Math. Stat. **31,** No. 4, 929–938 (Dec. 1960).

A comment on the NRL solar Lyman-Alpha results, J. T. Jefferies and R. N. Thomas, Astrophys. J. **133,** No. 2, 606–607 (Mar. 1961).

The nation's electronic standards program: where do we now stand? H. W. Lance, IRE Trans. Instrumentation **I–9,** No. 2, 94–100 (Sept. 1960).

Hard gallium alloys for use as low contact resistance electrodes and for bonding thermocouples into samples, G. C. Harmon, Rev. Sci. Instr. **31,** No. 7, 717–720 (July 1960).

Scattering of photons by deformed nuclei, E. G. Fuller and E. Hayward, Proc. Intern. Conf. Nuclear Structure, 763–766 (Kingston, Canada, 1960).

Publications for which a price is indicated (except for Technical Notes) are available only from the Superintendent of Documents, U.S. Government Printing Office, Washington 25, D.C. (foreign postage, one-fourth additional).

Technical Notes are available only from the Office of Technical Services, U.S. Department of Commerce, Washington 25, D.C. (Order by PB number). Reprints from outside journals and the NBS Journal of Research may often be obtained directly from the authors.

U.S. GOVERNMENT PRINTING OFFICE: 1961

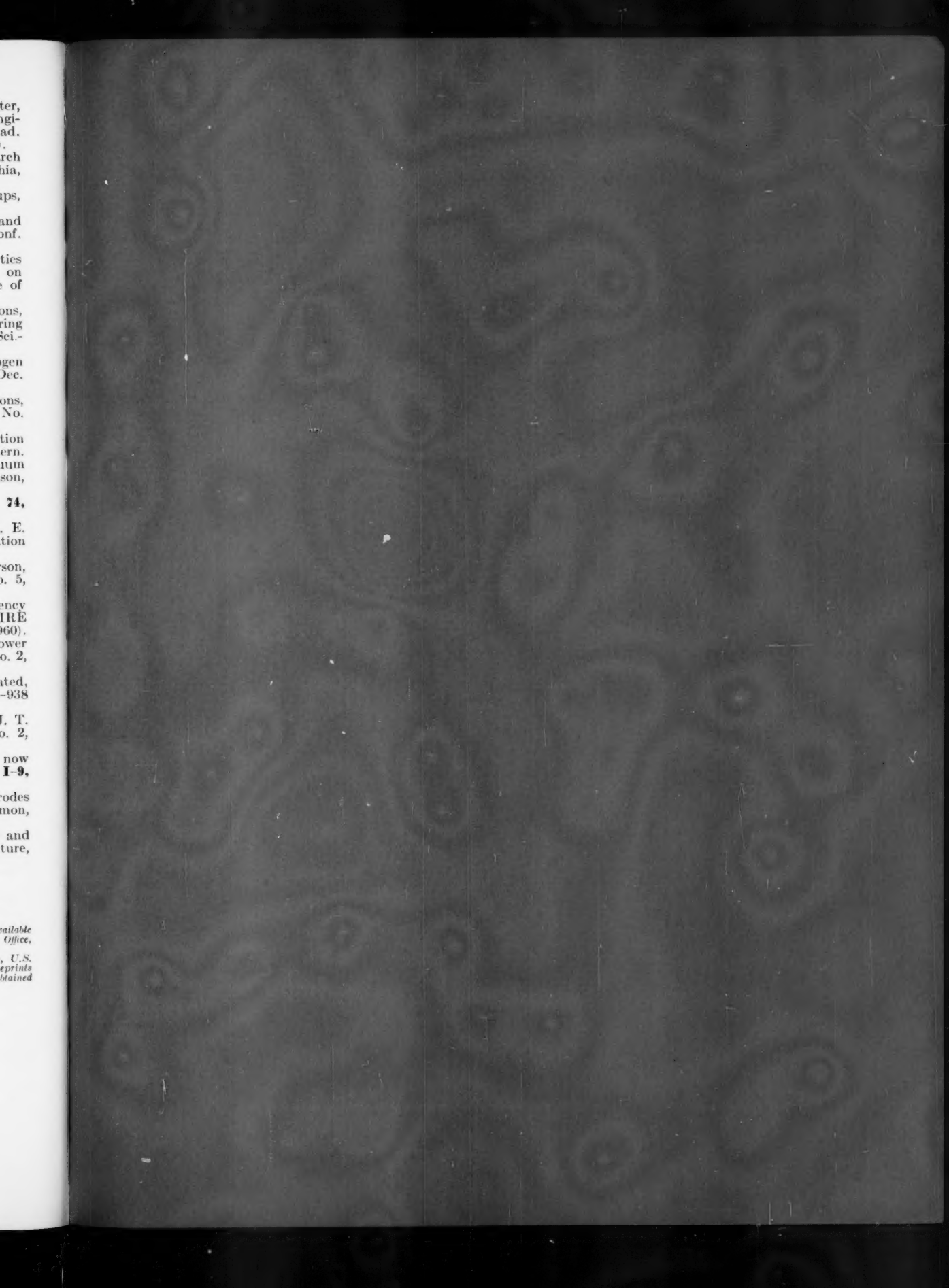

UNIVERSITY OF MICHIGAN
ORD # 56-160074
PHYSICS LIBRARY 2035 RANDALL LAB
ANN ARBOR MICH
SJR A DEC D-18220

UNI
GOVERNMEN
DIVISION OF PUBLIC DOCUMENTS
WASHINGTON 25, D.C.
OFFICIAL BUSINESS

PENALTY FOR PRIVATE USE TO AVOID PAYMENT OF POSTAGE, $300 (GPO)

JOURNAL OF RESEARCH of the National Bureau of Standards Vol. 65A, No. 5 September–October 1961
A. Physics and Chemistry

Contents

Page

Calibration of a monitor for use in bremsstrahlung beams. E. G. Fuller and Evans Hayward. 401

Mass spectrometric study of NF_3, NF_2, N_2F_2, and N_2F_4. John T. Herron and Vernon H. Dibeler 405

Rate of the reaction NO+N, and some heterogeneous reactions observed in the ion source of a mass spectrometer. John T. Herron. 411

Synthesis of the humites $nMg_2SiO_4 \cdot Mg(F,OH)_2$. A. Van Valkenburg. 415

Phase equilibria in systems involving the rare earth oxides. Part III. The Eu_2O_3–In_2O_3 system. S. J. Schneider. 429

Heats of hydrolysis and formation of dimethoxychloroborane. Marthada V. Kilday, Walter H. Johnson, and Edward J. Prosen. 435

Tritium-labeled compounds VII. Isotope effects in the oxidation of D-mannitols-C^{14} and D-mannitols-t to D-fructoses. Lorna T. Sniegoski, Harriet L. Frush, and Horace S. Isbell. 441

Franck-Condon factors to high vibrational quantum numbers I: N_2 and N_2^+. R. W. Nicholls. 451

Publications of the National Bureau of Standards. 461

For sale by the Superintendent of Documents, U.S. Government Printing Office, Washington 25, D.C. Price 70 cents (single copy)
Subscription price: $4.00 a year; 75 cents additional for foreign mailing.

UNITED STATES GOVERNMENT PRINTING OFFICE, WASHINGTON : 1961